ISSN 1948-0210 (online)

World Journal of *Stem Cells*

World J Stem Cells 2023 November 26; 15(11): 989-1034

Published by Baishideng Publishing Group Inc

WJSC

World Journal of Stem Cells

Contents

Monthly Volume 15 Number 11 November 26, 2023

MINIREVIEWS

989 How to enhance the ability of mesenchymal stem cells to alleviate intervertebral disc degeneration

Zhang QX, Cui M

ORIGINAL ARTICLE

Basic Study

999 Hypoxia and inflammatory factor preconditioning enhances the immunosuppressive properties of human umbilical cord mesenchymal stem cells

Li H, Ji XQ, Zhang SM, Bi RH

1017 Dissecting molecular mechanisms underlying ferroptosis in human umbilical cord mesenchymal stem cells: Role of cystathionine γ-lyase/hydrogen sulfide pathway

Hu B, Zhang XX, Zhang T, Yu WC

World Journal of Stem Cells

Monthly Volume 15 Number 11 November 26, 2023

Contents

ABOUT COVER

Editorial Board Member of *World Journal of Stem Cells*, Jyoti Anand Kode, MSc, PhD, Associate Professor, Senior Scientist, Principal Investigator, Kode Lab, Tumor Immunology and Immunotherapy Group, Facility for Immunomodulatory Activity Testing, Anti-Cancer Drug Screening Facility, Advanced Centre for Treatment, Research and Education in Cancer, Tata Memorial Centre, Homi Bhabha National Institute, Navi Mumbai 410210, Maharashtra, India.jkode@actrec.gov.in

AIMS AND SCOPE

The primary aim of *World Journal of Stem Cells* (*WJSC*, *World J Stem Cells*) is to provide scholars and readers from various fields of stem cells with a platform to publish high-quality basic and clinical research articles and communicate their research findings online. *WJSC* publishes articles reporting research results obtained in the field of stem cell biology and regenerative medicine, related to the wide range of stem cells including embryonic stem cells, germline stem cells, tissue-specific stem cells, adult stem cells, mesenchymal stromal cells, induced pluripotent stem cells, embryonal carcinoma stem cells, hemangioblasts, lymphoid progenitor cells, *etc*.

INDEXING/ABSTRACTING

The *WJSC* is now abstracted and indexed in Science Citation Index Expanded (SCIE, also known as SciSearch®), Journal Citation Reports/Science Edition, PubMed, PubMed Central, Scopus, Biological Abstracts, BIOSIS Previews, Reference Citation Analysis, China National Knowledge Infrastructure, China Science and Technology Journal Database, and Superstar Journals Database. The 2023 Edition of Journal Citation Reports® cites the 2022 impact factor (IF) for *WJSC* as 4.1; IF without journal self cites: 3.9; 5-year IF: 4.5; Journal Citation Indicator: 0.53; Ranking: 15 among 29 journals in cell and tissue engineering; Quartile category: Q3; Ranking: 99 among 191 journals in cell biology; and Quartile category: Q3. The *WJSC*'s CiteScore for 2022 is 8.0 and Scopus CiteScore rank 2022: Histology is 9/57; Genetics is 68/325; Genetics (clinical) is 19/90; Molecular Biology is 119/380; Cell Biology is 95/274.

RESPONSIBLE EDITORS FOR THIS ISSUE

NAME OF JOURNAL
World Journal of Stem Cells

ISSN
ISSN 1948-0210 (online)

LAUNCH DATE
December 31, 2009

FREQUENCY
Monthly

EDITORS-IN-CHIEF
Shengwen Calvin Li, Carlo Ventura

EDITORIAL BOARD MEMBERS
https://www.wjgnet.com/1948-0210/editorialboard.htm

PUBLICATION DATE
November 26, 2023

INSTRUCTIONS TO AUTHORS
https://www.wjgnet.com/bpg/gerinfo/204

GUIDELINES FOR ETHICS DOCUMENTS
https://www.wjgnet.com/bpg/GerInfo/287

GUIDELINES FOR NON-NATIVE SPEAKERS OF ENGLISH
https://www.wjgnet.com/bpg/gerinfo/240

PUBLICATION ETHICS
https://www.wjgnet.com/bpg/GerInfo/288

PUBLICATION MISCONDUCT
https://www.wjgnet.com/bpg/gerinfo/208

ARTICLE PROCESSING CHARGE
https://www.wjgnet.com/bpg/gerinfo/242

STEPS FOR SUBMITTING MANUSCRIPTS
https://www.wjgnet.com/bpg/GerInfo/239

ONLINE SUBMISSION
https://www.f6publishing.com

E-mail: bpgoffice@wjgnet.com https://www.wjgnet.com

World Journal of Stem Cells

Submit a Manuscript: https://www.f6publishing.com

World J Stem Cells 2023 November 26; 15(11): 989-998

DOI: 10.4252/wjsc.v15.i11.989

ISSN 1948-0210 (online)

MINIREVIEWS

How to enhance the ability of mesenchymal stem cells to alleviate intervertebral disc degeneration

Qing-Xiang Zhang, Min Cui

Specialty type: Cell and tissue engineering

Provenance and peer review: Unsolicited article; Externally peer reviewed.

Peer-review model: Single blind

Peer-review report's scientific quality classification

Grade A (Excellent): 0
Grade B (Very good): B; B
Grade C (Good): C, C
Grade D (Fair): D, D
Grade E (Poor): 0

P-Reviewer: Jabbarpour Z, United Kingdom; Trebol J, Spain; Wongkajornsilp A, Thailand; Li SC, United States; Ventura C, Italy

Received: July 17, 2023
Peer-review started: July 17, 2023
First decision: August 22, 2023
Revised: September 14, 2023
Accepted: November 16, 2023
Article in press: November 16, 2023
Published online: November 26, 2023

Qing-Xiang Zhang, Department of Critical Care Medicine, Union Hospital, Tongji Medical College, Huazhong University of Science and Technology, Wuhan 430022, Hubei Province, China

Qing-Xiang Zhang, Department of Critical Care Medicine, Wuhan Jinyintan Hospital, Tongji Medical College, Huazhong University of Science and Technology, Wuhan 430048, Hubei Province, China

Min Cui, Department of Orthopedics, Union Hospital, Tongji Medical College, Huazhong University of Science and Technology, Wuhan 430022, Hubei Province, China

Corresponding author: Min Cui, MD, PhD, Associate Chief Physician, Associate Professor, Doctor, Department of Orthopedics, Union Hospital, Tongji Medical College, Huazhong University of Science and Technology, No. 1277 Jiefang Avenue, Wuhan 430022, Hubei Province, China. cm95588@hust.edu.cn

Abstract

Intervertebral disc (ID) degeneration (IDD) is one of the main causes of chronic low back pain, and degenerative lesions are usually caused by an imbalance between catabolic and anabolic processes in the ID. The environment in which the ID is located is harsh, with almost no vascular distribution within the disc, and the nutrient supply relies mainly on the diffusion of oxygen and nutrients from the blood vessels located under the endplate. The stability of its internal environment also plays an important role in preventing IDD. The main feature of disc degeneration is a decrease in the number of cells. Mesenchymal stem cells have been used in the treatment of disc lesions due to their ability to differentiate into nucleus pulposus cells in a nonspecific anti-inflammatory manner. The main purpose is to promote their regeneration. The current aim of stem cell therapy is to replace the aged and metamorphosed cells in the ID and to increase the content of the extracellular matrix. The treatment of disc degeneration with stem cells has achieved good efficacy, and the current challenge is how to improve this efficacy. Here, we reviewed current treatments for disc degeneration and summarize studies on stem cell vesicles, enhancement of therapeutic effects when stem cells are mixed with related substances, and improvements in the efficacy of stem cell therapy by adjuvants under adverse conditions. We reviewed the new approaches and ideas for stem cell treatment of disc degeneration in order to contribute to the development of new therapeutic approaches to meet current challenges.

Key Words: Mesenchymal stem cells; Intervertebral disc degeneration; Extracellular vesicles; Nucleus pulposus cells; Tissue regeneration

Core Tip: Mesenchymal stem cells have a strong self-renewal capacity and multidirectional differentiation potential, and their secreted vesicles promote regeneration of myeloid cells, increase extracellular matrix production, and alleviate inflammatory status. We reviewed the current relevant targets of stem cell exosomes for the treatment of intervertebral discs and the adjuvant tools used in conjunction with stem cell therapy. This will help to improve the therapeutic efficacy of stem cells and their exosomes, which will also contribute to development of more efficient treatment strategies and approaches for the restoration of disc degeneration.

Citation: Zhang QX, Cui M. How to enhance the ability of mesenchymal stem cells to alleviate intervertebral disc degeneration. *World J Stem Cells* 2023; 15(11): 989-998
URL: https://www.wjgnet.com/1948-0210/full/v15/i11/989.htm
DOI: https://dx.doi.org/10.4252/wjsc.v15.i11.989

INTRODUCTION

Intervertebral discs (IDs) have a complex structure with a unique internal environment. They contain nucleus pulposus cells, fibrous rings, and extracellular matrix (ECM)[1], Mesenchymal stem cells (MSCs), a class of pluripotent stem cells with the capacity for self-renewal and the ability to differentiate into a variety of tissues in vitro, were first mentioned in 1970 in guinea pig bone marrow[2]. Isolation and culture of MSCs from human bone marrow was first described in 1992. Since then, MSCs have been isolated and cultured from different human tissues, such as fat, amniotic membrane, gingiva, thymus, and placenta. MSCs from different sources differ in phenotype and function[3], for example, in solving the problem of ID withdrawal, umbilical cord-derived MSCs have a greater capacity for cell proliferation and osteogenesis than bone marrow-derived MSCs[4]. Stem cell therapy is designed to restore this balance of secreting exosomes and vesicles, mixing other substances to promote their differentiation into nucleus pulposus cells, regulating the content of the ECM, and when treated accordingly resisting interference by the harsh environment of the IDs[5,6]. These synergistic approaches provide new possibilities for stem cell therapy of (IDD)[7,8].

MIRNA IN EXOSOMES

For signal transduction pathways, many miRNAs play a crucial role in the growth and development of IDs. MSCs deliver miRNA-31 to the nucleus pulposus and upregulate the Wnt/β-catenin pathway to inhibit apoptosis of nucleus pulposus cells and regulate production of the ECM[9]. Similarly, under the stimulation of external effects, miRNA-21 can be transfected into mesenchymal cell exosomes, enhancing the ability of MSCs to differentiate into osteoblasts and promote vascular regeneration[10]. In other related studies, exosomes derived from bone marrow MSCs inhibited apoptosis and inflammation by upregulating autophagy through the protein kinase β/mammalian target of rapamycin signaling pathway[11]. MSCs-derived exosomes can also inhibit apoptosis of nucleus pulposus cells through miRNA-532-5p transport, demonstrating that this transport is also effective in IDD therapy[12].

Exosome-delivered exogenous miRNA-26a-5p can also be delivered to IDs, as METTL14 is highly expressed in patients with IDD, and the level of NOD-like receptor family pyrin domain containing 3 regulated by it leads to an increase in proinflammatory factors and apoptosis of nucleus pulposus cells. Exogenous miRNA-26a-5p inhibits METTL4 expression and thus treats disc degeneration[13]. It has also been found that miRNA-15a in exosomes can participate in the protein balance regulated by the phosphatidylinositol 3-kinase/protein kinase β and Wnt3a/β-catenin axes of IDD and downregulate matrix metalloproteinase-3. Therefore, type II collagen and aggrecan levels can be increased, along with differentiation of MSCs to nucleus pulposus cells[14,15]. BTB-and-CNC homologue 1 is a transcription inhibitor of heme oxygenase 1, which activates autophagy in nucleus pulposus cells. miRNA-155 in exosomes inhibits BTB-and-CNC homologue 1 expression by binding to the 3′ untranslated region of this transcription inhibitor, thereby treating IDD[16] (Table 1).

SPECIAL GENETICS AND MSCsS

Microtubules are an important part of the cytoskeleton that can regulate the assembly of proteins and the transport of substances within the cell. The stability of microtubules may extend their own life and ensure their normal basic functions. A decrease in transforming growth factor (TGF)-β1 is one of the possible factors involved in ID metamorphosis.

Table 1 Effects of mRNA in vesicles on differentiation of mesenchymal stromal cells into myeloid cells, for extracellular matrix production, and for inflammatory status

Differentiation to myeloid cells	Extracellular matrix production	Inflammatory state	RNA	Target	Ref.
Promotion			lncRNA CAHM	M1 macrophages	Li *et al*[26]
Promotion		Repression	miR-199a	GREM1	Wen *et al*[35]
Promotion			miR-140-5p	KLF5/N-cadherin/MDM2/Slug	Wang *et al*[34]
Promotion			miR-105-5p	Sirt6	Sun *et al*[33]
Promotion		Repression	miR-129-5p	p38 MAPK	Cui *et al*[31]
Promotion	Promotion		miR-17-5p	TLR4	Zhou *et al*[29]
Promotion			miR-194-5p	TRAF6	Sun *et al*[12]
Promotion			miR-21	p38 MAPK	Wang *et al*[10]
Promotion		Repression	miR-26a-5p	METTL14	Xuan *et al*[13]
Promotion			miR-532-5p	AKT-mTOR	Sun *et al*[12]
Promotion		Repression	miR-31	Wnt/β-Catenin	Wang *et al*[9]
Promotion			miR-155	BACH1	Shi *et al*[16]
	Promotion		miR-15a	PI3K/Akt	Zhang *et al*[14]
	Promotion		miR-217	EZH2	Hao *et al*[27]
Promotion	Promotion		cirRNA0050205	GPX4	Yu *et al*[25]
Promotion	Promotion		cirRNA0072464	NRF2	Yu *et al*[24]

AKT: Protein kinase B; BACH1: BTB-and-CNC homologue 1; EZH2: Enhancer of zeste homolog 2; GPX4: Glutathione peroxidase 4; GREM1: Gremlin1; KLF5: Kruppel-like factor 5; lncRNA CAHM: Long non-coding RNA colorectal adenocarcinoma hypermethylated; MAPK: Mitogen-activated protein kinase; MDM2: Murine double minute 2; mTOR: Mechanistic target of rapamycin; NRF2: Nuclear factor erythroid 2-related factor 2; PI3K: Phosphoinositide 3-kinase; TRAF6: Tumor necrosis factor receptor associated factor 6.

Stabilization of microtubules can promote the expression of collagen type 2 and SRY-box transcription factor 9 (SOX9) in nucleus pulposus cells[17], which alleviates and reduces IDD. SOX9 and TGF-β1 can be used to transfect bone marrow MSCs, and MSCs can successfully differentiate into chondrocytes, promote formation of ECM, restore ID integrity, improve the inflammatory state, and reduce pain and further IDD. Similarly, MSCs and induced cartilage progenitor cells also increase the level of SOX9 and TGF-β1 during differentiation into nucleus pulposus cells, with the purpose of regulating inflammatory states and increasing differentiation[15,18,19].

METABOLITES AND MSCsS

MSCs-derived exosomes contain martrilin-3, which regulates the content of TGF-β1 in the IDs and differentiation of nucleus pulposus cells, promotes production of ECM, and inhibits release of inflammatory mediators[20]. Urolithin A was able to hinder hydrogen peroxide in inducing the aging of nucleus pulposus cells and destroying mitochondrial function. The silent information regulator 1/peroxisome proliferator-activated receptor gamma coactivator 1-alpha signaling pathway was activated by urolithin A *in vitro*, which protected the normal physiological function of mitochondria, linked nucleus pulposus cell aging, and increased the survival time of ECM while preventing further IDD [21,22]. The compression produced by the degenerated ID can promote reactive oxygen species production by nucleus pulposus cells and cause oxidative stress, which leads to further apoptosis of nucleus pulposus cells. MSCs-derived exosomes can inhibit apoptosis of myeloid cells caused by excessive oxidative stress and ameliorate compression-induced mitochondrial damage, which relieves the pain caused by IDD[23].

GEL-LOADED MSCsS

Heat-responsive hydrogel can act as a carrier of the extracellular vesicles of MSCs. These vectors deliver vesicles in a continuous box, which contains vasorin (a type I transmembrane glycoprotein regulated by hypoxia-inducible factor 1) to the disc environment. Vasorin can regulate the expression of relevant matrix metalloenzymes in the nucleus pulposus

cells through Notch1 signaling, enhance the ability of nucleus pulposus cells to proliferate, migrate, and anabolize, and inhibit the apoptotic cells to release inflammatory mediators, preventing further exacerbation of IDD. However, whether vasorin can promote the proliferation and differentiation of MSCs has not been confirmed[21]. Therefore, the strategy of helping stem cells to treat IDD through gels is worth further study.

The combination of heat-sensitive decellularized ECM hydrogels with adipocyte-derived MSCs exosomes does not damage the therapeutic activity of MSCs. The heat-sensitive dECM@exo hydrogel system produces gelation in situ to help MSCs differentiate into nucleus pulposus cells and maintains the content of ECM. This hydrogel also creates a suitable environment for the proliferation and differentiation of nucleus pulposus cells[22]. Previous studies have demonstrated transport of MSCs with hyaluronic acid and platelet-rich hydrogels. This method enhances MSCs activity, promotes IDs to increase keratin 19 gene expression, induces differentiation of MSCs into nucleus pulposus cells, and maintains the original ID height and normal physiological activity of the ID environment[23]. This situation leads to increased expression of keratin genes, and it has been demonstrated that porcine nucleus pulposus-rich cell matrix induces differentiation into nucleus pulposus cells by stimulating porcine chordate cells[24].

CIRCULAR RNA AND EXOSOMES

Circular RNA, such as circ_0050205 and circ_0072464, is transmitted through exosomes into nucleus pulposus cells to promote cell proliferation and ECM synthesis[24,25]. Endogenous long non-coding RNA colorectal adenocarcinoma hypermethylated delivery by MSCs exosomes inhibits M1-type macrophage polarization, which reduces nucleus pulposus apoptosis, the release of inflammatory factors, and a reduction in ECM to prevent further IDD[26]. In the MSCs exosomes, miRNA-217 is transferred to the ID and binds to the forkhead box O_3 promoter by targeting enhancer of zeste homolog 2. This maintains ID homeostasis and stimulates autophagy, thereby promoting collagen II and aggrecan content and inhibiting degradation of nucleus pulposus cells[15,27,28].

In other vesicles, overexpression of miRNA-194-5p inhibits the occurrence of disc degeneration by targeting tumor necrosis factor receptor associated factor 6. Lentiviral vectors have been shown to transport the growth and differentiation factor 5 (*GDF5)* gene and integrate it into the chromosomal genome of nucleus pulposus MSCs, which then express *GDF5* along with the MSCs genes. *GDF5* can also increase the level of proteoglycan and type II collagen[12]. If vesicles are subjected to hypoxia, miRNA-17-5p regulates the proliferation and differentiation of human nucleus pulposus cells and the proliferation and synthesis of ECM through the toll-like receptor 4 pathway, alleviating progression of IDD. This is more effective than the direct injection of MSCs into the ID[29].

During disc degeneration, the release of inflammatory factors also leads to a decrease in the uptake of extracellular vesicles. Vesicles prevent excess death of nucleus pulposus cells by delivering peroxidase 2 and reversing the decline in therapeutic effectiveness of MSCs due to tumor necrosis factor-α damage[30]. miRNA-129-5p in vesicles increases MSCs proliferation and differentiation into nucleus pulposus cells by blocking the lrg1-mediated p38 mitogen-activated protein kinase pathway and polarizing macrophages to the M1 phenotype, ultimately alleviating disc degeneration[31].

The combination of electromagnetic radiation and tissue engineering can stimulate the bone morphogenetic protein/Smad and mitogen-activated protein kinase-related p38 signaling pathway of ID stem cells to regulate differentiation of MSCs and increase their osteogenic capacity for the treatment of IDD[32]. Vesicles can also transmit exogenous miRNA-105-5p to revitalized nucleus pulposus cells, and transmit miRNA-140-3p to regulate the kruppel-like factor 5/N-cadherin/Murine double minute 2/Slug axis; all of which can slow down progression of IDD and restore normal ID physiological function[33,34]. miRNA-199a also exists in MSCs exosomes, which targets gremlin1 downregulation of the TGF-β pathway to prevent apoptosis of nucleus pulposus cells and inhibit progression of IDD[35].

MSCs MIXTURE

MSCs therapy alone has been shown to be effective in IDD, but its efficacy still falls short of expectations[36]. A recent study has shown that MSCs can be mixed with cell-free bioresorbable ultra-purified alginate gel for the treatment of IDD [37]. Such mixed preparations inhibit cell necrosis in the IDs and the release of inflammatory factors and consolidate the therapeutic effect of MSCs. Similarly, the combination of MSCs with in situ bioresorbable gel (dMD-001) produced the above therapeutic effects in IDD and was used after discectomy to prevent IDD[38]. Similarly, when MSCs are combined with coenzyme Q10 for the treatment of most ID lesions, it reduces oxidative stress in the ID, inhibits degradation of nucleus pulposus cells, and steadily improves the efficacy of IDD treatment[39].

Gelatin microparticles can also be mixed with MSCs, which can regulate the release of TGF-β1 and bone morphogenetic protein-2 to promote regeneration of osteochondral tissue[38]. When bone marrow MSCs are injected into the human body, leakage and decreased viability of MSCs occur, and gelatin colloidal hydrogels using nanostructures can effectively prevent these conditions. Under the load of gelatin colloid, MSCs promote regeneration of IDs and increase the number of nucleus pulposus cells between the IDs, ECM content, and the ID height[39]. Selective cell retention technology can concentrate MSCs and then the gelatin vector described above is used, which has been shown to enhance the effect of carrier materials on MSCs in the treatment of IDD[40].

A novel amphiphilic copolymer, polyethylene glycol-PAPO, fused with lipophilic kartogenin into a complex, is an esterase-reactive micelle that can carry MSCs and maintain their activity. When this combination is injected into IDs, it protects them from oxidative stress, activates autophagy of MSCs, regulates gene expression in the ECM, promotes ECM production, and increases ID height and hydration between the IDs[41]. Previous studies have found that collagen

hydrogel can promote differentiation of MSCs[42]. A more recent study found that biocompatible earthworm gel fused with MSCs induced their differentiation into nucleus pulposus cells in a targeted manner and improved their differentiation ability and efficiency[43]. For the expression of special genes such as *SOX9*, *ACAN* and *COL2* in nucleus pulposus cells, the study found that MSCs increased the expression of appeal genes after superoxide dismutase 2 and catalase processing, thereby reducing the deterioration of inflammatory states and promoting repair of ID tissue[44]. MSCs can also fuse with connective tissue growth factor and TGF-β3, transport polydopamine nanoparticles to the corresponding positions between the nuclei of the IDs, and finally induce MSCs to differentiate into nucleus pulposus cells and fibrous ring cells, reconstructing the mechanical environment of the IDs[45] (Figure 1).

STIMULATION INDUCTION WITH MSCsS

Sustained mechanical stimulation is an innovative method of induced differentiation in MSCs, which can be continuously stimulated in a special microgel attached to them[46]. Repeated continuous stretching regulates transient receptor potential vanilloid 4 and Piezo1 channel proteins, regulates the value-added differentiation of MSCs into chondrocytes, regenerates the intercellular matrix, increases the water content in the IDs, and restores the normal structure of degenerated IDs[47]. In addition, formation of ECM has been found to correlate with tissue specificity. Therefore, the isolated nucleus pulposus cells and fiber rings are processed into corresponding hydrogels, which are specific in composition and space structure. Viscous fibrinogen-thrombin-genipin gels act specifically through the RhoA/LATS/YAP1 signaling pathway to direct differentiation of MSCs into nucleus pulposus cells or fibrous rings. This helps patients with IDD to reduce the number of nucleus pulposus cells and fibrous ring damage, which may provide a new direction for the treatment of IDD[46,48]. In the treatment of IDD and recovery of ID height by using bleomycin to induce MSCs fibrosis and by stimulating the TGFβ-SMAD2/3 signaling pathway, the gene expression of related collagen and ECM is maintained, thereby maintaining the height of the ID and increasing its ability to resist wear[49].

HARSH ENVIRONMENT OF THE ID

The treatment of IDD with MSCs has been widely applied, and the role of MSCs in delaying ID lesions has been proven [50]. However, the stability and efficacy of MSCs entering the ID are affected by the microenvironment of the ID. The IDs are located in an environment of nutritional deficiency, high tension, low pH, hypoxia, and high mechanical load[51]. In this environment with progression of IDD, most of the nucleus pulposus cells begin to die, resulting in a series of malignant chain reactions that lead to aggravation of oxidative stress, secretion of inflammatory substances, and aggravation of pain[5] (Figure 2).

Many studies have reported that the microenvironment in which cells are located has an important impact on their biological activity[52]. The low pH of IDs significantly inhibits acid-sensitive ion channels (ASICs), which are key receptors for extracellular protons in central and peripheral neurons related to IDD[53]. Due to the decreased activity of ASICs, MSCs differentiate into nucleus pulposus cells. When the number of nucleus pulposus cells decreases and production of ECM decreases, this increases the short-function peptide fragments that can recognize ASIC blockers, as ASICs can activate cell aging pathways, such as p53-p21/p27 and p16-Rb1 signaling factors, to induce apoptosis of nucleus pulposus cells[54]. ASIC blockers can significantly help stem cells overcome the acidic environment during IDD treatment, improve the ability of MSCs to proliferate and differentiate into nucleus pulposus cells, and help restore the normal state of IDs. $1,25(OH)_2D_3$-treated nucleus pulposus MSCs have better tolerance to the hypertonic and acidic microenvironment in which the IDs are located[55]. This reduces apoptosis of nucleus pulposus mesenchymal cells, restores the height between the IDs, and delays occurrence of IDD.

The large changes in pressure between the degenerative IDs leads to a decrease in the survival and differentiation of MSCs[56]. Medullary pulposus cell-derived hydrogels help MSCs differentiate into nucleus pulposus cells[57]. A recent study found that the current methanipine cross-linked decellularization nucleus pulposus hydrogel-like cell delivery system can transport MSCs to the IDs[58]. The changes in ID pressure ensure that MSCs differentiate into nucleus pulposus cells, repair the reduced ECM, and maintain ID height to delay IDD.

MSCs pretreated with lithium chloride can increase the adaptability of MSCs[59], as lithium chloride helps MSCs antagonize oxidative stress and protect nucleus pulposus cells by activating more extracellular signal-regulated kinase 1/2[60]. Extracellular signal-regulated kinase 1/2 plays a vital role in fighting inflammation, which is one of the main ways it works in the harsh environment of the IDs. This conduction pathway ultimately also helps to improve the ability of MSCs to reduce nucleus pulposus cell death, increase ECM production, and improve inflammatory status and IDD.

Significant progress has been made in the treatment of IDD by MSCs, but due to the harsh environment of the IDs[5], the therapeutic effect of MSCs is reduced due to the lack of oxygen in the environment[61]. However, it has been found that the differentiation of MSCs to chondrocytes under hypoxic conditions can be helped by the addition of leptin[62], which provides energy for cell differentiation through its dependent glycolysis.

FUTURE DIRECTIONS FOR STEM-CELL-BASED THERAPY

Stem cell-based therapy offers promise for disc degeneration. Related studies have applied exogenous stem cells such as

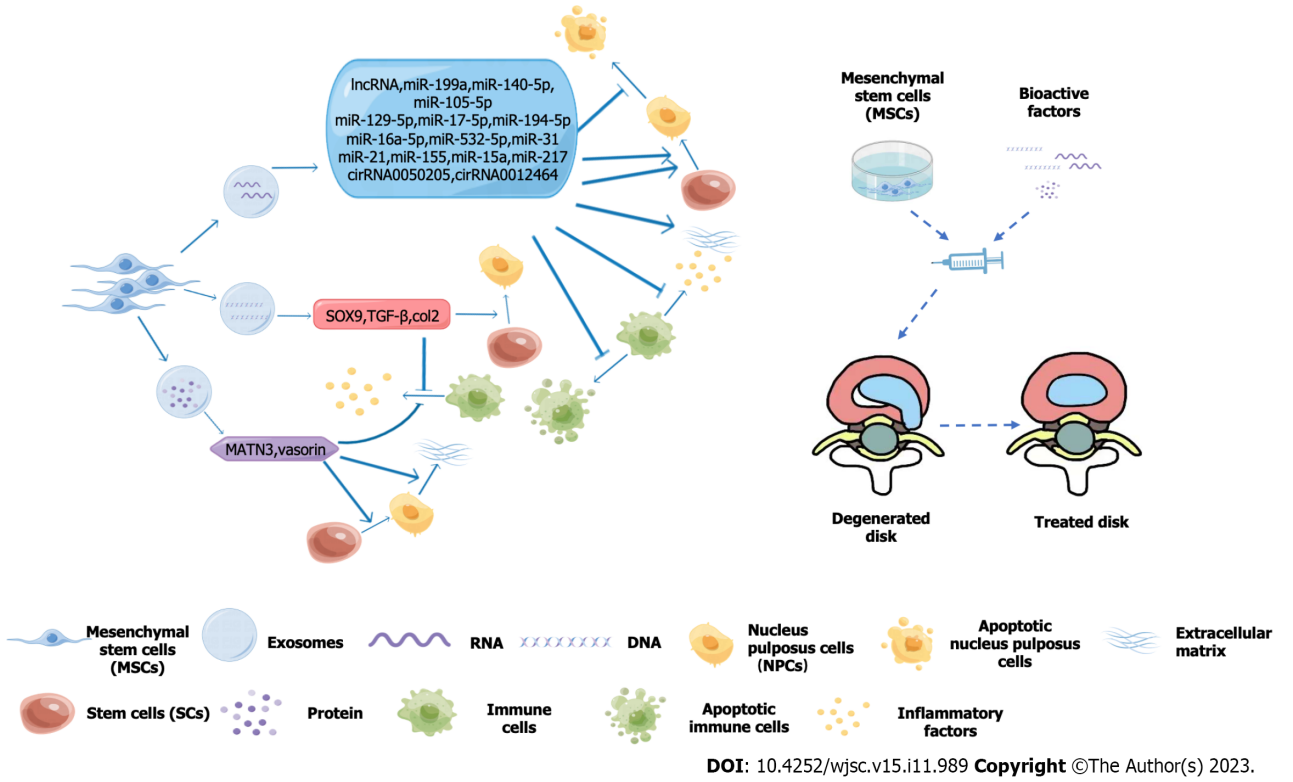

DOI: 10.4252/wjsc.v15.i11.989

Figure 1 Mesenchymal stromal cell exosomes can treat disc degeneration through the appropriate target. The extracellular vesicles secreted by mesenchymal stromal cells can be enriched with a variety of RNAs, DNAs, and proteins that can be targeted to treat disc degeneration. They have been shown to have a corresponding effect in promoting stem cell differentiation into myeloid cells, increasing extracellular matrix production, and reducing the release of inflammatory factors (pain reduction). MATN3: Martrilin-3; SOX9: SRY-box transcription factor 9; TGF: Transforming growth factor.

MSCs to treat disc degeneration with promising results[63]. As the field of stem cells continues to be studied[64], the histology of the IDs becomes clearer, and studies targeting the way in which stem cells restore disc structure are becoming more advanced. How to improve the efficiency of stem cell therapy for disc degeneration and how to resist the harsh disc environment for stem cell therapy are the focus of research[65]. This also includes how to help stem cells restore the normal physiological structure of the IDs under hypoxia and lack of blood supply[5]. This is a new direction that needs to be developed in the field of stem cells.

Sometimes it is not the stem cell therapy that is ineffective, as the way MSCs are administered similarly affects their behavior once inside the body. Overall, factors such as injection point site, syringe, carrier material, and buffer can affect the therapeutic efficacy of stem cells. Different injection sites may lead to variations in reflux of the cellular injection fluid [66], and the syringe (needle size/shape) may lead to variations in the shear rate and shear stress of the cellular injection fluid, which can affect the viability of the injected cells. There are various challenges in the clinical application of stem cells, both for local administration and circulatory system administration[65]. Therefore, does the appropriate route of administration always guarantee the clinical outcome of MSCs? Obviously not. While performing stem cell therapy, we not only need to choose the appropriate delivery method but also need to consider the individualization of the patient at the same time. We need to consider all these factors together in order to make the most appropriate stem cell treatment plan, thus improving the efficiency of MSCs treatment[67].

Different sources of MSCs have their own advantages and disadvantages in terms of therapeutic efficacy, and one of the major dilemmas that needs to be explored further is the production of stable MSCs at the production site[68]. Current research allows us to understand the current potential of MSCs for cell transplantation, tissue engineering, and cell-based therapies to improve the lives of those affected by disc injuries[65]. This requires us to deepen our understanding of MSCs, refine therapeutic approaches, and address the challenges of translating research findings into clinical practice. We can do this by further optimizing the sources of MSCs[69], delivery methods and timing of interventions, as well as standardized protocols for isolation, expansion, and characterization. Conducting well-designed clinical trials will help evaluate the safety, efficacy, and long-term outcomes of MSCs-based therapies[70]. As the clinical application of MSCs continues to be studied globally, stem cell therapeutic drugs are gradually being introduced, and more research teams and medical institutions are involved, this will gradually deepen the clinical application of stem cell therapy and bring hope to the majority of lumbar disc patients.

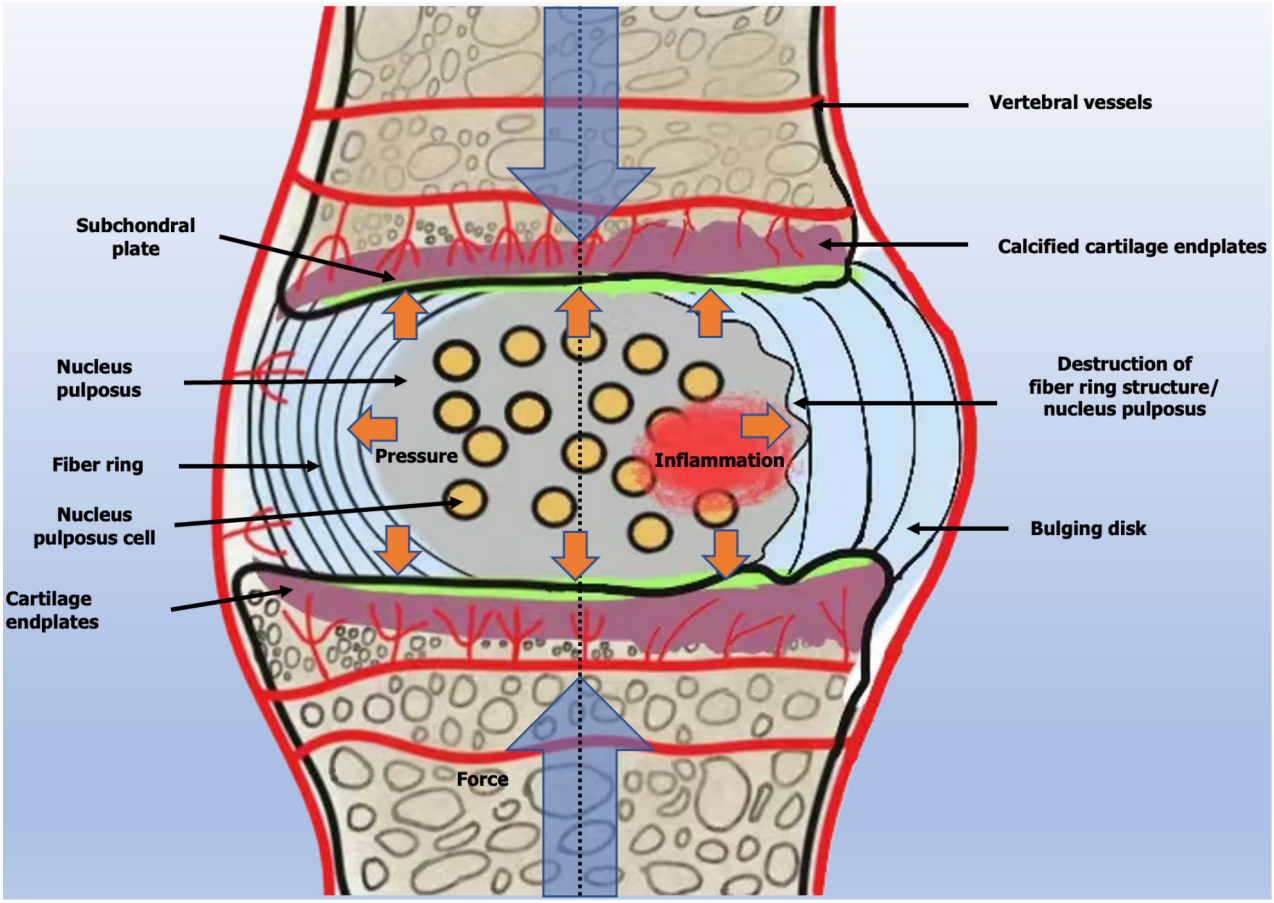

DOI: 10.4252/wjsc.v15.i11.989

Figure 2 The harsh environment in which the intervertebral discs are located. There is almost no vascular distribution in the intervertebral discs, and the nutrient supply relies mainly on the diffusion of oxygen and nutrients in the subendothelial vessels. The closer to the center of the nucleus pulposus, the lower the partial pressure of oxygen and the concentration of proteoglycans, which results in an extreme microenvironment, such as nutrient deficiency, high osmotic pressure, and acidic PH.

CONCLUSION

IDs have a complex structure with a unique internal environment. They contain nucleus pulposus cells, fibrous rings, and ECM, which are in a dynamic balance of self-renewal. Stem cells therapy is designed to restore this balance of secreting exosomes and vesicles, mixing other substances to promote their differentiation into nucleus pulposus cells, regulating the content of the ECM, and when treated accordingly resisting interference by the harsh environment of the IDs. These synergistic approaches provide new possibilities for stem cell therapy of IDD. They contain nucleus pulposus cells, annulus fibrosus, and ECM, and as the nucleus pulposus cells age and the ECM is lost, among other things, the disc becomes less stable. Stem cell therapy aims to restore the structure of the disc by secreting exosomes and vesicles, it mixes other substances to promote their differentiation into nucleus pulposus cells, regulates the content of the ECM and resists interference from the hostile environment of the IDs when treated accordingly. These synergistic approaches offer new possibilities for stem cell therapy for IDD. In the future, as people continue to explore the field of stem cells in disc therapy, stem cells will bring more hope to disc degeneration.

FOOTNOTES

Author contributions: Zhang QX wrote the manuscript and collected the data; Cui M revised and approved the manuscript; all authors read and approved the final manuscript.

Supported by National Natural Science Foundation of China, No. 82202766; Natural Science Foundation of Hubei Province of China, No. 2022CFB686; Science Foundation of Union Hospital, No. 2021xhyn102; Scientific Research Training Program for Young Talents in Union Hospital, Tongji Medical College, Huazhong University of Science and Technology, China.

Conflict-of-interest statement: There is no conflict of interest associated with this manuscript.

Country/Territory of origin: China

ORCID number: Min Cui 0000-0002-2638-3287.

S-Editor: Qu XL
L-Editor: Filipodia
P-Editor: Zhang XD

REFERENCES

1 **Shen D**, Wang Z, Wang H, Zhu H, Jiang C, Xie F, Zhang H, Lv Q, Liu Q, Qi N. Evaluation of preclinical efficacy of human umbilical cord mesenchymal stem cells in ankylosing spondylitis. *Front Immunol* 2023; **14**: 1153927 [PMID: 37063838 DOI: 10.3389/fimmu.2023.1153927]
2 **Steck E**, Bertram H, Abel R, Chen B, Winter A, Richter W. Induction of intervertebral disc-like cells from adult mesenchymal stem cells. *Stem Cells* 2005; **23**: 403-411 [PMID: 15749935 DOI: 10.1634/stemcells.2004-0107]
3 **Hass R**, Kasper C, Böhm S, Jacobs R. Different populations and sources of human mesenchymal stem cells (MSCs): A comparison of adult and neonatal tissue-derived MSCs. *Cell Commun Signal* 2011; **9**: 12 [PMID: 21569606 DOI: 10.1186/1478-811X-9-12]
4 **Li C**, Chen X, Qiao S, Liu X, Liu C, Zhu D, Su J, Wang Z. Effects of Wharton's jelly cells of the human umbilical cord on acute spinal cord injury in rats, and expression of interleukin-1β and nerve growth factor in spinal cord tissues. *Artif Cells Nanomed Biotechnol* 2016; **44**: 1254-1258 [PMID: 25801039 DOI: 10.3109/21691401.2015.1019671]
5 **Chu G**, Zhang W, Han F, Li K, Liu C, Wei Q, Wang H, Liu Y, Li B. The role of microenvironment in stem cell-based regeneration of intervertebral disc. *Front Bioeng Biotechnol* 2022; **10**: 968862 [PMID: 36017350 DOI: 10.3389/fbioe.2022.968862]
6 **Guan M**, Liu C, Zheng Q, Chu G, Wang H, Jin J, Wu H, Chen J, Huang Q, Deng Z, Wang Y. Exosome-laden injectable self-healing hydrogel based on quaternized chitosan and oxidized starch attenuates disc degeneration by suppressing nucleus pulposus senescence. *Int J Biol Macromol* 2023; **232**: 123479 [PMID: 36731695 DOI: 10.1016/j.ijbiomac.2023.123479]
7 **Zhao Y**, Xiang Q, Cheng Y, Lin J, Jiang S, Li W. Mesenchymal Stem Cells May Alleviate the Intervertebral Disc Degeneration by Reducing the Oxidative Stress in Nucleus Pulposus Cells. *Stem Cells Int* 2022; **2022**: 6082377 [PMID: 36238530 DOI: 10.1155/2022/6082377]
8 **Orozco L**, Soler R, Morera C, Alberca M, Sánchez A, García-Sancho J. Intervertebral disc repair by autologous mesenchymal bone marrow cells: a pilot study. *Transplantation* 2011; **92**: 822-828 [PMID: 21792091 DOI: 10.1097/TP.0b013e3182298a15]
9 **Wang B**, Xu N, Cao L, Yu X, Wang S, Liu Q, Wang Y, Xu H, Cao Y. miR-31 from Mesenchymal Stem Cell-Derived Extracellular Vesicles Alleviates Intervertebral Disc Degeneration by Inhibiting NFAT5 and Upregulating the Wnt/β-Catenin Pathway. *Stem Cells Int* 2022; **2022**: 2164057 [PMID: 36311041 DOI: 10.1155/2022/2164057]
10 **Wang T**, Zhao H, Jing S, Fan Y, Sheng G, Ding Q, Liu C, Wu H, Liu Y. Magnetofection of miR-21 promoted by electromagnetic field and iron oxide nanoparticles *via* the p38 MAPK pathway contributes to osteogenesis and angiogenesis for intervertebral fusion. *J Nanobiotechnology* 2023; **21**: 27 [PMID: 36694219 DOI: 10.1186/s12951-023-01789-3]
11 **Xiao Q**, Zhao Z, Teng Y, Wu L, Wang J, Xu H, Chen S, Zhou Q. BMSCs-Derived Exosomes Alleviate Intervertebral Disc Degeneration by Modulating AKT/mTOR-Mediated Autophagy of Nucleus Pulposus Cells. *Stem Cells Int* 2022; **2022**: 9896444 [PMID: 35855812 DOI: 10.1155/2022/9896444]
12 **Sun Z**, Tang X, Li Q, Wang H, Sun H, Tian J. Mesenchymal stem cell extracellular vesicles-derived microRNA-194-5p delays the development of intervertebral disc degeneration by targeting TRAF6. *Regen Ther* 2022; **19**: 88-96 [PMID: 35127996 DOI: 10.1016/j.reth.2021.12.001]
13 **Yuan X**, Li T, Shi L, Miao J, Guo Y, Chen Y. Human umbilical cord mesenchymal stem cells deliver exogenous miR-26a-5p *via* exosomes to inhibit nucleus pulposus cell pyroptosis through METTL14/NLRP3. *Mol Med* 2021; **27**: 91 [PMID: 34412584 DOI: 10.1186/s10020-021-00355-7]
14 **Zhang Q**, Shen Y, Zhao S, Jiang Y, Zhou D, Zhang Y. Exosomes miR-15a promotes nucleus pulposus-mesenchymal stem cells chondrogenic differentiation by targeting MMP-3. *Cell Signal* 2021; **86**: 110083 [PMID: 34252537 DOI: 10.1016/j.cellsig.2021.110083]
15 **Zhang X**, Shu S, Feng Z, Qiu Y, Bao H, Zhu Z. Microtubule stabilization promotes the synthesis of type 2 collagen in nucleus pulposus cell by activating hippo-yap pathway. *Front Pharmacol* 2023; **14**: 1102318 [PMID: 36778003 DOI: 10.3389/fphar.2023.1102318]
16 **Shi M**, Zhao Y, Sun Y, Xin D, Xu W, Zhou B. Therapeutic effect of co-culture of rat bone marrow mesenchymal stem cells and degenerated nucleus pulposus cells on intervertebral disc degeneration. *Spine J* 2021; **21**: 1567-1579 [PMID: 34000376 DOI: 10.1016/j.spinee.2021.05.007]
17 **Ekram S**, Khalid S, Bashir I, Salim A, Khan I. Human umbilical cord-derived mesenchymal stem cells and their chondroprogenitor derivatives reduced pain and inflammation signaling and promote regeneration in a rat intervertebral disc degeneration model. *Mol Cell Biochem* 2021; **476**: 3191-3205 [PMID: 33864569 DOI: 10.1007/s11010-021-04155-9]
18 **Khalid S**, Ekram S, Ramzan F, Salim A, Khan I. Co-regulation of Sox9 and TGFβ1 transcription factors in mesenchymal stem cells regenerated the intervertebral disc degeneration. *Front Med (Lausanne)* 2023; **10**: 1127303 [PMID: 37007782 DOI: 10.3389/fmed.2023.1127303]
19 **Khalid S**, Ekram S, Salim A, Chaudhry GR, Khan I. Transcription regulators differentiate mesenchymal stem cells into chondroprogenitors, and their in vivo implantation regenerated the intervertebral disc degeneration. *World J Stem Cells* 2022; **14**: 163-182 [PMID: 35432734 DOI: 10.4252/wjsc.v14.i2.163]
20 **Guo Z**, Su W, Zhou R, Zhang G, Yang S, Wu X, Qiu C, Cong W, Shen N, Guo J, Liu C, Yang SY, Xing D, Wang Y, Chen B, Xiang H. Exosomal MATN3 of Urine-Derived Stem Cells Ameliorates Intervertebral Disc Degeneration by Antisenescence Effects and Promotes NPC Proliferation and ECM Synthesis by Activating TGF-β. *Oxid Med Cell Longev* 2021; **2021**: 5542241 [PMID: 34136064 DOI: 10.1155/2021/5542241]

21 **Shi PZ**, Wang JW, Wang PC, Han B, Lu XH, Ren YX, Feng XM, Cheng XF, Zhang L. Urolithin a alleviates oxidative stress-induced senescence in nucleus pulposus-derived mesenchymal stem cells through SIRT1/PGC-1α pathway. *World J Stem Cells* 2021; **13**: 1928-1946 [PMID: 35069991 DOI: 10.4252/wjsc.v13.i12.1928]

22 **Xing H**, Zhang Z, Mao Q, Wang C, Zhou Y, Zhou X, Ying L, Xu H, Hu S, Zhang N. Injectable exosome-functionalized extracellular matrix hydrogel for metabolism balance and pyroptosis regulation in intervertebral disc degeneration. *J Nanobiotechnology* 2021; **19**: 264 [PMID: 34488795 DOI: 10.1186/s12951-021-00991-5]

23 **Russo F**, Ambrosio L, Peroglio M, Guo W, Wangler S, Gewiess J, Grad S, Alini M, Papalia R, Vadalà G, Denaro V. A Hyaluronan and Platelet-Rich Plasma Hydrogel for Mesenchymal Stem Cell Delivery in the Intervertebral Disc: An Organ Culture Study. *Int J Mol Sci* 2021; **22** [PMID: 33803999 DOI: 10.3390/ijms22062963]

24 **Yu X**, Xu H, Liu Q, Wang Y, Wang S, Lu R, Jiang Y, Kang H, Hu W. circ_0072464 Shuttled by Bone Mesenchymal Stem Cell-Secreted Extracellular Vesicles Inhibits Nucleus Pulposus Cell Ferroptosis to Relieve Intervertebral Disc Degeneration. *Oxid Med Cell Longev* 2022; **2022**: 2948090 [PMID: 35814268 DOI: 10.1155/2022/2948090]

25 **Yu XJ**, Liu QK, Lu R, Wang SX, Xu HR, Wang YG, Bao Y, Jiang YQ, Li MW, Kang H. Bone Marrow Mesenchymal Stem Cell-Derived Extracellular Vesicles Carrying circ_0050205 Attenuate Intervertebral Disc Degeneration. *Oxid Med Cell Longev* 2022; **2022**: 8983667 [PMID: 35847582 DOI: 10.1155/2022/8983667]

26 **Li W**, Xu Y, Chen W. Bone mesenchymal stem cells deliver exogenous lncRNA CAHM *via* exosomes to regulate macrophage polarization and ameliorate intervertebral disc degeneration. *Exp Cell Res* 2022; **421**: 113408 [PMID: 36334792 DOI: 10.1016/j.yexcr.2022.113408]

27 **Hao Y**, Zhu G, Yu L, Ren Z, Zhang P, Zhu J, Cao S. Extracellular vesicles derived from mesenchymal stem cells confer protection against intervertebral disc degeneration through a microRNA-217-dependent mechanism. *Osteoarthritis Cartilage* 2022; **30**: 1455-1467 [PMID: 36041665 DOI: 10.1016/j.joca.2022.08.009]

28 **Chuah YJ**, Wu Y, Chia YQ, Cheong MLS, Joshua JJN, Kang Y, Hee HT. The co-influence of hyaluronic acid and collagen on the development of an engineered annulus tissue model with bone marrow stromal cells. *Biomed Mater* 2022; **17** [PMID: 35764078 DOI: 10.1088/1748-605X/ac7cac]

29 **Zhou ZM**, Bao JP, Peng X, Gao JW, Vlf C, Zhang C, Sun R, Kun-Wang, Wu XT. Small extracellular vesicles from hypoxic mesenchymal stem cells alleviate intervertebral disc degeneration by delivering miR-17-5p. *Acta Biomater* 2022; **140**: 641-658 [PMID: 34879291 DOI: 10.1016/j.actbio.2021.11.044]

30 **Liao Z**, Liu H, Ma L, Lei J, Tong B, Li G, Ke W, Wang K, Feng X, Hua W, Li S, Yang C. Engineering Extracellular Vesicles Restore the Impaired Cellular Uptake and Attenuate Intervertebral Disc Degeneration. *ACS Nano* 2021; **15**: 14709-14724 [PMID: 34476937 DOI: 10.1021/acsnano.1c04514]

31 **Cui S**, Zhang L. microRNA-129-5p shuttled by mesenchymal stem cell-derived extracellular vesicles alleviates intervertebral disc degeneration *via* blockade of LRG1-mediated p38 MAPK activation. *J Tissue Eng* 2021; **12**: 20417314211021679 [PMID: 34377430 DOI: 10.1177/20417314211021679]

32 **Li W**, Huang C, Ma T, Wang J, Liu W, Yan J, Sheng G, Zhang R, Wu H, Liu C. Low-frequency electromagnetic fields combined with tissue engineering techniques accelerate intervertebral fusion. *Stem Cell Res Ther* 2021; **12**: 143 [PMID: 33597006 DOI: 10.1186/s13287-021-02207-x]

33 **Sun Y**, Zhang W, Li X. Induced pluripotent stem cell-derived mesenchymal stem cells deliver exogenous miR-105-5p *via* small extracellular vesicles to rejuvenate senescent nucleus pulposus cells and attenuate intervertebral disc degeneration. *Stem Cell Res Ther* 2021; **12**: 286 [PMID: 33985571 DOI: 10.1186/s13287-021-02362-1]

34 **Wang Z**, Zhang S, Zhao Y, Qu Z, Zhuang X, Song Q, Leng J, Liu Y. MicroRNA-140-3p alleviates intervertebral disc degeneration *via* KLF5/N-cadherin/MDM2/Slug axis. *RNA Biol* 2021; **18**: 2247-2260 [PMID: 33904383 DOI: 10.1080/15476286.2021.1898176]

35 **Wen T**, Wang H, Li Y, Lin Y, Zhao S, Liu J, Chen B. Bone mesenchymal stem cell-derived extracellular vesicles promote the repair of intervertebral disc degeneration by transferring microRNA-199a. *Cell Cycle* 2021; **20**: 256-270 [PMID: 33499725 DOI: 10.1080/15384101.2020.1863682]

36 **Wu X**, Sun W. Extracellular Vesicles Derived From Stem Cells in Intervertebral Disc Degeneration. *Front Cell Dev Biol* 2021; **9**: 793363 [PMID: 35096823 DOI: 10.3389/fcell.2021.793363]

37 **Suzuki H**, Ura K, Ukeba D, Suyama T, Iwasaki N, Watanabe M, Matsuzaki Y, Yamada K, Sudo H. Injection of Ultra-Purified Stem Cells with Sodium Alginate Reduces Discogenic Pain in a Rat Model. *Cells* 2023; **12** [PMID: 36766847 DOI: 10.3390/cells12030505]

38 **Bello AB**, Kim Y, Park S, Muttigi MS, Kim J, Park H, Lee S. Matrilin3/TGFβ3 gelatin microparticles promote chondrogenesis, prevent hypertrophy, and induce paracrine release in MSCs spheroid for disc regeneration. *NPJ Regen Med* 2021; **6**: 50 [PMID: 34480032 DOI: 10.1038/s41536-021-00160-0]

39 **Wang Y**, Zhang Y, Chen K, Shao F, Wu Y, Guo C, Wu H, Zhang D, Li W, Kong Q, Wang H. Injectable nanostructured colloidal gels resembling native nucleus pulposus as carriers of mesenchymal stem cells for the repair of degenerated intervertebral discs. *Mater Sci Eng C Mater Biol Appl* 2021; **128**: 112343 [PMID: 34474893 DOI: 10.1016/j.msec.2021.112343]

40 **Xu B**, Zhang H, Du L, Yuan Q, Zhang K, Xu H, Ma X, Liu Y, Jiang H, Li N. Selective Retention of Bone Marrow Stromal Cells with Gelatin Sponge for Repair of Intervertebral Disc Defects after Microendoscopic Discectomy: A Prospective Controlled Study and 2-Year Follow-Up. *Biomed Res Int* 2021; **2021**: 4822383 [PMID: 34337012 DOI: 10.1155/2021/4822383]

41 **Yu C**, Li D, Wang C, Xia K, Wang J, Zhou X, Ying L, Shu J, Huang X, Xu H, Han B, Chen Q, Li F, Tang J, Liang C, Slater N. Injectable kartogenin and apocynin loaded micelle enhances the alleviation of intervertebral disc degeneration by adipose-derived stem cell. *Bioact Mater* 2021; **6**: 3568-3579 [PMID: 33842742 DOI: 10.1016/j.bioactmat.2021.03.018]

42 **Huang D**, Li Y, Ma Z, Lin H, Zhu X, Xiao Y, Zhang X. Collagen hydrogel viscoelasticity regulates MSCs chondrogenesis in a ROCK-dependent manner. *Sci Adv* 2023; **9**: eade9497 [PMID: 36763657 DOI: 10.1126/sciadv.ade9497]

43 **Binch ALA**, Ratcliffe LPD, Milani AH, Saunders BR, Armes SP, Hoyland JA. Site-Directed Differentiation of Human Adipose-Derived Mesenchymal Stem Cells to Nucleus Pulposus Cells Using an Injectable Hydroxyl-Functional Diblock Copolymer Worm Gel. *Biomacromolecules* 2021; **22**: 837-845 [PMID: 33470795 DOI: 10.1021/acs.biomac.0c01556]

44 **Xiao L**, Xu SJ, Liu C, Wang J, Hu B, Xu HG. Sod2 and catalase improve pathological conditions of intervertebral disc degeneration by modifying human adipose-derived mesenchymal stem cells. *Life Sci* 2021; **267**: 118929 [PMID: 33359244 DOI: 10.1016/j.lfs.2020.118929]

45 **Sun B**, Lian M, Han Y, Mo X, Jiang W, Qiao Z, Dai K. A 3D-Bioprinted dual growth factor-releasing intervertebral disc scaffold induces nucleus pulposus and annulus fibrosus reconstruction. *Bioact Mater* 2021; **6**: 179-190 [PMID: 32913927 DOI: 10.1016/j.bioactmat.2020.06.022]

46 **Deng R**, Kang R, Jin X, Wang Z, Liu X, Wang Q, Xie L. Mechanical stimulation promotes MSCs healing the lesion of intervertebral disc annulus fibrosus. *Front Bioeng Biotechnol* 2023; **11**: 1137199 [PMID: 36845186 DOI: 10.3389/fbioe.2023.1137199]

47 **Huang X**, Chen D, Liang C, Shi K, Zhou X, Zhang Y, Li Y, Chen J, Xia K, Shu J, Yang B, Wang J, Xu H, Yu C, Cheng F, Wang S, Wang C, Ying L, Li H, Han M, Li F, Tao Y, Zhao Q, Chen Q. Swelling-Mediated Mechanical Stimulation Regulates Differentiation of Adipose-Derived Mesenchymal Stem Cells for Intervertebral Disc Repair Using Injectable UCST Microgels. *Adv Healthc Mater* 2023; **12**: e2201925 [PMID: 36250343 DOI: 10.1002/adhm.202201925]

48 **Peng Y**, Qing X, Lin H, Huang D, Li J, Tian S, Liu S, Lv X, Ma K, Li R, Rao Z, Bai Y, Chen S, Lei M, Quan D, Shao Z. Decellularized Disc Hydrogels for hBMSCs tissue-specific differentiation and tissue regeneration. *Bioact Mater* 2021; **6**: 3541-3556 [PMID: 33842740 DOI: 10.1016/j.bioactmat.2021.03.014]

49 **Yang X**, Chen Z, Chen C, Han C, Zhou Y, Li X, Tian H, Cheng X, Zhang K, Qin A, Zhou T, Zhao J. Bleomycin induces fibrotic transformation of bone marrow stromal cells to treat height loss of intervertebral disc through the TGFβR1/Smad2/3 pathway. *Stem Cell Res Ther* 2021; **12**: 34 [PMID: 33413668 DOI: 10.1186/s13287-020-02093-9]

50 **Xin J**, Wang Y, Zheng Z, Wang S, Na S, Zhang S. Treatment of Intervertebral Disc Degeneration. *Orthop Surg* 2022; **14**: 1271-1280 [PMID: 35486489 DOI: 10.1111/os.13254]

51 **Ran R**, Wu Y, Zhang HH. Acid-sensing Ion Channels: Implications for Intervertebral Disc Degeneration. *Curr Pharm Biotechnol* 2023; **24**: 1343-1350 [PMID: 36503387 DOI: 10.2174/1389201024666221209163234]

52 **Han L**, Wang Z, Chen H, Li J, Zhang S, Shao S, Zhang Y, Shen C, Tao H. Sa12b-Modified Functional Self-Assembling Peptide Hydrogel Enhances the Biological Activity of Nucleus Pulposus Mesenchymal Stem Cells by Inhibiting Acid-Sensing Ion Channels. *Front Cell Dev Biol* 2022; **10**: 822501 [PMID: 35252187 DOI: 10.3389/fcell.2022.822501]

53 **Ding J**, Zhang R, Li H, Ji Q, Cheng X, Thorne RF, Hondermarck H, Liu X, Shen C. ASIC1 and ASIC3 mediate cellular senescence of human nucleus pulposus mesenchymal stem cells during intervertebral disc degeneration. *Aging (Albany NY)* 2021; **13**: 10703-10723 [PMID: 33824228 DOI: 10.18632/aging.202850]

54 **Cai F**, Hong X, Tang X, Liu NC, Wang F, Zhu L, Xie XH, Xie ZY, Wu XT. ASIC1a activation induces calcium-dependent apoptosis of BMSCs under conditions that mimic the acidic microenvironment of the degenerated intervertebral disc. *Biosci Rep* 2019; **39** [PMID: 31696219 DOI: 10.1042/BSR20192708]

55 **Wang JW**, Zhu L, Shi PZ, Wang PC, Dai Y, Wang YX, Lu XH, Cheng XF, Feng XM, Zhang L. 1,25(OH)(2)D(3) Mitigates Oxidative Stress-Induced Damage to Nucleus Pulposus-Derived Mesenchymal Stem Cells through PI3K/Akt Pathway. *Oxid Med Cell Longev* 2022; **2022**: 1427110 [PMID: 35340208 DOI: 10.1155/2022/1427110]

56 **Liu Y**, Gao GM, Yang KY, Nong LM. Construction of tissue-engineered nucleus pulposus by stimulation with periodic mechanical stress and BMP-2. *iScience* 2022; **25**: 104405 [PMID: 35633940 DOI: 10.1016/j.isci.2022.104405]

57 **Zhang C**, Gullbrand SE, Schaer TP, Boorman S, Elliott DM, Chen W, Dodge GR, Mauck RL, Malhotra NR, Smith LJ. Combined Hydrogel and Mesenchymal Stem Cell Therapy for Moderate-Severity Disc Degeneration in Goats. *Tissue Eng Part A* 2021; **27**: 117-128 [PMID: 32546053 DOI: 10.1089/ten.TEA.2020.0103]

58 **Yu L**, Liu Y, Wu J, Wang S, Yu J, Wang W, Ye X. Genipin Cross-Linked Decellularized Nucleus Pulposus Hydrogel-Like Cell Delivery System Induces Differentiation of ADSCs and Retards Intervertebral Disc Degeneration. *Front Bioeng Biotechnol* 2021; **9**: 807883 [PMID: 35004657 DOI: 10.3389/fbioe.2021.807883]

59 **Zhu Z**, Xing H, Tang R, Qian S, He S, Hu Q, Zhang N. The preconditioning of lithium promotes mesenchymal stem cell-based therapy for the degenerated intervertebral disc *via* upregulating cellular ROS. *Stem Cell Res Ther* 2021; **12**: 239 [PMID: 33853670 DOI: 10.1186/s13287-021-02306-9]

60 **Sun J**, Yang F, Wang L, Yu H, Yang Z, Wei J, Vasilev K, Zhang X, Liu X, Zhao Y. Delivery of coenzyme Q10 loaded micelle targets mitochondrial ROS and enhances efficiency of mesenchymal stem cell therapy in intervertebral disc degeneration. *Bioact Mater* 2023; **23**: 247-260 [PMID: 36439087 DOI: 10.1016/j.bioactmat.2022.10.019]

61 **Tong B**, Liao Z, Liu H, Ke W, Lei C, Zhang W, Liang H, Wang H, He Y, Lei J, Yang K, Zhang X, Li G, Ma L, Song Y, Hua W, Feng X, Wang K, Wu X, Tan L, Gao Y, Yang C. Augmenting Intracellular Cargo Delivery of Extracellular Vesicles in Hypoxic Tissues through Inhibiting Hypoxia-Induced Endocytic Recycling. *ACS Nano* 2023; **17**: 2537-2553 [PMID: 36730125 DOI: 10.1021/acsnano.2c10351]

62 **Li X**, Fu X, Li H, Gao Y, Wang W, Liu Z, Shen Y. Leptin accelerates BMSCs transformation into vertebral epiphyseal plate chondrocytes by activating SENP1-mediated deSUMOylation of SIRT3. *FEBS Open Bio* 2023; **13**: 293-306 [PMID: 36537765 DOI: 10.1002/2211-5463.13539]

63 **Zhang W**, Sun T, Li Y, Yang M, Zhao Y, Liu J, Li Z. Application of stem cells in the repair of intervertebral disc degeneration. *Stem Cell Res Ther* 2022; **13**: 70 [PMID: 35148808 DOI: 10.1186/s13287-022-02745-y]

64 **Jia Z**, Liu D, Xu J, Wang Q, Zhang L, Yin S, Qian B, Li X, Wu Y, Zhang Y, Li W, Wen T. An international analysis of stem cell research in intervertebral disc degeneration. *Stem Cell Res* 2023; **67**: 103044 [PMID: 36796251 DOI: 10.1016/j.scr.2023.103044]

65 **Widjaja G**, Jalil AT, Budi HS, Abdelbasset WK, Efendi S, Suksatan W, Rita RS, Satria AP, Aravindhan S, Saleh MM, Shalaby MN, Yumashev AV. Mesenchymal stromal/stem cells and their exosomes application in the treatment of intervertebral disc disease: A promising frontier. *Int Immunopharmacol* 2022; **105**: 108537 [PMID: 35101851 DOI: 10.1016/j.intimp.2022.108537]

66 **Rascón-Ramírez FJ**, Esteban-García N, Barcia JA, Trondin A, Nombela C, Sánchez-Sánchez-Rojas L. Are We Ready for Cell Therapy to Treat Stroke? *Front Cell Dev Biol* 2021; **9**: 621645 [PMID: 34249901 DOI: 10.3389/fcell.2021.621645]

67 **Ullah I**, Subbarao RB, Rho GJ. Human mesenchymal stem cells - current trends and future prospective. *Biosci Rep* 2015; **35** [PMID: 25797907 DOI: 10.1042/BSR20150025]

68 **Xia Y**, Yang R, Hou Y, Wang H, Li Y, Zhu J, Fu C. Application of mesenchymal stem cell-derived exosomes from different sources in intervertebral disc degeneration. *Front Bioeng Biotechnol* 2022; **10**: 1019437 [PMID: 36277386 DOI: 10.3389/fbioe.2022.1019437]

69 **Wu PH**, Kim HS, Jang IT. Intervertebral Disc Diseases PART 2: A Review of the Current Diagnostic and Treatment Strategies for Intervertebral Disc Disease. *Int J Mol Sci* 2020; **21** [PMID: 32244936 DOI: 10.3390/ijms21062135]

70 **Watanabe T**, Sakai D, Yamamoto Y, Iwashina T, Serigano K, Tamura F, Mochida J. Human nucleus pulposus cells significantly enhanced biological properties in a coculture system with direct cell-to-cell contact with autologous mesenchymal stem cells. *J Orthop Res* 2010; **28**: 623-630 [PMID: 19953600 DOI: 10.1002/jor.21036]

World Journal of Stem Cells

Submit a Manuscript: https://www.f6publishing.com

World J Stem Cells 2023 November 26; 15(11): 999-1016

DOI: 10.4252/wjsc.v15.i11.999

ISSN 1948-0210 (online)

ORIGINAL ARTICLE

Basic Study

Hypoxia and inflammatory factor preconditioning enhances the immunosuppressive properties of human umbilical cord mesenchymal stem cells

Hang Li, Xiao-Qing Ji, Shu-Ming Zhang, Ri-Hui Bi

Specialty type: Cell and tissue engineering

Provenance and peer review: Unsolicited article; Externally peer reviewed.

Peer-review model: Single blind

Peer-review report's scientific quality classification

Grade A (Excellent): A
Grade B (Very good): B
Grade C (Good): C
Grade D (Fair): 0
Grade E (Poor): 0

P-Reviewer: Al-Hashmi S, Oman; Li SC, United States

Received: August 15, 2023
Peer-review started: August 15, 2023
First decision: September 5, 2023
Revised: September 28, 2023
Accepted: October 30, 2023
Article in press: October 30, 2023
Published online: November 26, 2023

Hang Li, Department of Histology and Embryology, Shanxi Medical University, Taiyuan 030001, Shanxi Province, China

Xiao-Qing Ji, Shu-Ming Zhang, School of Pharmaceutical Science, Shanxi Medical University, Taiyuan 030001, Shanxi Province, China

Ri-Hui Bi, Department of Hepatobiliary Surgery, Shanxi Bethune Hospital, Shanxi Academy of Medical Sciences, Tongji Hospital Affiliated to Shanxi Medical University, The Third Hospital of Shanxi Medical University, Taiyuan 030002, Shanxi Province, China

Corresponding author: Ri-Hui Bi, MD, Surgeon, Department of Hepatobiliary Surgery, Shanxi Bethune Hospital, Shanxi Academy of Medical Sciences, Tongji Hospital Affiliated to Shanxi Medical University, The Third Hospital of Shanxi Medical University, No. 99 Longcheng, Xiaodian District, Taiyuan 030002, Shanxi Province, China. birihui@sxmu.edu.cn

Abstract

BACKGROUND

Mesenchymal stem cells (MSCs) have great potential for the treatment of various immune diseases due to their unique immunomodulatory properties. However, MSCs exposed to the harsh inflammatory environment of damaged tissue after intravenous transplantation cannot exert their biological effects, and therefore, their therapeutic efficacy is reduced. In this challenging context, an *in vitro* preconditioning method is necessary for the development of MSC-based therapies with increased immunomodulatory capacity and transplantation efficacy.

AIM

To determine whether hypoxia and inflammatory factor preconditioning increases the immunosuppressive properties of MSCs without affecting their biological characteristics.

METHODS

Umbilical cord MSCs (UC-MSCs) were pretreated with hypoxia (2% O_2) exposure and inflammatory factors (interleukin-1β, tumor necrosis factor-α, interferon-γ) for 24 h. Flow cytometry, polymerase chain reaction, enzyme-linked immunosorbent assay and other experimental methods were used to evaluate the biological characteristics of pretreated UC-MSCs and to determine whether pretreatment

affected the immunosuppressive ability of UC-MSCs in coculture with immune cells.

RESULTS

Pretreatment with hypoxia and inflammatory factors caused UC-MSCs to be elongated but did not affect their viability, proliferation or size. In addition, pretreatment significantly decreased the expression of coagulation-related tissue factors but did not affect the expression of other surface markers. Similarly, mitochondrial function and integrity were retained. Although pretreatment promoted UC-MSC apoptosis and senescence, it increased the expression of genes and proteins related to immune regulation. Pretreatment increased peripheral blood mononuclear cell and natural killer (NK) cell proliferation rates and inhibited NK cell-induced toxicity to varying degrees.

CONCLUSION

In summary, hypoxia and inflammatory factor preconditioning led to higher immunosuppressive effects of MSCs without damaging their biological characteristics.

Key Words: Mesenchymal stem cells; Umbilical cord; Preconditioning; Hypoxia, Inflammatory factors; Immune regulation

Core Tip: Mesenchymal stem cells (MSCs) are potential candidates for treating many immune diseases due to their unique immunomodulatory abilities, but low survival rates and weakened function after venous transplantation reduces their treatment potential. Therefore, our study reveals a combination pretreatment method based on *in vitro* hypoxia exposure and inflammatory factor treatment that simulates the harsh *in vivo* environment to protect MSCs from injury after intravenous transfusion and promote high immunosuppressive effects of MSCs.

Citation: Li H, Ji XQ, Zhang SM, Bi RH. Hypoxia and inflammatory factor preconditioning enhances the immunosuppressive properties of human umbilical cord mesenchymal stem cells. *World J Stem Cells* 2023; 15(11): 999-1016
URL: https://www.wjgnet.com/1948-0210/full/v15/i11/999.htm
DOI: https://dx.doi.org/10.4252/wjsc.v15.i11.999

INTRODUCTION

In recent years, mesenchymal stem cells (MSCs) have been shown to have a variety of biological properties, such as self-renewal[1], multilineage differentiation[2,3], immunomodulation functions[4,5], tissue repair effects[6], anti-aging and regeneration activity[7]. Furthermore, due to the abundance and ready availability of MSCs[8], they do not lead to rejection after allografting[9]; thus, MSCs have great economic value, importance in the cell therapy field and broad application prospects. Although many questions remain unanswered, the immunomodulatory effects of MSCs make them candidates for cell-based tissue repair and disease treatment[10-12]. For example, MSCs have great potential in treating graft-*versus*-host disease[13], cardiovascular disease[14,15], liver disease[16,17], systemic lupus erythematosus [18], autoimmune encephalomyelitis[19] and spinal cord injury[20]. Studies have shown that the immunomodulatory ability of MSCs is primarily regulated by cytokines and other soluble factors, including prostaglandin E2 (PGE2), tumor necrosis factor (TNF)-α-stimulated gene protein-6 (TSG-6), inducible indoleamine 2,3-dioxygenase (IDO), interleukin-10 (IL-10) and transforming growth factor-β1 (TGF-β1)[21]. They contribute to MSC-mediated immunosuppression by inhibiting natural killer (NK) cell proliferation, cytotoxicity and cytokine secretion[22], inhibiting T-cell proliferation, promoting regulatory T cell production[5,23,24], and inhibiting B-cell proliferation and immunoglobulin release[25,26].

It has been shown that when MSCs are injected into the body and migrate to damaged tissues or organs, the activation of innate immune cells leads to increased chemokine and cytokine release (such as TNF-α, IL-1α and IL-1β)[27] and is accompanied by the development of a harsh environment caused by hypoxic stress[28], leading to decreased MSC activity. Therefore, *in vitro* preconditioning culture developed through hypoxia exposure and inflammatory factor supplementation can effectively mimic the *in vivo* microenvironment. Preconditioning MSCs *in vitro* activates various signaling pathways, influencing the biological activities of MSCs *in vitro* and *in vivo*, thereby preparing them to survive the harsh environment to which they are subjected during *in vivo* administration and protecting them from damage[29, 30]. In addition, preconditioning can induce MSCs to secrete immunosuppressive molecules to target innate and adaptive immune cells, thereby mediating immune regulation by releasing water-soluble factors[31,32]. Therefore, pretreatment is an adaptive strategy to enhance the efficacy of MSC therapy, which can not only prolong MSC survival and function after transplantation but also endows them with higher immunomodulatory activity levels. Studies have shown that preconditioning with inflammatory factors such as TNF-α and interferon (IFN)-γ can increase MSC immunoregulatory ability[33, 34]. Hypoxia preconditioning is often used to enhance the therapeutic effect of MSCs by inducing the expression of survival genes, chemokines, growth factors, and angiogenic factors (such as vascular endothelial growth factor), enabling the MSCs to adapt to the harsh environment of damaged tissue[35,36].

Although different preconditioning methods can enhance cell properties and increase their function, many are accompanied by safety concerns. In contrast to the aforementioned positive outcomes of pretreatment, improper pretreatment can negatively impact cell morphology and function, damage mitochondrial function[37], and affect MSC surface marker expression. For example, previous studies have shown that tissue factor (TF/CD142) binds to coagulation factor VII/VIIB to initiate the exogenous coagulation system. The relative cell surface expression of TF is strongly correlated with procoagulant activity[38]. MSCs expressing surface TF show high coagulant activity and promote blood and plasma coagulation[39]. Therefore, high TF expression on MSCs increases the risk of thrombosis after intravenous injection[40-43].

We found that most studies have been focused on bone marrow- or adipose-derived MSCs (AD-MSCs), but human umbilical cord-derived MSCs (hUC-MSCs) are more suitable for clinical research and large-scale use because they are not associated with ethical problems, are abundant and highly proliferative. Therefore, we chose hUC-MSCs to study. To our knowledge, studies using a combination of hypoxia (2% O_2) exposure and inflammatory factor (IL-1β, TNF-α, IFN-γ) treatment to precondition hUC-MSCs are rare, and our study supports the current theory. Our aim was to simulate the injury-induced environment *in vitro* using a combination of hypoxia and inflammatory factor preconditioning to determine whether preconditioning increases the immunosuppressive properties of MSCs without affecting their biological characteristics.

MATERIALS AND METHODS

UC-MSC extraction and culture

Umbilical cord and cord blood were obtained with the approval of the Medical Ethics Committee of Shanxi Medical University and the consent of the donors, and experiments were performed in accordance with the Declaration of Helsinki.

Umbilical cord tissue was provided by one hospital, and the donors gave informed consent. After obtaining the umbilical cords, two veins and one artery were removed, and Wharton's jelly was cut into pieces and placed into a 10 cm^2 petri dish (Nice) with 5 mL of DMEM/F12 culture medium (Thermo Fisher Scientific, Waltham, MA, United States) containing 2.5% serum substitute (Shanxi Yinshi Cell Technology, Xian, China). Approximately 14 d later, the UC-MSCs were passaged, and P4 generation cells were used for experiments. UC-MSCs were cultured in a carbon dioxide incubator (Thermo Fisher Scientific) at standard oxygen tension with 5% carbon dioxide, 95% air, and 37 °C (*i.e.* normoxia). When UC-MSCs were 70%-80% confluent, a mixture of IFN-γ (R&D), TNF-α (R&D Systems, Minneapolis, MN, United States) and IL-1β (PeproTech, Cranbury, NJ, United States) was added to the medium. The cells were then immediately placed into a three-gas incubator (Panasonic, Osaka, Japan) with 2% O_2, 5% CO_2, and 93% N_2 at 37 °C (*i.e.* hypoxia). After 24 h, primed UC-MSCs (PUC-MSCs) were obtained. Therefore, our experiments were divided into two groups: Control (UC-MSCs) with no treatment and an experimental group (PUC-MSCs) in which cells were exposed to hypoxia and inflammatory factor supplementation.

Extraction and culture of peripheral blood mononuclear cells

Umbilical cord blood was obtained and centrifuged at 700 × *g* for 10 min and the plasma was extracted and placed into a water bath at 56 °C for 30 min for heat inactivation. The plasma was removed from the water bath, centrifuged at 850 × *g* for 10 min, and placed in a refrigerator at 4 °C for later use. The blood cells were resuspended in phosphate buffered saline (PBS) and mixed. The cell suspension was slowly added into a centrifuge tube containing Ficoll human peripheral blood lymphocyte isolation medium (Tianjin Haoyang Biological Products Technology Co., Ltd., Tianjin, China). After centrifugation at 400 × *g* for 30 min, white cells were extracted and washed twice with PBS. The cells [(1-2) × 10^6 cells/mL] were inoculated in peripheral blood mononuclear cell (PBMC) medium containing 10% of the heat-inactivated autologous plasma (Shanxi Yin Cell Technology Co., Ltd., Hebei, China) in the presence or absence of UC-MSCs or PUC-MSCs. The PBMCs were treated with 100 U/mL IL-2 (PeproTech). For coculture experiments, PBMCs were inoculated with UC-MSCs or PUC-MSCs at a PBMC/MSC ratio of 3:1 so that the cells were in direct contact, which is the appropriate proportion of cells to obtain MSC-mediated inhibition of PBMC proliferation.

NK cell extraction and culture

Umbilical cord blood was obtained and centrifuged at 700 × *g* for 10 min, and the plasma was placed into a water bath at 56 °C for 30 min for heat inactivation. The plasma was removed, centrifuged at 850 × *g* for 10 min, and placed into a refrigerator at 4 °C for later use. The blood cells were resuspended in PBS, mixed, and incubated at room temperature for 20 min with RosetteSepT NK Enrichment Cocktail. The cell suspension was slowly added into a centrifuge tube containing Ficoll human peripheral blood lymphocyte isolation medium (Tianjin Haoyang Biological Products Technology Co., Ltd.). After centrifugation at 400 × *g* for 30 min, white cells were extracted and washed twice with PBS. The cells [(1-2) × 10^6 cells/mL] were inoculated into NK medium containing 10% heat-inactivated autologous plasma (Shanxi Yin Cell Technology Co., Ltd.). NK cells were cultured with or without UC-MSCs or PUC-MSCs and treated with 100 U/mL IL-2 (PeproTech).

Cell survival rate and cell size detection

Double fluorescence acridine orange/propidium iodide (AO/PI) cell viability counting was performed. The AO/PI reagent consists of the DNA-binding dye AO, which fluoresces green, and the DNA-binding dye PI, which fluoresces red.

AO can pass through a complete cell membrane and enter the nuclei of all cells (living and dead cells), emitting green fluorescence. PI can only pass through an incomplete cell membrane and enter the nuclei of dead cells, resulting in red fluorescence. After mixing 10 μL of cell suspension with 10 μL of AOPI reagent, the viability and size of the cells in suspension were measured by a Countstar Rigel S2 (Shanghai Rui Yu Biotech, Shanghai, China).

Monoclonal antibodies and cytofluorometric analysis

Flow cytometry analysis of UC-MSCs and PUC-MSCs was performed. The cells were resuspended in staining buffer after centrifugation, and the corresponding antibodies were added to the buffer. Cells were incubated for 30 min, neutralized and washed 1-2 times. The UC-MSC or PUC-MSC antigen markers (BD Biosciences, San Jose, CA, United States) were CD105-APC, CD90-FITC, CD73-PE, CD142-PC5.5, CD29-PE, CD34-PE, CD14-PE, CD45-APC, human leukocyte antigen (HLA)-ABC-APC, CD47-APC, CD166-PE, CD44-PE, and CD31-APC.

Reactive oxygen species measurement

Mitochondrial reactive oxygen species (ROS) production was measured by flow cytometry (Beckman Coulter Life Sciences, Brea, CA, United States) using a ROS detection kit (Biyuntian, Shanghai, China). 2,7-dichlorodihydrofluorescein diacetate (DCFH-DA) was diluted in serum-free medium at 1:1000 to a final concentration of 10 μmol/L. After collection, 1 million to 20 million/mL cells were suspended in diluted DCFH-DA and incubated in an infrared carbon dioxide incubator (Thermo Fisher Scientific) at 37 °C for 20 min. The cells were turned over and mixed every 3-5 min to ensure that the probe was in full contact with the cells. The cells were washed with serum-free cell culture solution three times to fully remove excess DCFH-DA. Finally, the results were detected by flow cytometry.

Measurement of mitochondrial membrane potential

Mitochondrial membrane potential (MMP) was detected using MMP detection reagent JC-1 (Beyotime, Jiangsu, China). The culture medium was removed and the cells were washed twice with PBS. JC-1 staining solution (1 mL) was added, mixed thoroughly, and incubated with cells in an infrared carbon dioxide incubator (Thermo Fisher Scientific) at 37 °C for 20 min. During the incubation period, JC-1 staining buffer (1×) was prepared by adding approximately 4 mL distilled water to approximately 1 mL JC-1 staining buffer (5×), and the buffer was placed in an ice bath. After incubation at 37 °C, the supernatant was removed, and the cells were washed twice with JC-1 staining buffer (1×). Finally, 2 mL of the cell culture solution was added. Images were obtained with an inverted fluorescence microscope (CKX53; Olympus, Tokyo, Japan).

Real time-polymerase chain reaction

TRIzol (Invitrogen, Waltham, MA, United States) was used to lyse the cells, total RNA was extracted, and an ultratrace nucleic acid protein detector (Shanghai Jiapeng Materials, Shanghai, China) was used to determine RNA concentration. mRNA expression levels were quantitatively analyzed on a real-time polymerase chain reaction (RT-PCR) instrument (Bio-Rad, Hercules, CA, United States) using a One Step TB Green PrimeScript PLUS RT□PCR Kit (Takara Bio Inc., Shiga, Japan) to measure the levels of the following transcripts: Catalase, Istanniocalcin-1 (STC1), hemeoxygenase-1 (HOMX1), B-cell lymphoma 2-associated protein (Bax), B-cell lymphoma 2 (Bcl2), silencing information regulator 2-related enzyme 1 (SIRT1), P53, P16, P21, PGE2, kynurenine (KYN), IDO, IL-1 receptor antagonist (IL-1ra), cyclooxygenaese-2 (COX2), IL-10, TGF-β1, HLA-G5, TSG-6, ligands for programmed cell death 1 (PD-L1). All primer sequences for qRT-PCR are listed in Table 1.

Enzyme-linked immunosorbent assays

UC-MSCs and PUC-MSCs supernatants were collected and centrifuged at 210 × *g* for 5 min, and the suspended cells were removed and stored at -80 °C. The protein levels of PGE2, TSG-6, IDO, IL-10 and TGF-β1 secreted by UC-MSCs and PUC-MSCs were measured by enzyme-linked immunosorbent assay (ELISA) kits (Wuhan Eliret Biotechnology Co, Ltd., Wuhan, China). Finally, the optical density (OD) value of each well was measured on the basis of enzyme label (Thermo Fisher Scientific) absorption at 450 nm.

Annexin V-FITC apoptosis detection

UC-MSC and PUC-MSC suspensions were obtained and washed twice with PBS. Annexin V-FITC apoptosis reagent (Biyuntian) was added and incubated with the cells at room temperature for 10-20 min in the dark, and flow cytometry was performed. Annexin V-FITC emits green fluorescence, and PI emits red fluorescence.

β-galactosidase (SA-β-gal) activity detection

The cell culture medium was removed, the cells were washed once with PBS, and 1 mL/well β-galactosidase (SA-β-gal) staining fixation solution (Solarbio, Beijing, China) was added and incubated at room temperature for 15 min. Fixative was removed, and the cells were washed 3 times with PBS for 3 min each. The PBS was removed, and 1 mL of staining solution was added to each well. The plate was incubated at 37°C overnight and sealed with plastic wrap to prevent evaporation. The positive expression of blue particles was observed under an inverted microscope (CKX53; Olympus), and the number of positive cells per 100 cells was quantified. Each experiment was repeated three times.

Proliferation experiment

NK cells were cultured in the presence or absence of UC-MSCs or PUC-MSCs for 3 d at a 3:1 ratio. The cells were prelabelled with carboxyfluorescein diacetate succinimidyl ester (CFSE) dye (BioLegend, San Diego, CA, United States)

Table 1 Primer used to amplify the human transcripts during real-time quantitative polymerase chain reaction

Gene	Sequence, 5' to 3'	Application
Catalae (human)	Upper: TTCTGTTGAAGATGCGGCGAGAC	qRT-PCR
	Lower: GGGGTACTTTCCTGTGGCAATGG	
STC-1 (human)	Upper: CCATGAGGCGGAGCAGAATGAC	qRT-PCR
	Lower: GCCGACCTGTAGAGCACTGTTG	
HMOX1 (human)	Upper: TGCCAGTGCCACCAAGTTCAAG	qRT-PCR
	Lower: TGTTGAGCAGGAACGCAGTCTTG	
Bax (human)	Upper: ACCAAGAAGCTGAGCGAGTGTC	qRT-PCR
	Lower: TGTCCACGGCGGCAATCATC	
Bcl2 (human)	Upper: TGAGTTCGGTGGGGTCATGT	qRT-PCR
	Lower: TTCCACAAAGGCATCCCAGC	
SIRT1 (human)	Upper: CCTGGACAATTCCAGCCATCT	qRT-PCR
	Lower: TGCAAAGGAACCATGACACTGA	
P53 (human)	Upper: GCCCATCCTCACCATCATCACAC	qRT-PCR
	Lower: GCACAAACACGCACCTCAAAGC	
P16 (human)	Upper: CCGTGGACCTGGCTGAGGAG	qRT-PCR
	Lower: CGGGGATGTCTGAGGGACCTTC	
P21 (human)	Upper: CTTGTACCCTTGTGCCTCGC	qRT-PCR
	Lower: AGAAGATCAGCCGGCGTTTG	
β-actin (human)	Upper: AGTGTGACGTGGACATCCGCA	qRT-PCR
	Lower: ATCCACATCTGCTGGAAGGTGGAC	
PGE2 (human)	Upper: ATTCTCCTGGCTATCATGAC	qRT-PCR
	Lower: GAACAGGAGGCCTAAGGATG	
IDO (human)	Upper: CTCTGCCAAATCCACAGGAAA	qRT-PCR
	Lower: ATGACCTTTGCCCCACACAT	
KYN (human)	Upper: CAAGCGAAGGGTTGTTATGTTGGC	qRT-PCR
	Lower: GGAACACCAGCAGGCAAAATCAAC	
COX2 (human)	Upper: AATCTGGCTGCGGGAACACAAC	qRT-PCR
	Lower: TGTCTGGAACAACTGCTCATCACC	
IL-1ra (human)	Upper: GTGCCTGTCCTGTGTCAAGTCTG	qRT-PCR
	Lower: GCCACTGTCTGAGCGGATGAAG	
IL-10 (human)	Upper: GCCAAGCCTTGTCTGAGATGATCC	qRT-PCR
	Lower: GCCTTGATGTCTGGGTCTTGGTTC	
TGF-β1 (human)	Upper: AGCAACAATTCCTGGCGATACCTC	qRT-PCR
	Lower: TCAACCACTGCCGCACAACTC	
HLA-G5 (human)	Upper: AGAGGAGACACGGAACACCAAGG	qRT-PCR
	Lower: CAGGTCGCAGCCAATCATCCAC	
TSG-6 (human)	Upper: AGAGAAGCACGGTCTGGCAAATAC	qRT-PCR
	Lower: GCCATCCATCCAGCAGCACAG	
PD-L1 (human)	Upper: TGACCTACTGGCATTTGCTGAACG	qRT-PCR
	Lower: CACTGCTTGTCCAGATGACTTCGG	

Bax: B-cell lymphoma 2-associated protein; Bcl2: B-cell lymphoma 2; COX2: Cyclooxygenaese-2; HLA-G5: Human leukocyte antigen-G5; HOMX1: Hemeoxygenase-1; IDO: Idoleamine-2,3-dioxygenase; IL-1ra: Interleukin-1 receptor antagonist; IL-10: Interleukin-10; KYN: Kynurenine; PD-L1: Ligands for programmed cell death 1; PGE2: Prostaglandin E2; qRT-PCR: Quantitative real-time polymerase chain reaction; SIRT1: Silencing information regulator 2-related enzyme 1; STC1: Stanniocalcin-1; TGF-β1: Transforming growth factor-beta 1; TSG-6: Tumor necrosis factor-α-induced protein-6.

and the fluorescence intensity of CFSE was measured by flow cytometry.

Cell growth and proliferation

UC-MSCs and PUC-MSCs were collected for DNA extraction and DNA concentration was determined by an ultramicro nucleic acid protein detector (Shanghai Jiapeng Materials) to evaluate the cell proliferation rate. PBMCs were cultured in the presence or absence of UC-MSCs or PUC-MSCs at a ratio of 3:1. The number of cells (Countstar Rigel S2; Shanghai Rui Yu Biotech) was counted by a cell imaging analyzer for 5 consecutive days and the growth curve was plotted.

Cytotoxicity of K562 target cells

NK cells were cultured alone or in direct contact with MSCs (NK: UC-MSCs or PUC-MSCs = 3:1 ratio) for 72 h. NK cells were then collected and cocultured with CFSE-stained (Biolegend) K562 target cells for 4 h at the effective target ratio of 1:5. All cells were collected and washed twice with PBS. K562 cell apoptosis was analyzed by PI staining (Biyuntian), and the fluorescence intensity was measured by flow cytometry.

Statistical analysis

SPSS 19.0.0 and GraphPad Prism 7 (GraphPad Prism, La Jolla, CA, United States) statistical software were used for data processing. All experimental data are expressed as the mean ± SD. A *t* test was performed to compare two datasets, and $P < 0.05$ was considered statistically significant.

RESULTS

Effects of hypoxia and inflammatory factor pretreatment on UC-MSC morphology, size, proliferation and viability

We evaluated the effects of hypoxia and inflammatory factor pretreatment on UC-MSC morphology, vitality and size. The morphological differences between UC-MSCs and PUC-MSCs were compared under a microscope when cell confluency reached 80% to 90%. Untreated UC-MSCs appeared as either short rods or long spindles in an adherent state and were arranged in a spiral pattern. After 24 h of exposure to hypoxia and inflammatory factors, cell morphology changed from short and rod-like to thin and elongated (Figure 1A), but the proliferation rate did not change (Figure 1B). We further evaluated the effects of pretreatment on UC-MSC viability and size using AOPI staining and a cell imaging analyzer. UC-MSC viability (Figure 1C) in suspension was 93.59% ± 3.87% ($n = 5$) and the mean diameter (Figure 1D) was 18.216 ± 0.78 μm ($n = 5$), while PUC-MSC viability (Figure 1C) was 92.89% ± 4.13% ($n = 5$) and the mean diameter (Figure 1D) was 18.628 ± 0.76 μm ($n = 5$). These results showed that pretreated MSCs became elongated, the measured viability slightly decreased ($P = 0.84$), and the cells were slightly enlarged ($P = 0.47$), but these differences were not statistically significant.

MSC surface marker expression

We further evaluated whether preconditioning altered the cellular phenotype by analyzing MSC surface marker expression by flow cytometry. UC-MSCs (Figure 2A) and PUC-MSCs (Figure 2B) from three donors were positive for CD105, CD90, CD73, CD29, CD166, CD47 and HLA-ABC surface expression and negative for CD31, CD45, CD14 and CD34. The results showed that surface marker expression was consistent between PUC-MSCs and UC-MSCs. Interestingly, CD142 expression (59.3%) (Figure 2B) was significantly lower in PUC-MSCs compared to UC-MSCs (99.6%) (Figure 2A).

Effect of pretreatment on UC-MSC mitochondrial function

ROS play key roles in the proapoptotic signaling cascade, and excess ROS attacks the mitochondrial membrane and loss of MMP, leading to MSC apoptosis[44]. Therefore, we used flow cytometry to examine the effect of MSC pretreatment on ROS production. Intracellular ROS levels showed a three-fold increase in DCFH-DA fluorescence intensity in PUC-MSCs compared to untreated UC-MSCs (Figure 3A), but all the effects were within the range of values obtained in positive controls. STC1, catalase and HOMX1 expression levels increased (Figure 3B), indicating that the antioxidant capacity of the cells was increased and that mitochondrial ROS removal was increased, enhancing antioxidant defense effects and preventing ROS-induced DNA damage. Maintaining a stable MMP (Ψm) is essential to ensure efficient ROS clearance and prevent apoptosis or other stress-related events caused by excessive ROS[45]. Therefore, we further determined whether hypoxia and inflammatory factor preconditioning induced MMP dysfunction in UC-MSCs. We used the sensitive fluorescent probe JC-1 to evaluate the effect of pretreatment. We determined whether the membrane potential changed in UC-MSCs by measuring a change in JC-1 red fluorescence to green fluorescence. Microscopically, untreated UC-MSCs showed a normal MMP, as shown by red fluorescence staining with JC-1 (Figure 3C). Neither the red and green fluorescence nor the MMP was significantly different between PUC-MSCs and UC-MSCs. We further measured the

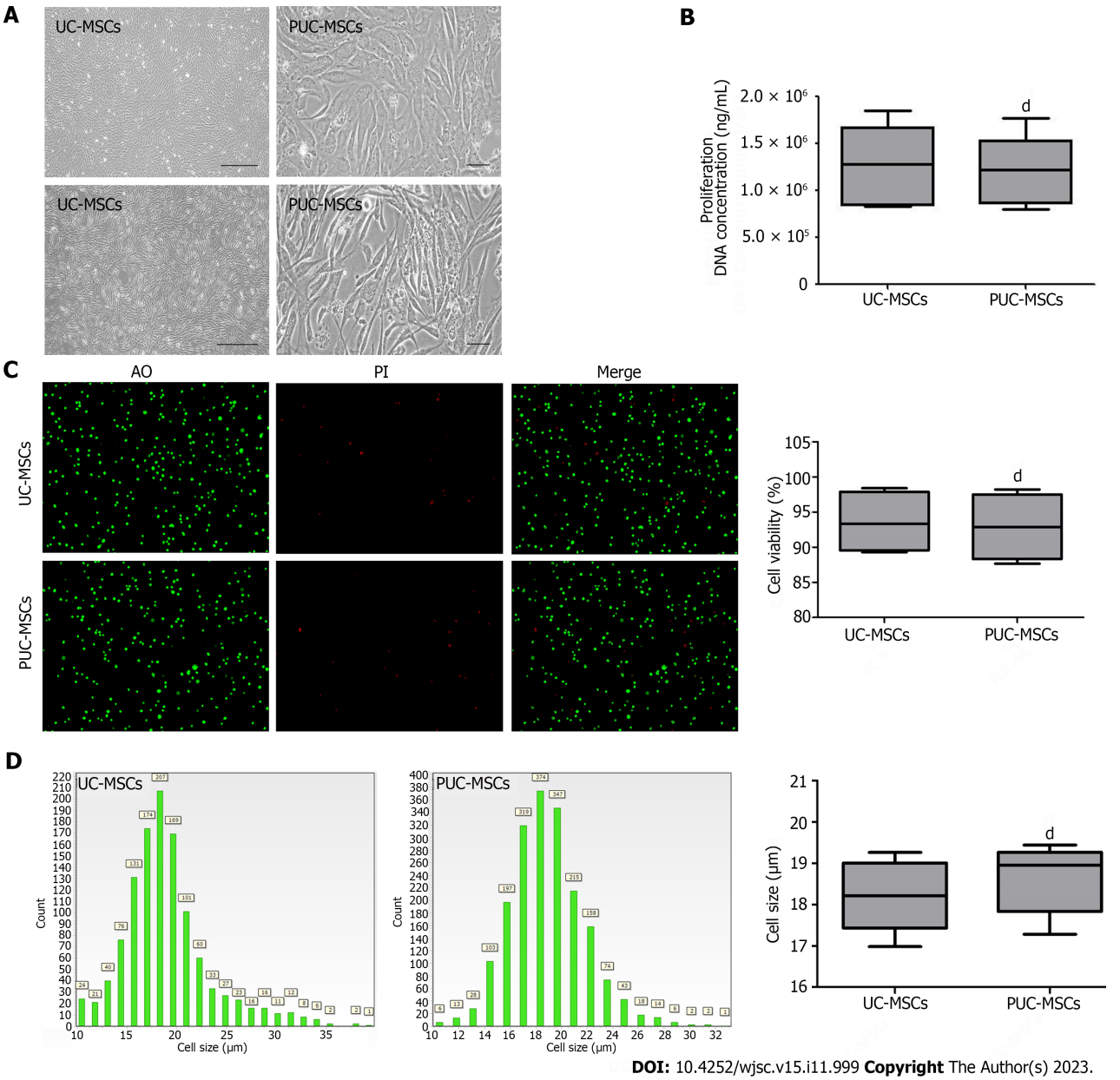

DOI: 10.4252/wjsc.v15.i11.999

Figure 1 Morphology, viability, proliferation, and size of mesenchymal stem cells. A: Representative micrographs showing umbilical cord mesenchymal stem cells (UC-MSCs) and primed umbilical cord mesenchymal stem cells (PUC-MSCs). Microscopy observation of cell morphology revealed that UC-MSCs were elongated after hypoxia and inflammatory factor pretreatment (Bar = 200 μm); B: The DNA concentration was measured by an ultramicro nucleic acid protein detector. The DNA concentration of PUC-MSCs was not significantly different from that of UC-MSCs, and pretreatment had no effect on their proliferation; C: Cell viability was determined by an acridine orange (AO) propidium iodide (PI) staining cell image analyzer, and no significant difference between UC-MSCs and PUC-MSCs was observed; D: Cell size was determined with a cell imaging analyzer, and the sizes of the UC-MSCs and PUC-MSCs were comparable. $^{d}P > 0.05$.

JC-1 red/green fluorescence ratio by flow cytometry and confirmed our microscopy results (Figure 3D). These results showed that mitochondrial function in UC-MSCs was not damaged by hypoxia and inflammatory factor pretreatment.

Hypoxia and inflammatory factor preconditioning induces UC-MSC apoptosis and senescence

Bax expression decreased and Bcl2 and SIRT1 expression increased after pretreatment, suggesting that the anti-apoptotic capacity increased after pretreatment (Figure 4A). The expression of the senescence-related genes P53, P16 and P21 was upregulated by pretreatment (Figure 4B). We analyzed apoptosis by Annexin V-PI staining and flow cytometry. We compared the proportion of cells that were positive for both Annexin V-FITC and PI (necrotic cells), and the apoptotic index of PUC-MSCs (15.08% ± 4.11%) significantly increased (Figure 4C) compared to UC-MSCs (6.22% ± 3.03%). Next, we investigated the effect of preconditioning on cell senescence. SA-β-gal has been the most widely accepted senescence marker since Dimri first published its use in 1995[46], so we performed SA-β-gal staining to evaluate cell senescence ratios. SA-β-gal levels increased in PUC-MSCs (14.83% ± 1.57%) compared to UC-MSCs (4.83% ± 1.34%) (Figure 4D). These results suggest that hypoxia and inflammatory factor preconditioning not only induces UC-MSC apoptosis and senescence but also increases anti-apoptotic factor levels.

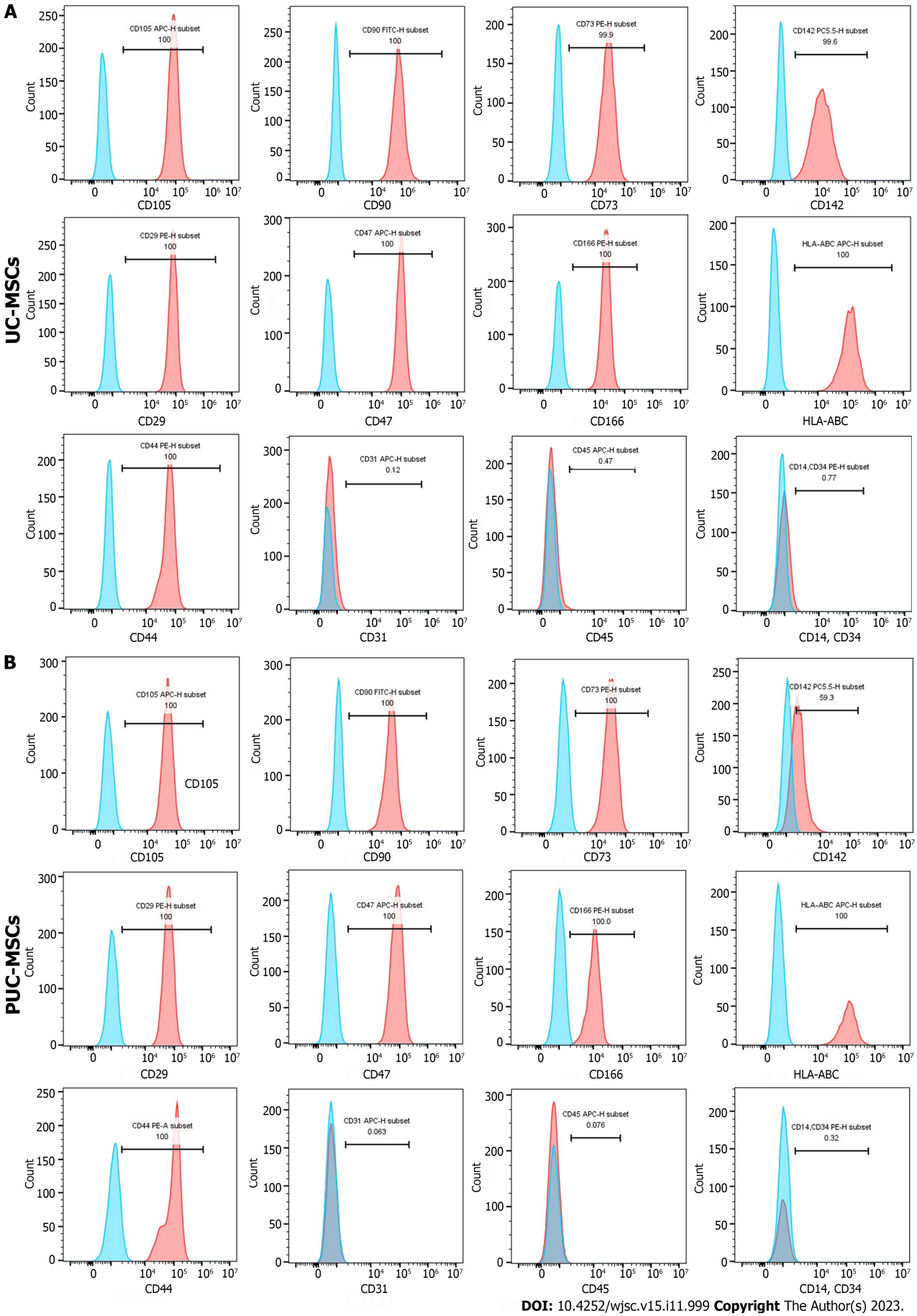

DOI: 10.4252/wjsc.v15.i11.999

Figure 2 Phenotypes of mesenchymal stem cells were detected by flow cytometry. A: Cell surface markers of umbilical cord mesenchymal stem cells

(UC-MSCs); B: Cell surface markers of primed umbilical cord mesenchymal stem cells (PUC-MSCs). The signals from the unstained control cells are shown in blue in the histogram, and the signals from stained cells are shown in red in the histogram. HLA: Human leukocyte antigen.

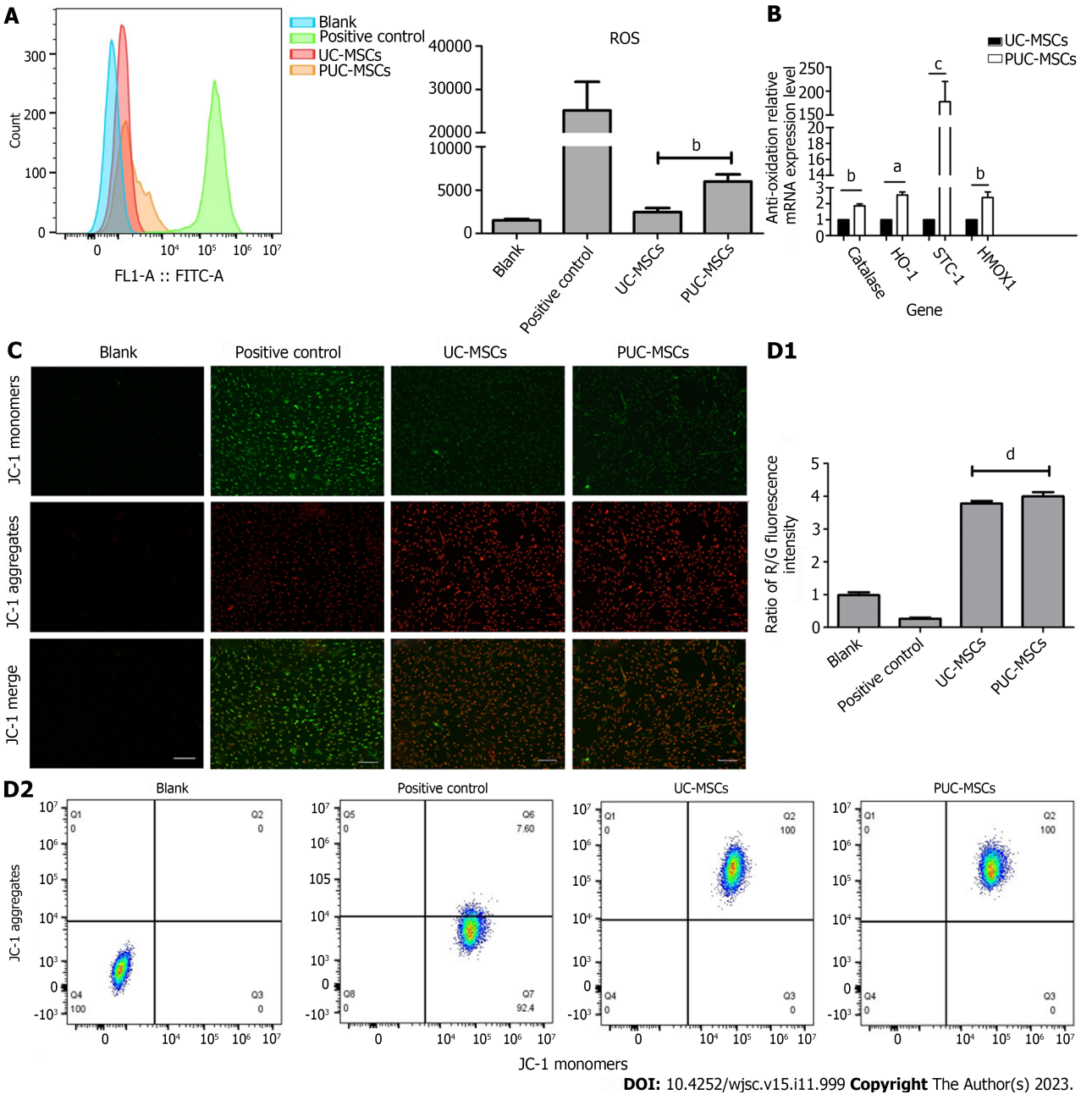

DOI: 10.4252/wjsc.v15.i11.999

Figure 3 Mitochondrial function. A: Reactive oxygen species (ROS) levels in umbilical cord mesenchymal stem cells (UC-MSCs) and primed UC-MSCs (PUC-MSCs) were analyzed by flow cytometry. The fluorescence intensity of 2,7-dichlorodihydrofluorescein (DCFH-DA) in PUC-MSCs increased by 3-fold compared to UC-MSCs; B: The expression of the antioxidant-related genes catalase, stanniocalcin-1 (STC1), and hemeoxygenase-1 (HOMX1) was increased; C: Representative image showing the mitochondrial membrane potential (MMP) of mesenchymal stem cells stained with JC-1. The red fluorescence of potential-dependent JC-1 aggregation in each group and the green fluorescence of the JC-1 monomer in the cytoplasm after depolarization of the mitochondrial membrane were observed. Fluorescence microscopy showed no significant difference in red and green fluorescence between UC-MSCs and PU-MSCs; Bar = 200 μm; D: Flow cytometry was used to detect the red and green fluorescence of the JC-1 probe in UC-MSCs and PUC-MSCs. There was no difference in the ratios of red and green fluorescence. [a] $P < 0.05$; [b]$P < 0.01$; [c]$P < 0.001$; [d]$P > 0.05$.

Hypoxia and inflammatory factor preconditioning enhances UC-MSC immunosuppressive properties

MSCs are pluripotent stem cells that have been shown to hold promise in tissue regeneration due to their ability to self-renew and differentiate and their broad immunomodulatory properties[1-5]. We evaluated whether UC-MSC immunomodulatory activities increased after pretreatment. qRT-PCR analysis revealed that the expression of PGE2, IDO, KYN, COX2, IL-10, TGF-β1, TSG-6, HLA-G5, and PD-L1 increased in PUC-MSCs compared to untreated UC-MSCs. IL-1ra expression was slightly elevated, but the difference was not statistically significant (Figure 5A). Because paracrine activity

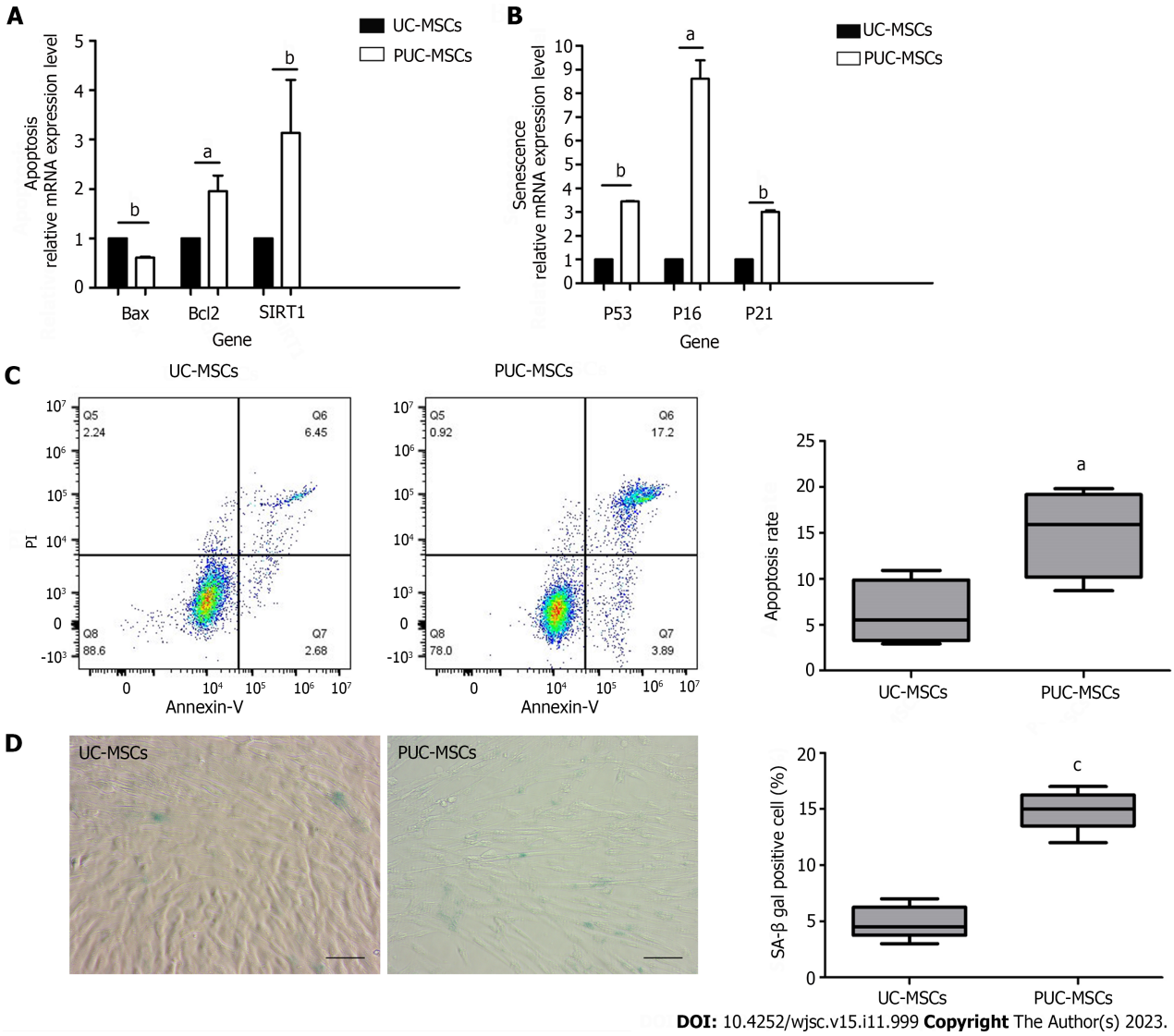

DOI: 10.4252/wjsc.v15.i11.999

Figure 4 Effects of pretreatment on apoptosis and senescence in mesenchymal stem cells. A: Apoptosis-related gene analysis showed that the expression of B-cell lymphoma 2 (BCL-2)-associated protein (Bax) was decreased and the expression of Bcl2 and silencing information regulator 2-related enzyme 1 (SIRT1) was increased after hypoxia and inflammatory factor pretreatment; B: Expression of P53, P16 and P21 was upregulated after hypoxia and inflammatory factor pretreatment; C: Umbilical cord mesenchymal stem cells (UC-MSCs) and primed UC-MSCs (PUC-MSCs) were stained with Annexin V-FITC apoptosis assay kit reagents and apoptotic cells were detected by flow cytometry. The results showed that the apoptosis index of PUC-MSCs increased; D: Representative images of β-galactosidase (SA-β-gal) staining and quantitative analysis of positive SA-β-gal staining. Compared with that of the UC-MSCs, the number of SA-β-gal-positive PUC-MSCs was significantly increased; Bar = 100 μm. $^{a}P < 0.05$; $^{b}P < 0.01$; $^{c}P < 0.001$.

is a key mechanism underlying MSC effects, we compared the bioactive factor secretion levels in PUC-MSCs and untreated UC-MSCs. We assessed MSC paracrine function by measuring the protein levels of immunosuppression-related soluble factors released into the culture supernatant, including IDO, PGE2, TGF-β1, TSG-6, and IL-10 by ELISAs. IDO, PGE2, TGF-β1 and TSG-6 levels significantly increased in the PUC-MSC supernatant, while IL-10 levels slightly increased but did not reach statistical significance (Figure 5B). In summary, these data strongly suggest that UC-MSC preconditioning with hypoxia and inflammatory factors upregulates the expression of soluble immunomodulatory factors and enhances their immunomodulatory activity.

Hypoxia and inflammatory factor preconditioning increases UC-MSC immunosuppressive properties

Considering the high expression of immunomodulatory molecules in PUC-MSCs, we evaluated their immunosuppressive capacity. We compared UC-MSC and PUC-MSC immunosuppressive capacity using PBMC and NK cell proliferation assays by analyzing growth dynamics of PBMCs cultured alone, with UC-MSCs or with PUC-MSCs (Figure 6A). Both UC-MSCs and PUC-MSCs significantly inhibited PBMC proliferation compared to PBMCs cultured alone. However, PUC-MSCs had a stronger inhibitory effect on PBMC proliferation, further indicating that pretreatment enhanced UC-MSC immunosuppressive abilities. We further investigated MSC-mediated inhibition of NK cell proliferation in the presence of the two MSC populations. We cultured CFSE-stained NK cells in the presence of IL-2 alone or with UC-MSCs or PUC-MSCs and analyzed CFSE fluorescence intensity by flow cytometry after 3 d. The proliferation rate of NK cells was reduced in cocultures with UC-MSCs or PUC-MSCs compared to NK cells cultured alone, but the PUC-MSC group

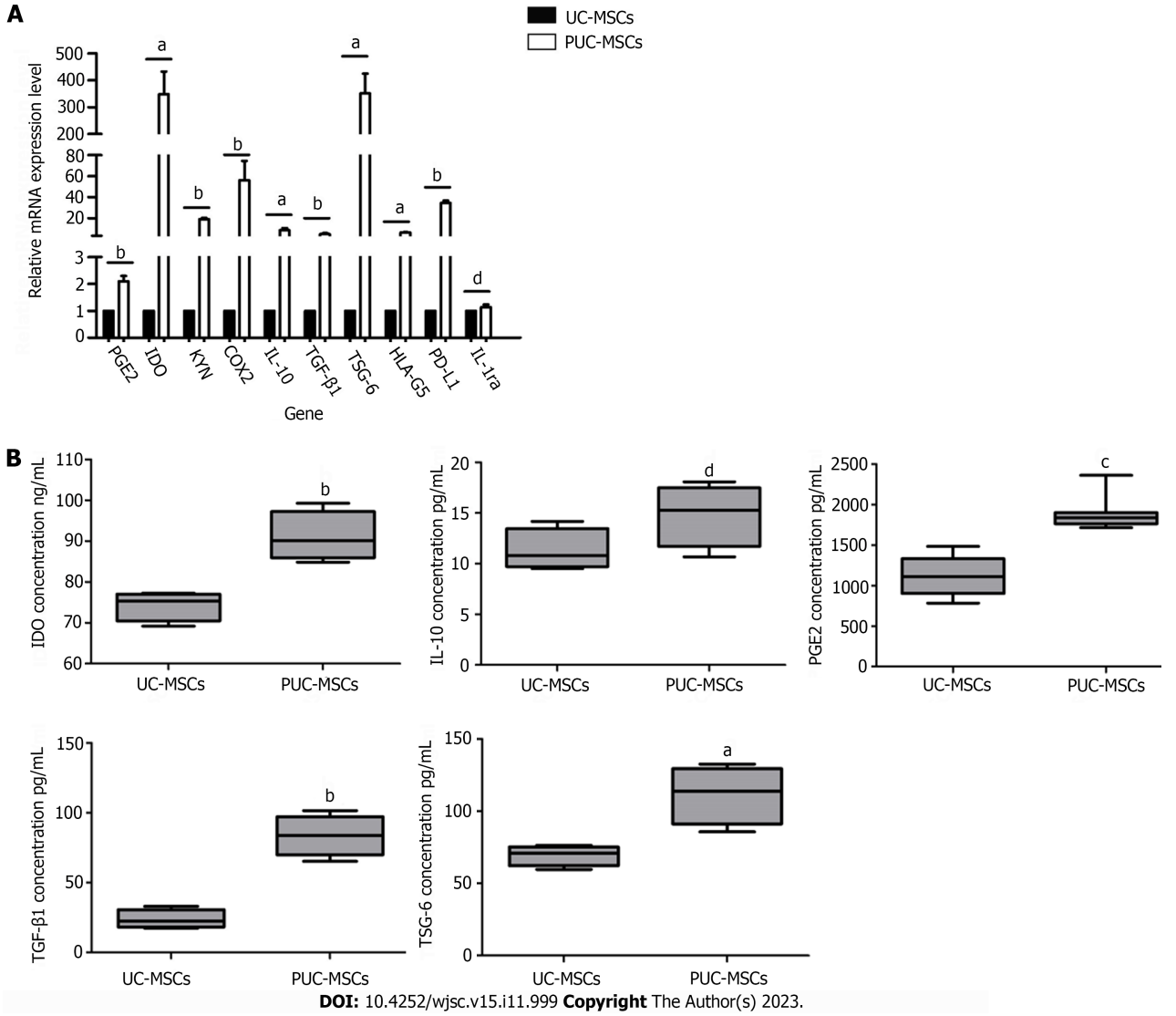

DOI: 10.4252/wjsc.v15.i11.999

Figure 5 Relative expression of immunomodulatory genes and proteins in umbilical cord mesenchymal stem cells after pretreatment. A: Gene expression levels of umbilical cord mesenchymal stem cells (UC-MSCs) and primed UC-MSCs (PUC-MSCs) were analyzed by quantitative real-time polymerase chain reaction. Expression levels of prostaglandin E2 (PGE2), kynurenine, idoleamine-2,3-dioxygenase (IDO), cyclooxygenaese-2 (COX2), interleukin-10 (IL-10), transforming growth factor-beta 1 (TGF-β1), human leukocyte antigen-G5 (HLA-G5), tumor necrosis factor-α-induced protein-6 (TSG-6) and ligands for programmed cell death 1 (PD-L1) were all increased after hypoxia and inflammatory factor preconditioning. IL-1 receptor antagonist (IL-1ra) was not significantly different between the two groups; B: Levels of immunoregulatory proteins in UC-MSCs and PUC-MSCs were detected by enzyme-linked immunosorbent assay. After hypoxia and inflammatory factor pretreatment, the protein levels of IDO, PGE2, TGF-β1 and TSG-6 were increased, while the expression of IL-10 was not significantly different, as determined *via* three independent experiments. $^{a}P < 0.05$; $^{b}P < 0.01$; $^{c}P < 0.001$; $^{d}P > 0.05$.

exerted stronger inhibitory effects on NK cells compared to UC-MSCs (Figure 6B).

Finally, we evaluated the effect of UC-MSC pretreatment with hypoxia exposure and inflammatory factor treatment on NK cell cytotoxic activity. NK cells were cultured alone or with UC-MSCs/PUC-MSCs at a 3:1 ratio for 72 h, then collected and incubated with CFSE-stained K562 target cells at an effective target ratio (E:T = 1:5) for 4 h. The cells were collected, and K562 cell apoptosis was analyzed by PI staining. The results showed that NK cells cocultured with UC-MSCs or PUC-MSCs had lower cytolytic activity, and the inhibition of NK cell-mediated cytotoxic activity was higher with PUC-MSCs than UC-MSCs (Figure 6C).

DISCUSSION

Intravenous injection of MSCs has been increasingly used in clinical research and has shown great potential in the treatment of various diseases. Because of their immunomodulatory functions, MSCs have become a promising alternative treatment for inflammatory diseases. MSCs come from a wide range of sources. Currently, the most studied MSCs are derived from bone marrow and adipose tissue, followed by those from umbilical cord tissue[47]. Compared with those from other sources, umbilical cord-derived MSCs are abundant, easy to collect, genetically stable, and do not readily

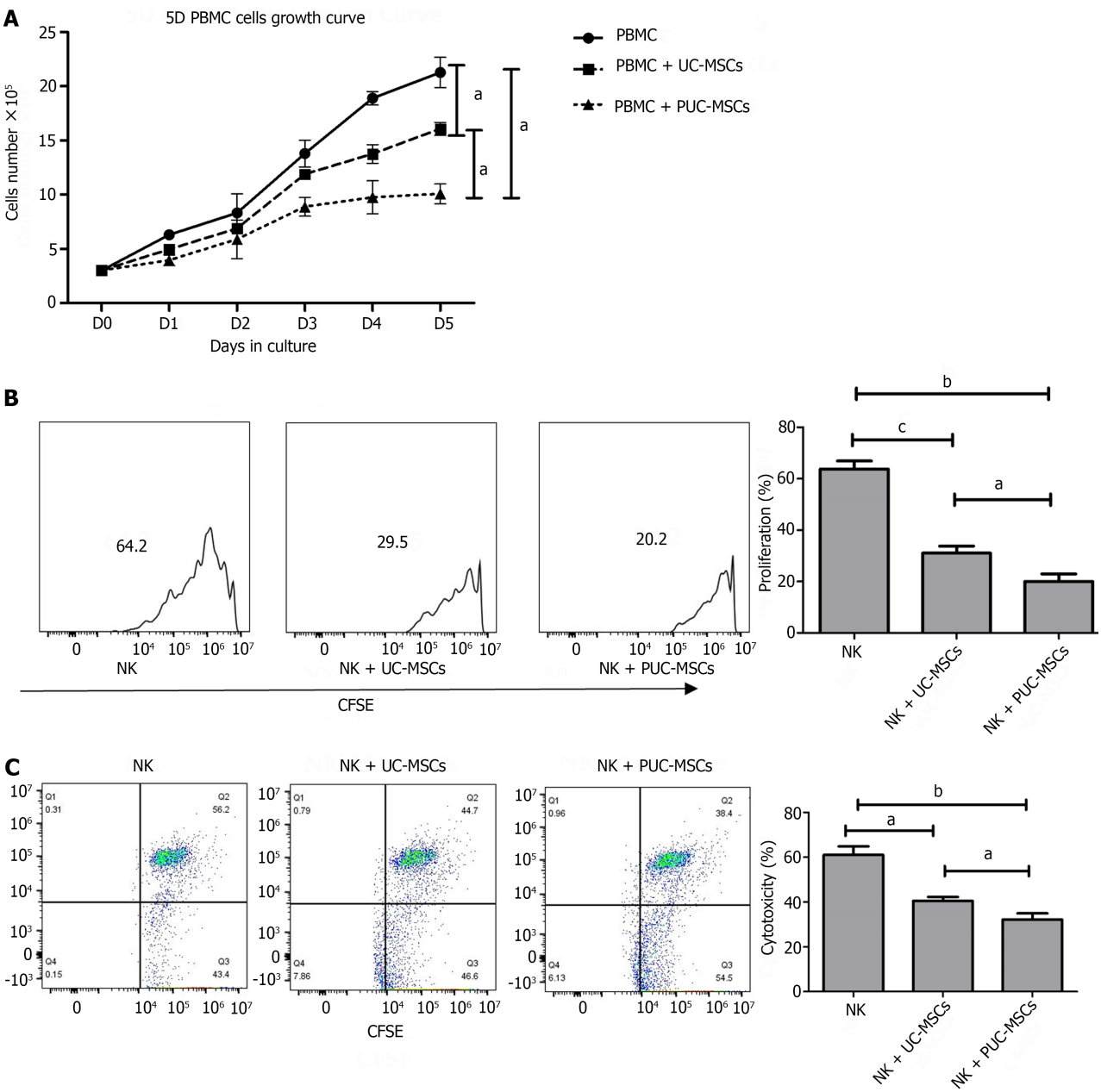

DOI: 10.4252/wjsc.v15.i11.999

Figure 6 Detection of the immunomodulatory function of umbilical cord mesenchymal stem cells after preconditioning. A: Peripheral blood mononuclear cells (PBMCs) alone or directly exposed to umbilical cord mesenchymal stem cells (UC-MSCs/primed UC-MSCs) for 5 d in a 3:1 ratio. The number of PBMCs in three groups was measured daily and the growth curve was plotted; B: Carboxyfluorescein diacetate succinimidyl ester (CFSE)-stained natural killer (NK) cells were cultured alone or cocultured with UC-MSCs/PUC-MSCs at a 3:1 ratio for 72 h. NK cells were harvested, and the fluorescence intensity of CFSE was measured by flow cytometry to measure the proliferation rate of NK cells; C: NK cells were collected and incubated with CFSE-stained K562 target cells for 4 h at an effector ratio (E:T = 1:5). Effector cell (NK cell)-mediated cytotoxicity of K562 cells was analyzed by flow cytometry. $^{a}P < 0.05$; $^{b}P < 0.01$; $^{c}P < 0.001$; $^{d}P > 0.05$.

mutate. Therefore, umbilical cord MSCs have broad application prospects in the cell therapy field[48-50]. Therefore, we focused on UC-MSCs in this study.

In addition to the effects of their origin, MSCs exhibit decreased biological performance when subjected to vein transplantation and exposure to the harsh inflammatory environment of damaged tissue[29]. Studies have shown that preconditioning cells by exposing them to the external environment can enhance their therapeutic effects by preparing them for the harsh conditions they encounter when injected into the body. Antebi *et al*[51] showed that hypoxic preconditioning of bone marrow MSCs enhanced the therapeutic function of these cells. Gorgun *et al*[34] analyzed the effects of hypoxia and inflammatory factor (TNF-α, IL-1α) pretreatment on AD-MSC angiogenic potential. In addition, Rodriguez *et al*[52] pretreated AD-MSCs with a mixture of inflammatory factors under anoxic culture conditions, which significantly enhanced their functional characteristics and immunosuppressive and immunoregulatory functions.

In this study, we developed a combination strategy of hypoxia plus a mixture of TNF-α, IL-1β, and IFN-γ preconditioning to enhance hUC-MSC immunomodulatory capacity. To our knowledge, this is a previously unanalyzed combination pretreatment. We found that this preconditioning approach successfully mimicked the harsh inflammatory

environment and effectively enhanced the immunosuppressive function of MSCs. To simulate hypoxia, we cultured UC-MSCs in a special three-gas incubator containing 2% O_2, 5% CO_2 and 93% N_2 at 37°C for 24 h. We had previously evaluated these gas conditions and found them to be most suitable for preserving the functional characteristics of MSCs. To simulate the harsh inflammatory environment, we independently developed and utilized a mixture of IL-1β, IFN-γ and TNF-α. After pretreatment, we found that the cells became elongated, but their proliferation, viability and size did not significantly change. Notably, Klinker *et al*[53] recently demonstrated that the morphological characteristics of MSCs were significantly correlated with their immunosuppressive ability and can be used to predict their overall immunosuppressive effects[53]. The results of the study by Klinker *et al*[53] showed that pretreated UC-MSCs became elongated and had stronger immunosuppressive ability, consistent with the results of our study.

Although different forms of preconditioning have been shown to successfully enhance cell properties and increase cell function, there are still noteworthy safety concerns. Because pretreatment may have negative effects on cell function, we used flow cytometry to characterize MSC phenotypes. The expression of specific MSC surface markers can be used as indicators of cell differentiation potential, lineage commitment, aging, and therapeutic function[54]. The International Society for Cell and Gene Therapy defines minimum standards for MSC characterization, and most experiments are conducted on this basis[55]. However, we examined additional MSC surface markers. We found that UC-MSCs and PUC-MSCs from three donors retained high expression levels of CD105, CD90, CD73, CD29, CD166, CD47 and HLA-ABC and were negative for CD31, CD45, CD14, and CD34 expression. These findings indicated that UC-MSCs retained MSC properties after pretreatment. Interestingly, we found that CD142 expression significantly decreased after pretreatment. Oeller *et al*[39] found that UC-MSCs showed higher procoagulant activity than adipose-derived MSCs, and UC-MSCs showed extensive TF (CD142) expression and long-lasting clotting; a higher cell number significantly increased clot formation, which was partially dependent on coagulation factors[43]. Our study showed that CD142 expression in UC-MSCs without treatment exceeded 99% and CD142 expression significantly decreased after pretreatment (59.3%). Our experiment showed significant decreases in TF expression, which has been shown to be closely related to procoagulant activity[38]. However, Rodriguez *et al*[52] demonstrated that bone marrow-derived MSCs (BM-MSCs) and AD-MSCs that were pretreated with a combination of hypoxia and inflammatory factors showed increased CD142 expression, which was inconsistent with previous studies[53]. We determined that these discrepancies may be due to different origins of MSCs, MSC heterogeneity and/or differences between culture systems. However, we found pretreatment significantly reduced CD142 expression. In addition, studies have suggested the use of anticoagulants or genetic methods to inhibit TF activity for the clinical application of MSCs to maximize clinical benefits for patients, which also underscores the importance of insights into the mechanisms underlying safety issues related to nonhematopoietic cell transplantation[43].

The efficacy of MSCs depends on the full function of their mitochondria, which can be damaged after cell exposure to harmful environments[56]. Therefore, we examined the effects of hypoxia and inflammatory factor pretreatment on mitochondrial function. ROS levels were increased after pretreatment but were within the range of those in the positive controls. In addition, the increased expression of antioxidants such as STC1, catalase and HOMX1 can eliminate ROS to maintain cell redox homeostasis[57]. Previous studies have shown that both HMOX1 and catalase play key roles in protecting cells from ROS-induced damage[58,59]. Therefore, although ROS levels increased after pretreatment, the antioxidant capacity of the cells also correspondingly increased and the ROS removal rate increased. In addition, the MMP (Δψm) plays a key role in important mitochondrial functions, and its dissipation is an indicator of mitochondrial dysfunction[60]. Maintaining a stable MMP (Ψm) is essential for ensuring efficient ROS clearance and preventing apoptosis or other stress-related events caused by excessive ROS. Therefore, we examined the MMP and found that pretreatment had no effect on MMP. In summary, although ROS levels increased after pretreatment, the antioxidant capacity also increased, and the MMP did not change, indicating that there was no damage to mitochondrial function after pretreatment.

We next examined the effect of pretreatment on MSC apoptosis and senescence and found that the apoptosis index of UC-MSCs increased to a certain extent after pretreatment. Galleu *et al*[61] showed that all patients can receive apoptotic MSCs for *in vivo* injection and that these cells can induce receptor-mediated immune regulation. MSC apoptosis of is critical to their therapeutic functions[62]. BCL-2, BAX and SIRT1 genes play important roles in the apoptosis pathway. In this study, we found increased expression of the SIRT1 gene, which protected cells from apoptosis by activating autophagy[63]. The ratio of BAX/BCL-2 is closely related to the apoptosis potential of cells[64]. In this study, an inverse proportional relationship between BAX and BCL-2 indicated that MSCs exerted stronger anti-apoptosis effects after pretreatment. This may indicate that the cells were protecting themselves from the harmful inflammatory environment. In addition, MSCs showed increased SA-β-gal activity and p53, P16 and p21 expression after hypoxia and inflammatory factor pretreatment, suggesting that MSCs underwent senescence after pretreatment. Salminen *et al*[65] found that aging MSCs exert stronger immunosuppressive effects. The experimental results showed that even when some of the pretreated UC-MSCs underwent senescence and apoptosis, these effects did not reduce their immunoregulatory abilities, and even apoptotic and senescent MSCs showed increased immunosuppressive abilities.

The pleiotropic effect of MSCs is mostly mediated by soluble paracrine factors, and active paracrine factors produced by these cells regulate cellular immunity when they come into contact with the host[66]. Therefore, we investigated the response of paracrine factors involved in the immune regulation of MSCs to preconditioning. Many bioactive molecules produced by MSCs, such as IDO, PGE2, IL-10, TSG-6, and TGF-β1, effectively regulate innate and adaptive immunity and play a key role in the immunosuppressive effect of MSCs[67]. The detection of immunomodulation-related genes showed that the expression levels of PGE2, KYN, IDO, COX2, IL-10, TGF-β1, TSG-6, HLA-G5 and PD-L1 were significantly increased in addition to that of IL-1ra. In addition, PGE2, TSG-6, TGF-β1 and IDO protein levels in the supernatant were significantly increased. IL-10 levels were slightly increased, but the difference between the pretreatment and control groups was not significant. These results showed that preconditioning can promote the production of immunomodulatory paracrine factors in UC-MSCs and increase their immunomodulatory effect.

Finally, we studied the immunosuppressive effects of MSCs on PBMCs and NK cells. We found that UC-MSCs and PUC-MSCs inhibited PBMCs and NK cell proliferation, but PUC-MSCs exerted a stronger inhibitory effect. Some work has been done to characterize the interaction between BM-MSCs and NK cells[22,68,69]. However, the interaction of UC-MSCs with NK cells has been largely unexplored. Our results add to our understanding of the immunosuppressive effects of UC-MSCs[70,71]. In addition, we found that PUC-MSCs exerted a stronger inhibitory effect on NK cell-mediated cytotoxic activity. Reportedly, IDO and PGE2 or TGF-β1 produced by MSCs are critical for inhibiting NK cell cytotoxicity[22,72]. PUC-MSCs may exert stronger inhibitory effects on NK cell-mediated toxicity due to increased IDO, TGF-β1 and PGE2 expression.

We acknowledge that this study has limitations. Whether the combination of hypoxia (2% O_2) and inflammatory factors (IL-1β, TNF-α, IFN-γ) is superior to other preconditioning methods is unclear. However, our study shows a preconditioning strategy that adds to the existing experimental options to use in further research. In addition, whether these cells exhibit superior immunomodulatory functions under harsh *in vivo* inflammatory conditions remains to be demonstrated and is the focus of our future work. Moreover, although TF expression is reduced by preconditioning, the mechanism is unclear. Thromboembolism may still have significant clinical consequences for patients who receive MSCs after preconditioning. Therefore, for whole-body cell administration, it is still necessary to use anticoagulants during the clinical application of MSCs to inhibit TF activity and increase the clinical benefits to patients.

CONCLUSION

In conclusion, we successfully developed an *in vitro* preconditioning method that mimics the impaired environment through a combination of hypoxia (2% O_2) and inflammatory factors (IL-1β, TNF-α, IFN-γ) to enhance UC-MSC immunosuppressive ability without compromising their biological characteristics. Most notably, this approach greatly reduced the expression of the clotting-related TF in MSCs, which was a surprising result.

ARTICLE HIGHLIGHTS

Research background

Mesenchymal stem cells (MSCs) have great potential in the treatment of a variety of immune-related diseases due to their unique immunomodulatory and anti-inflammatory abilities. However, after intravenous transplantation, MSCs cannot effectively exert their biological effects when they encounter a harsh environment *in vivo*, which reduces the efficacy of cell therapy. To increase transplantation efficacy, appropriate pretreatment methods are particularly important.

Research motivation

Although a variety of pretreatment methods are used to increase MSC transplantation efficacy, suitable and effective *in vitro* pretreatment methods are still worth studying.

Research objectives

To evaluate whether umbilical cord MSCs (UC-MSCs) pretreated with hypoxia exposure and inflammatory factors show enhanced immunosuppressive effects without affecting cell biological characteristics.

Research methods

In this study, we used a combination of hypoxia (2% O_2) and inflammatory factors (interleukin-1β, tumor necrosis factor-α , interferon-γ) to pretreat UC-MSCs for 24 h to simulate the *in vivo* injury environment. We then comprehensively evaluated the biological properties of pretreated UC-MSCs and investigated their immunosuppressive properties.

Research results

Our results showed that compared to UC-MSCs, pretreated UC-MSCs were morphologically elongated, but their viability, proliferation and size were not affected, the expression of coagulation-related tissue factors was significantly reduced, and mitochondria maintained their function and integrity. Although some cells underwent apoptosis or senescence, polymerase chain reactions and enzyme-linked immunosorbent assays revealed a significant increase in the levels of immunomodulation-related factors. Coculture with peripheral blood mononuclear cell and natural killer cells exerted a stronger immunosuppressive effect.

Research conclusions

The combined pretreatment of hypoxia exposure and inflammatory factors enhanced the immunosuppressive ability of MSCs but did not affect the biological characteristics of these cells.

Research perspectives

Our study provides new strategies for the preconditioning of UC-MSCs.

ACKNOWLEDGEMENTS

I would like to thank the people who helped me in the process of writing this article, the Second Hospital of Shanxi Medical University for technical support, and my friends and colleagues for their help during the experiments.

FOOTNOTES

Author contributions: Li H, Ji XQ, Zhang SM, and Bi RH designed and coordinated the study; Li H performed experiments and wrote the manuscript; Ji XQ acquired and analyzed the data; Bi RH contributed to ideas, supervision, review and editing; All authors approved the final version of the article.

Supported by the National Natural Science Foundation of China, No. 31200899.

Institutional review board statement: This study was approved by the Medical Ethics Committee of Shanxi Medical University (Approval No. 2018LL016).

Conflict-of-interest statement: The authors report no relevant conflicts of interest for this article.

Data sharing statement: No additional data are available.

Country/Territory of origin: China

ORCID number: Hang Li 0000-0003-1815-4369; Ri-Hui Bi 0009-0005-6212-1910.

S-Editor: Wang JJ
L-Editor: Filipodia
P-Editor: Cai YX

REFERENCES

1 **Yu M**, Ma L, Yuan Y, Ye X, Montagne A, He J, Ho TV, Wu Y, Zhao Z, Sta Maria N, Jacobs R, Urata M, Wang H, Zlokovic BV, Chen JF, Chai Y. Cranial Suture Regeneration Mitigates Skull and Neurocognitive Defects in Craniosynostosis. *Cell* 2021; **184**: 243-256.e18 [PMID: 33417861 DOI: 10.1016/j.cell.2020.11.037]

2 **Berebichez-Fridman R**, Montero-Olvera PR. Sources and Clinical Applications of Mesenchymal Stem Cells: State-of-the-art review. *Sultan Qaboos Univ Med J* 2018; **18**: e264-e277 [PMID: 30607265 DOI: 10.18295/squmj.2018.18.03.002]

3 **Stefańska K**, Nemcova L, Blatkiewicz M, Pieńkowski W, Ruciński M, Zabel M, Mozdziak P, Podhorska-Okołów M, Dzięgiel P, Kempisty B. Apoptosis Related Human Wharton's Jelly-Derived Stem Cells Differentiation into Osteoblasts, Chondrocytes, Adipocytes and Neural-like Cells-Complete Transcriptomic Assays. *Int J Mol Sci* 2023; **24** [PMID: 37373173 DOI: 10.3390/ijms241210023]

4 **Zhou T**, Yuan Z, Weng J, Pei D, Du X, He C, Lai P. Challenges and advances in clinical applications of mesenchymal stromal cells. *J Hematol Oncol* 2021; **14**: 24 [PMID: 33579329 DOI: 10.1186/s13045-021-01037-x]

5 **Gao F**, Chiu SM, Motan DA, Zhang Z, Chen L, Ji HL, Tse HF, Fu QL, Lian Q. Mesenchymal stem cells and immunomodulation: current status and future prospects. *Cell Death Dis* 2016; **7**: e2062 [PMID: 26794657 DOI: 10.1038/cddis.2015.327]

6 **Li F**, Guo X, Chen SY. Function and Therapeutic Potential of Mesenchymal Stem Cells in Atherosclerosis. *Front Cardiovasc Med* 2017; **4**: 32 [PMID: 28589127 DOI: 10.3389/fcvm.2017.00032]

7 **Ha DH**, Kim HK, Lee J, Kwon HH, Park GH, Yang SH, Jung JY, Choi H, Lee JH, Sung S, Yi YW, Cho BS. Mesenchymal Stem/Stromal Cell-Derived Exosomes for Immunomodulatory Therapeutics and Skin Regeneration. *Cells* 2020; **9** [PMID: 32392899 DOI: 10.3390/cells9051157]

8 **Tsuji M**, Mukai T, Sato Y, Azuma Y, Yamamoto S, Cayetanot F, Bodineau L, Onoda A, Nagamura-Inoue T, Coq JO. Umbilical cord-derived mesenchymal stromal cell therapy to prevent the development of neurodevelopmental disorders related to low birth weight. *Sci Rep* 2023; **13**: 3841 [PMID: 36882440 DOI: 10.1038/s41598-023-30817-3]

9 **Jiang Y**, Zhang P, Zhang X, Lv L, Zhou Y. Advances in mesenchymal stem cell transplantation for the treatment of osteoporosis. *Cell Prolif* 2021; **54**: e12956 [PMID: 33210341 DOI: 10.1111/cpr.12956]

10 **Kirwin T**, Gomes A, Amin R, Sufi A, Goswami S, Wang B. Mechanisms underlying the therapeutic potential of mesenchymal stem cells in atherosclerosis. *Regen Med* 2021; **16**: 669-682 [PMID: 34189963 DOI: 10.2217/rme-2021-0024]

11 **Liang J**, Zhang H, Kong W, Deng W, Wang D, Feng X, Zhao C, Hua B, Wang H, Sun L. Safety analysis in patients with autoimmune disease receiving allogeneic mesenchymal stem cells infusion: a long-term retrospective study. *Stem Cell Res Ther* 2018; **9**: 312 [PMID: 30428931 DOI: 10.1186/s13287-018-1053-4]

12 **Munir H**, McGettrick HM. Mesenchymal Stem Cell Therapy for Autoimmune Disease: Risks and Rewards. *Stem Cells Dev* 2015; **24**: 2091-2100 [PMID: 26068030 DOI: 10.1089/scd.2015.0008]

13 **Dunavin N**, Dias A, Li M, McGuirk J. Mesenchymal Stromal Cells: What Is the Mechanism in Acute Graft-Versus-Host Disease?

Biomedicines 2017; **5** [PMID: 28671556 DOI: 10.3390/biomedicines5030039]
14 **White IA**, Sanina C, Balkan W, Hare JM. Mesenchymal Stem Cells in Cardiology. *Methods Mol Biol* 2016; **1416**: 55-87 [PMID: 27236666 DOI: 10.1007/978-1-4939-3584-0_4]
15 **Brychtova M**, Thiele JA, Lysak D, Holubova M, Kralickova M, Vistejnova L. Mesenchymal stem cells as the near future of cardiology medicine - truth or wish? *Biomed Pap Med Fac Univ Palacky Olomouc Czech Repub* 2019; **163**: 8-18 [PMID: 30439932 DOI: 10.5507/bp.2018.071]
16 **Wang YH**, Wu DB, Chen B, Chen EQ, Tang H. Progress in mesenchymal stem cell-based therapy for acute liver failure. *Stem Cell Res Ther* 2018; **9**: 227 [PMID: 30143052 DOI: 10.1186/s13287-018-0972-4]
17 **Zhang Y**, Li Y, Zhang L, Li J, Zhu C. Mesenchymal stem cells: potential application for the treatment of hepatic cirrhosis. *Stem Cell Res Ther* 2018; **9**: 59 [PMID: 29523186 DOI: 10.1186/s13287-018-0814-4]
18 **Liang J**, Zhang H, Hua B, Wang H, Lu L, Shi S, Hou Y, Zeng X, Gilkeson GS, Sun L. Allogenic mesenchymal stem cells transplantation in refractory systemic lupus erythematosus: a pilot clinical study. *Ann Rheum Dis* 2010; **69**: 1423-1429 [PMID: 20650877 DOI: 10.1136/ard.2009.123463]
19 **Volkman R**, Offen D. Concise Review: Mesenchymal Stem Cells in Neurodegenerative Diseases. *Stem Cells* 2017; **35**: 1867-1880 [PMID: 28589621 DOI: 10.1002/stem.2651]
20 **Lo Furno D**, Mannino G, Giuffrida R. Functional role of mesenchymal stem cells in the treatment of chronic neurodegenerative diseases. *J Cell Physiol* 2018; **233**: 3982-3999 [PMID: 28926091 DOI: 10.1002/jcp.26192]
21 **Fan XL**, Zhang Y, Li X, Fu QL. Mechanisms underlying the protective effects of mesenchymal stem cell-based therapy. *Cell Mol Life Sci* 2020; **77**: 2771-2794 [PMID: 31965214 DOI: 10.1007/s00018-020-03454-6]
22 **Spaggiari GM**, Capobianco A, Abdelrazik H, Becchetti F, Mingari MC, Moretta L. Mesenchymal stem cells inhibit natural killer-cell proliferation, cytotoxicity, and cytokine production: role of indoleamine 2,3-dioxygenase and prostaglandin E2. *Blood* 2008; **111**: 1327-1333 [PMID: 17951526 DOI: 10.1182/blood-2007-02-074997]
23 **Fan XL**, Zeng QX, Li X, Li CL, Xu ZB, Deng XQ, Shi J, Chen D, Zheng SG, Fu QL. Induced pluripotent stem cell-derived mesenchymal stem cells activate quiescent T cells and elevate regulatory T cell response *via* NF-κB in allergic rhinitis patients. *Stem Cell Res Ther* 2018; **9**: 170 [PMID: 29921316 DOI: 10.1186/s13287-018-0896-z]
24 **Selmani Z**, Naji A, Zidi I, Favier B, Gaiffe E, Obert L, Borg C, Saas P, Tiberghien P, Rouas-Freiss N, Carosella ED, Deschaseaux F. Human leukocyte antigen-G5 secretion by human mesenchymal stem cells is required to suppress T lymphocyte and natural killer function and to induce CD4+CD25highFOXP3+ regulatory T cells. *Stem Cells* 2008; **26**: 212-222 [PMID: 17932417 DOI: 10.1634/stemcells.2007-0554]
25 **Augello A**, Tasso R, Negrini SM, Amateis A, Indiveri F, Cancedda R, Pennesi G. Bone marrow mesenchymal progenitor cells inhibit lymphocyte proliferation by activation of the programmed death 1 pathway. *Eur J Immunol* 2005; **35**: 1482-1490 [PMID: 15827960 DOI: 10.1002/eji.200425405]
26 **Corcione A**, Benvenuto F, Ferretti E, Giunti D, Cappiello V, Cazzanti F, Risso M, Gualandi F, Mancardi GL, Pistoia V, Uccelli A. Human mesenchymal stem cells modulate B-cell functions. *Blood* 2006; **107**: 367-372 [PMID: 16141348 DOI: 10.1182/blood-2005-07-2657]
27 **MacLeod AS**, Mansbridge JN. The Innate Immune System in Acute and Chronic Wounds. *Adv Wound Care (New Rochelle)* 2016; **5**: 65-78 [PMID: 26862464 DOI: 10.1089/wound.2014.0608]
28 **Hong WX**, Hu MS, Esquivel M, Liang GY, Rennert RC, McArdle A, Paik KJ, Duscher D, Gurtner GC, Lorenz HP, Longaker MT. The Role of Hypoxia-Inducible Factor in Wound Healing. *Adv Wound Care (New Rochelle)* 2014; **3**: 390-399 [PMID: 24804159 DOI: 10.1089/wound.2013.0520]
29 **Hu C**, Li L. Preconditioning influences mesenchymal stem cell properties in vitro and in vivo. *J Cell Mol Med* 2018; **22**: 1428-1442 [PMID: 29392844 DOI: 10.1111/jcmm.13492]
30 **Harrell CR**, Fellabaum C, Jovicic N, Djonov V, Arsenijevic N, Volarevic V. Molecular Mechanisms Responsible for Therapeutic Potential of Mesenchymal Stem Cell-Derived Secretome. *Cells* 2019; **8** [PMID: 31100966 DOI: 10.3390/cells8050467]
31 **Sarsenova M**, Kim Y, Raziyeva K, Kazybay B, Ogay V, Saparov A. Recent advances to enhance the immunomodulatory potential of mesenchymal stem cells. *Front Immunol* 2022; **13**: 1010399 [PMID: 36211399 DOI: 10.3389/fimmu.2022.1010399]
32 **Shi Y**, Wang Y, Li Q, Liu K, Hou J, Shao C. Immunoregulatory mechanisms of mesenchymal stem and stromal cells in inflammatory diseases. *Nat Rev Nephrol* 2018; **14**: 493-507 [PMID: 29895977 DOI: 10.1038/s41581-018-0023-5]
33 **Su Y**, Xu C, Cheng W, Zhao Y, Sui L. Pretreated Mesenchymal Stem Cells and Their Secretome: Enhanced Immunotherapeutic Strategies. *Int J Mol Sci* 2023; **24** [PMID: 36674790 DOI: 10.3390/ijms24021277]
34 **Gorgun C**, Ceresa D, Lesage R, Villa F, Reverberi D, Balbi C, Santamaria S, Cortese K, Malatesta P, Geris L, Quarto R, Tasso R. Dissecting the effects of preconditioning with inflammatory cytokines and hypoxia on the angiogenic potential of mesenchymal stromal cell (MSC)-derived soluble proteins and extracellular vesicles (EVs). *Biomaterials* 2021; **269**: 120633 [PMID: 33453634 DOI: 10.1016/j.biomaterials.2020.120633]
35 **Liu L**, Gao J, Yuan Y, Chang Q, Liao Y, Lu F. Hypoxia preconditioned human adipose derived mesenchymal stem cells enhance angiogenic potential *via* secretion of increased VEGF and bFGF. *Cell Biol Int* 2013; **37**: 551-560 [PMID: 23505143 DOI: 10.1002/cbin.10097]
36 **Ferreira JR**, Teixeira GQ, Santos SG, Barbosa MA, Almeida-Porada G, Gonçalves RM. Mesenchymal Stromal Cell Secretome: Influencing Therapeutic Potential by Cellular Pre-conditioning. *Front Immunol* 2018; **9**: 2837 [PMID: 30564236 DOI: 10.3389/fimmu.2018.02837]
37 **Paliwal S**, Chaudhuri R, Agrawal A, Mohanty S. Regenerative abilities of mesenchymal stem cells through mitochondrial transfer. *J Biomed Sci* 2018; **25**: 31 [PMID: 29602309 DOI: 10.1186/s12929-018-0429-1]
38 **Christy BA**, Herzig MC, Montgomery RK, Delavan C, Bynum JA, Reddoch KM, Cap AP. Procoagulant activity of human mesenchymal stem cells. *J Trauma Acute Care Surg* 2017; **83**: S164-S169 [PMID: 28628602 DOI: 10.1097/TA.0000000000001485]
39 **Oeller M**, Laner-Plamberger S, Hochmann S, Ketterl N, Feichtner M, Brachtl G, Hochreiter A, Scharler C, Bieler L, Romanelli P, Couillard-Despres S, Russe E, Schallmoser K, Strunk D. Selection of Tissue Factor-Deficient Cell Transplants as a Novel Strategy for Improving Hemocompatibility of Human Bone Marrow Stromal Cells. *Theranostics* 2018; **8**: 1421-1434 [PMID: 29507631 DOI: 10.7150/thno.21906]
40 **Tatsumi K**, Ohashi K, Matsubara Y, Kohori A, Ohno T, Kakidachi H, Horii A, Kanegae K, Utoh R, Iwata T, Okano T. Tissue factor triggers procoagulation in transplanted mesenchymal stem cells leading to thromboembolism. *Biochem Biophys Res Commun* 2013; **431**: 203-209 [PMID: 23313481 DOI: 10.1016/j.bbrc.2012.12.134]
41 **George MJ**, Prabhakara K, Toledano-Furman NE, Wang YW, Gill BS, Wade CE, Olson SD, Cox CS Jr. Clinical Cellular Therapeutics Accelerate Clot Formation. *Stem Cells Transl Med* 2018; **7**: 731-739 [PMID: 30070065 DOI: 10.1002/sctm.18-0015]

42 **Coppin L**, Sokal E, Stéphenne X. Thrombogenic Risk Induced by Intravascular Mesenchymal Stem Cell Therapy: Current Status and Future Perspectives. *Cells* 2019; **8** [PMID: 31569696 DOI: 10.3390/cells8101160]

43 **Stéphenne X**, Vosters O, Najimi M, Beuneu C, Dung KN, Wijns W, Goldman M, Sokal EM. Tissue factor-dependent procoagulant activity of isolated human hepatocytes: relevance to liver cell transplantation. *Liver Transpl* 2007; **13**: 599-606 [PMID: 17394166 DOI: 10.1002/Lt.21128]

44 **Maryanovich M**, Gross A. A ROS rheostat for cell fate regulation. *Trends Cell Biol* 2013; **23**: 129-134 [PMID: 23117019 DOI: 10.1016/j.tcb.2012.09.007]

45 **Brand MD**, Buckingham JA, Esteves TC, Green K, Lambert AJ, Miwa S, Murphy MP, Pakay JL, Talbot DA, Echtay KS. Mitochondrial superoxide and aging: uncoupling-protein activity and superoxide production. *Biochem Soc Symp* 2004; 203-213 [PMID: 15777023 DOI: 10.1042/bss0710203]

46 **Dimri GP**, Lee X, Basile G, Acosta M, Scott G, Roskelley C, Medrano EE, Linskens M, Rubelj I, Pereira-Smith O. A biomarker that identifies senescent human cells in culture and in aging skin in vivo. *Proc Natl Acad Sci U S A* 1995; **92**: 9363-9367 [PMID: 7568133 DOI: 10.1073/pnas.92.20.9363]

47 **Wang ZG**, He ZY, Liang S, Yang Q, Cheng P, Chen AM. Comprehensive proteomic analysis of exosomes derived from human bone marrow, adipose tissue, and umbilical cord mesenchymal stem cells. *Stem Cell Res Ther* 2020; **11**: 511 [PMID: 33246507 DOI: 10.1186/s13287-020-02032-8]

48 **Ding DC**, Chang YH, Shyu WC, Lin SZ. Human umbilical cord mesenchymal stem cells: a new era for stem cell therapy. *Cell Transplant* 2015; **24**: 339-347 [PMID: 25622293 DOI: 10.3727/096368915X686841]

49 **Mushahary D**, Spittler A, Kasper C, Weber V, Charwat V. Isolation, cultivation, and characterization of human mesenchymal stem cells. *Cytometry A* 2018; **93**: 19-31 [PMID: 29072818 DOI: 10.1002/cyto.a.23242]

50 **Beeravolu N**, McKee C, Alamri A, Mikhael S, Brown C, Perez-Cruet M, Chaudhry GR. Isolation and Characterization of Mesenchymal Stromal Cells from Human Umbilical Cord and Fetal Placenta. *J Vis Exp* 2017 [PMID: 28447991 DOI: 10.3791/55224]

51 **Antebi B**, Rodriguez LA 2nd, Walker KP 3rd, Asher AM, Kamucheka RM, Alvarado L, Mohammadipoor A, Cancio LC. Short-term physiological hypoxia potentiates the therapeutic function of mesenchymal stem cells. *Stem Cell Res Ther* 2018; **9**: 265 [PMID: 30305185 DOI: 10.1186/s13287-018-1007-x]

52 **Rodriguez LA 2nd**, Mohammadipoor A, Alvarado L, Kamucheka RM, Asher AM, Cancio LC, Antebi B. Preconditioning in an Inflammatory Milieu Augments the Immunotherapeutic Function of Mesenchymal Stromal Cells. *Cells* 2019; **8** [PMID: 31096722 DOI: 10.3390/cells8050462]

53 **Klinker MW**, Marklein RA, Lo Surdo JL, Wei CH, Bauer SR. Morphological features of IFN-γ-stimulated mesenchymal stromal cells predict overall immunosuppressive capacity. *Proc Natl Acad Sci U S A* 2017; **114**: E2598-E2607 [PMID: 28283659 DOI: 10.1073/pnas.1617933114]

54 **Yin JQ**, Zhu J, Ankrum JA. Manufacturing of primed mesenchymal stromal cells for therapy. *Nat Biomed Eng* 2019; **3**: 90-104 [PMID: 30944433 DOI: 10.1038/s41551-018-0325-8]

55 **Dominici M**, Le Blanc K, Mueller I, Slaper-Cortenbach I, Marini F, Krause D, Deans R, Keating A, Prockop Dj, Horwitz E. Minimal criteria for defining multipotent mesenchymal stromal cells. The International Society for Cellular Therapy position statement. *Cytotherapy* 2006; **8**: 315-317 [PMID: 16923606 DOI: 10.1080/14653240600855905]

56 **Meng Y**, Eirin A, Zhu XY, Tang H, Chanana P, Lerman A, van Wijnen AJ, Lerman LO. Obesity-induced mitochondrial dysfunction in porcine adipose tissue-derived mesenchymal stem cells. *J Cell Physiol* 2018; **233**: 5926-5936 [PMID: 29243809 DOI: 10.1002/jcp.26402]

57 **He L**, He T, Farrar S, Ji L, Liu T, Ma X. Antioxidants Maintain Cellular Redox Homeostasis by Elimination of Reactive Oxygen Species. *Cell Physiol Biochem* 2017; **44**: 532-553 [PMID: 29145191 DOI: 10.1159/000485089]

58 **Loboda A**, Damulewicz M, Pyza E, Jozkowicz A, Dulak J. Role of Nrf2/HO-1 system in development, oxidative stress response and diseases: an evolutionarily conserved mechanism. *Cell Mol Life Sci* 2016; **73**: 3221-3247 [PMID: 27100828 DOI: 10.1007/s00018-016-2223-0]

59 **Zhang ZH**, Zhu W, Ren HZ, Zhao X, Wang S, Ma HC, Shi XL. Mesenchymal stem cells increase expression of heme oxygenase-1 leading to anti-inflammatory activity in treatment of acute liver failure. *Stem Cell Res Ther* 2017; **8**: 70 [PMID: 28320485 DOI: 10.1186/s13287-017-0524-3]

60 **Audi SH**, Cammarata A, Clough AV, Dash RK, Jacobs ER. Quantification of mitochondrial membrane potential in the isolated rat lung using rhodamine 6G. *J Appl Physiol (1985)* 2020; **128**: 892-906 [PMID: 32134711 DOI: 10.1152/japplphysiol.00789.2019]

61 **Galleu A**, Riffo-Vasquez Y, Trento C, Lomas C, Dolcetti L, Cheung TS, von Bonin M, Barbieri L, Halai K, Ward S, Weng L, Chakraverty R, Lombardi G, Watt FM, Orchard K, Marks DI, Apperley J, Bornhauser M, Walczak H, Bennett C, Dazzi F. Apoptosis in mesenchymal stromal cells induces in vivo recipient-mediated immunomodulation. *Sci Transl Med* 2017; **9** [PMID: 29141887 DOI: 10.1126/scitranslmed.aam7828]

62 **Pang SHM**, D'Rozario J, Mendonca S, Bhuvan T, Payne NL, Zheng D, Hisana A, Wallis G, Barugahare A, Powell D, Rautela J, Huntington ND, Dewson G, Huang DCS, Gray DHD, Heng TSP. Mesenchymal stromal cell apoptosis is required for their therapeutic function. *Nat Commun* 2021; **12**: 6495 [PMID: 34764248 DOI: 10.1038/s41467-021-26834-3]

63 **He F**, Li Q, Sheng B, Yang H, Jiang W. SIRT1 Inhibits Apoptosis by Promoting Autophagic Flux in Human Nucleus Pulposus Cells in the Key Stage of Degeneration *via* ERK Signal Pathway. *Biomed Res Int* 2021; **2021**: 8818713 [PMID: 33728342 DOI: 10.1155/2021/8818713]

64 **Perlman H**, Zhang X, Chen MW, Walsh K, Buttyan R. An elevated bax/bcl-2 ratio corresponds with the onset of prostate epithelial cell apoptosis. *Cell Death Differ* 1999; **6**: 48-54 [PMID: 10200547 DOI: 10.1038/sj.cdd.4400453]

65 **Salminen A**, Kaarniranta K, Kauppinen A. Exosomal vesicles enhance immunosuppression in chronic inflammation: Impact in cellular senescence and the aging process. *Cell Signal* 2020; **75**: 109771 [PMID: 32896608 DOI: 10.1016/j.cellsig.2020.109771]

66 **Bhujel B**, Shin HE, Choi DJ, Han I. Mesenchymal Stem Cell-Derived Exosomes and Intervertebral Disc Regeneration: Review. *Int J Mol Sci* 2022; **23** [PMID: 35806304 DOI: 10.3390/ijms23137306]

67 **Gonzalez-Pujana A**, Igartua M, Santos-Vizcaino E, Hernandez RM. Mesenchymal stromal cell based therapies for the treatment of immune disorders: recent milestones and future challenges. *Expert Opin Drug Deliv* 2020; **17**: 189-200 [PMID: 31918562 DOI: 10.1080/17425247.2020.1714587]

68 **Sotiropoulou PA**, Perez SA, Gritzapis AD, Baxevanis CN, Papamichail M. Interactions between human mesenchymal stem cells and natural killer cells. *Stem Cells* 2006; **24**: 74-85 [PMID: 16099998 DOI: 10.1634/stemcells.2004-0359]

69 **Spaggiari GM**, Capobianco A, Becchetti S, Mingari MC, Moretta L. Mesenchymal stem cell-natural killer cell interactions: evidence that activated NK cells are capable of killing MSCs, whereas MSCs can inhibit IL-2-induced NK-cell proliferation. *Blood* 2006; **107**: 1484-1490 [PMID: 16239427 DOI: 10.1182/blood-2005-07-2775]

70 **Chatterjee D**, Marquardt N, Tufa DM, Hatlapatka T, Hass R, Kasper C, von Kaisenberg C, Schmidt RE, Jacobs R. Human Umbilical Cord-

Derived Mesenchymal Stem Cells Utilize Activin-A to Suppress Interferon-γ Production by Natural Killer Cells. *Front Immunol* 2014; **5**: 662 [PMID: 25584044 DOI: 10.3389/fimmu.2014.00662]

71 **Sarhan D**, Wang J, Sunil Arvindam U, Hallstrom C, Verneris MR, Grzywacz B, Warlick E, Blazar BR, Miller JS. Mesenchymal stromal cells shape the MDS microenvironment by inducing suppressive monocytes that dampen NK cell function. *JCI Insight* 2020; **5** [PMID: 32045384 DOI: 10.1172/jci.insight.130155]

72 **Chatterjee D**, Marquardt N, Tufa DM, Beauclair G, Low HZ, Hatlapatka T, Hass R, Kasper C, von Kaisenberg C, Schmidt RE, Jacobs R. Role of gamma-secretase in human umbilical-cord derived mesenchymal stem cell mediated suppression of NK cell cytotoxicity. *Cell Commun Signal* 2014; **12**: 63 [PMID: 25266361 DOI: 10.1186/s12964-014-0063-9]

World Journal of Stem Cells

Submit a Manuscript: https://www.f6publishing.com

World J Stem Cells 2023 November 26; 15(11): 1017-1034

DOI: 10.4252/wjsc.v15.i11.1017

ISSN 1948-0210 (online)

ORIGINAL ARTICLE

Basic Study

Dissecting molecular mechanisms underlying ferroptosis in human umbilical cord mesenchymal stem cells: Role of cystathionine γ-lyase/hydrogen sulfide pathway

Bin Hu, Xiang-Xi Zhang, Tao Zhang, Wan-Cheng Yu

Specialty type: Cell and tissue engineering

Provenance and peer review: Unsolicited article; Externally peer reviewed.

Peer-review model: Single blind

Peer-review report's scientific quality classification

Grade A (Excellent): 0
Grade B (Very good): B
Grade C (Good): C, C
Grade D (Fair): D
Grade E (Poor): 0

P-Reviewer: Jaing TH, Taiwan; Ventura C, Italy; Wang Q, China; Li SC, United States

Received: September 2, 2023
Peer-review started: September 2, 2023
First decision: October 19, 2023
Revised: October 25, 2023
Accepted: November 17, 2023
Article in press: November 17, 2023
Published online: November 26, 2023

Bin Hu, Xiang-Xi Zhang, Tao Zhang, Wan-Cheng Yu, Department of Cardiovascular Surgery, Shandong Provincial Hospital Affiliated to Shandong First Medical University, Jinan 250062, Shandong Province, China

Corresponding author: Wan-Cheng Yu, Doctor, MD, Postdoc, Surgeon, Department of Cardiovascular Surgery, Shandong Provincial Hospital Affiliated to Shandong First Medical University, No. 324 Jingwu Weiqi Road, Jinan 250062, Shandong Province, China.
yuwancheng123@126.com

Abstract

BACKGROUND

Ferroptosis can induce low retention and engraftment after mesenchymal stem cell (MSC) delivery, which is considered a major challenge to the effectiveness of MSC-based pulmonary arterial hypertension (PAH) therapy. Interestingly, the cystathionine γ-lyase (CSE)/hydrogen sulfide (H_2S) pathway may contribute to mediating ferroptosis. However, the influence of the CSE/H_2S pathway on ferroptosis in human umbilical cord MSCs (HUCMSCs) remains unclear.

AIM

To clarify whether the effect of HUCMSCs on vascular remodelling in PAH mice is affected by CSE/H_2S pathway-mediated ferroptosis, and to investigate the functions of the CSE/H_2S pathway in ferroptosis in HUCMSCs and the underlying mechanisms.

METHODS

Erastin and ferrostatin-1 (Fer-1) were used to induce and inhibit ferroptosis, respectively. HUCMSCs were transfected with a vector to overexpress or inhibit expression of CSE. A PAH mouse model was established using 4-wk-old male BALB/c nude mice under hypoxic conditions, and pulmonary pressure and vascular remodelling were measured. The survival of HUCMSCs after delivery was observed by *in vivo* bioluminescence imaging. Cell viability, iron accumulation, reactive oxygen species production, cystine uptake, and lipid peroxidation in HUCMSCs were tested. Ferroptosis-related proteins and S-sulfhydrated Kelch-like ECH-associating protein 1 (Keap1) were detected by western blot analysis.

RESULTS

In vivo, CSE overexpression improved cell survival after erastin-treated HUCMSC delivery in mice with hypoxia-induced PAH. *In vitro*, CSE overexpression improved H_2S production and ferroptosis-related indexes, such as cell viability, iron level, reactive oxygen species production, cystine uptake, lipid peroxidation, mitochondrial membrane density, and ferroptosis-related protein expression, in erastin-treated HUCMSCs. In contrast, *in vivo*, CSE inhibition decreased cell survival after Fer-1-treated HUCMSC delivery and aggravated vascular remodelling in PAH mice. *In vitro*, CSE inhibition decreased H_2S levels and restored ferroptosis in Fer-1-treated HUCMSCs. Interestingly, upregulation of the CSE/H_2S pathway induced Keap1 S-sulfhydration, which contributed to the inhibition of ferroptosis.

CONCLUSION

Regulation of the CSE/H_2S pathway in HUCMSCs contributes to the inhibition of ferroptosis and improves the suppressive effect on vascular remodelling in mice with hypoxia-induced PAH. Moreover, the protective effect of the CSE/H_2S pathway against ferroptosis in HUCMSCs is mediated *via* S-sulfhydrated Keap1/nuclear factor erythroid 2-related factor 2 signalling. The present study may provide a novel therapeutic avenue for improving the protective capacity of transplanted MSCs in PAH.

Key Words: Human umbilical cord mesenchymal stem cells; Cystathionine γ-lyase/hydrogen sulfide pathway; Ferroptosis; Pulmonary arterial hypertension; S-sulfhydration

Core Tip: Regulation of the cystathionine γ-lyase (CSE)/hydrogen sulfide (H_2S) pathway in human umbilical cord mesenchymal stem cells (HUCMSCs) contributes to the inhibition of ferroptosis and improves the suppressive effect of HUCMSCs on vascular remodelling in hypoxia-induced pulmonary arterial hypertension (PAH) mice. Moreover, the protective effect of the CSE/H_2S pathway against ferroptosis in HUCMSCs was mediated *via* S-sulfhydrated Kelch-like ECH-associating protein 1/nuclear factor erythroid 2-related factor 2 signalling. The present study may provide a novel therapeutic avenue for improving the protective capacity of transplanted MSCs in PAH.

Citation: Hu B, Zhang XX, Zhang T, Yu WC. Dissecting molecular mechanisms underlying ferroptosis in human umbilical cord mesenchymal stem cells: Role of cystathionine γ-lyase/hydrogen sulfide pathway. *World J Stem Cells* 2023; 15(11): 1017-1034
URL: https://www.wjgnet.com/1948-0210/full/v15/i11/1017.htm
DOI: https://dx.doi.org/10.4252/wjsc.v15.i11.1017

INTRODUCTION

Mesenchymal stem cells (MSCs), derived from placenta, bone marrow, adipose, or other tissues, have emerged as a new regenerative therapy for pulmonary arterial hypertension (PAH) over the last decade[1]. MSC delivery significantly inhibits pulmonary artery remodelling, resulting in the reduced progression of PAH. However, low cell retention and engraftment after cell delivery are considered major challenges to the effectiveness of MSC-based therapy[2]. Interestingly, increasing evidence indicates that programmed cell death (PCD) is closely linked to the low engraftment and survival rates of transplanted MSCs[3].

Ferroptosis is a novel type of PCD with distinct properties. Ferroptosis essentially consists of polyunsaturated fatty acid-containing phospholipid synthesis and peroxidation, iron metabolism, and mitochondrial metabolism, which result in oxidative stress and lipid peroxidation, triggering cell death[4]. Studies have shown a relationship between ferroptosis and MSCs; ferroptosis can be induced by erastin in MSCs[5,6]. Inhibiting ferroptosis maintained the viability and differentiation of MSCs[7,8]. Moreover, suppressing ferroptosis worsened MSC fate and enhanced the exposure and efficacy of transplanted MSCs in live disease[9]. However, few studies have directly evaluated the effect of ferroptosis on MSC delivery in PAH.

Decreased antioxidative stress can cause ferroptosis[10]. In addition, the mediation of antioxidative stress-related proteins, such as nuclear factor erythroid 2-related factor 2 (Nrf2), can inhibit ferroptosis[11]. Thus, understanding the signalling pathways that maintain redox balance will provide new approaches for inhibiting ferroptosis. The novel gaseous mediator hydrogen sulfide (H_2S) has been shown to exert protective effects, including its antioxidant properties [12]. Therefore, the impact of H_2S on the contribution of antioxidative stress to decreased ferroptosis is worth exploring. In mammalian cells, cystathionine γ-lyase (CSE) is predominantly responsible for endogenous H_2S production in the cardiovascular system[13]. However, the effect of CSE on the ferroptosis of MSCs remains unclear.

Hence, the present study aimed to clarify whether ferroptosis is involved in the therapeutic effect of human umbilical cord MSCs (HUCMSCs) in PAH mice. Furthermore, we investigated the role of the CSE/H_2S pathway in ferroptosis in HUCMSCs.

MATERIALS AND METHODS

Cell culture

Primary HUCMSCs were purchased from ScienCell Research Laboratories, Inc. HUCMSCs were cultured in MSC medium (7501, ScienCell Research Laboratories, United States) containing 5% foetal bovine serum, 1% penicillin/streptomycin, and 1% MSC growth supplement at 37 °C in a 5% CO_2 atmosphere. HUCMSCs at passages three to five were used in this study.

Cell transfection

HUCMSCs were transduced with a lentiviral vector expressing firefly luciferase (HBLV-LUC-BSD, Hanbio, China) in serum-free medium containing 3 μg/mL blasticidin (SBR00022, Sigma-Aldrich, United States) at a multiplicity of infection of 100. Transduction was analysed by luciferase imaging 72 h after transfection. The expression of LUC was confirmed by measuring luciferase activity [*in vivo* imaging system (IVIS) Lumina imaging station, Caliper Life Sciences]. Surface markers and the differentiation of HUCMSCs-LUC into osteoblasts and adipocytes were evaluated as previously described[14]. The antibodies that were used are shown in Supplementary Table 1.

Short hairpin RNAs targeting CSE were designed, cloned, and inserted into a modified pLKO.1-TRC vector by GenePharma Co. Ltd. (Shanghai, CHN). To genetically engineer cells to overexpress CSE, the open reading frame of human CSE was cloned and inserted into the vector pLVX-IRES-Puro by GenePharma Co. Ltd. (Shanghai, CHN). HUCMSCs-LUC were transfected with the PLKO.1-sh-CSE vector (HUCMSC/sh-CSE), negative control vector (HUCMSCs/sh-NC), PLVX-CSE-Puro vector (HUCMSCs/CSE), or PLVX-empty-Puro vector (HUCMSCs/NC) using Lipofectamine 2000 (11668019, Invitrogen, United States). After 48 h, the transfection efficacy was determined using western blot and real-time polymerase chain reaction (RT-PCR) (Supplementary Figure 1).

Drug treatments

Erastin (S7242), ferrostatin-1 (Fer-1, S7243), and the Nrf2 inhibitor brusatol (S7956, 10 nM, 6 h) were purchased from Selleck Chemicals (Houston, United States) and initially dissolved in DMSO before being diluted in the culture medium to their final concentration.

Quantification of cell viability

Cell Counting Kit-8 (CCK8, 96992, Sigma-Aldrich, United States) was used to examine cell viability according to the manufacturer's instructions. Briefly, cells were seeded at a density of 5000 cells/well in 96-well plates in three replicates and incubated overnight. At the end of the different treatments, CCK8 reagent was added to each well and incubated for 2 h. The optical density (OD) values at 450 nm were measured using a plate reader (Bio-Rad).

Lactase dehydrogenase release assay

Lactate dehydrogenase (LDH) release was measured using an LDH cytotoxicity detection kit (CK12, Dojindo Laboratory, JPN) in accordance with the manufacturer's instructions to evaluate cell membrane integrity. In brief, cells were seeded at a density of 5000 cells/well in 96-well plates. At the end of the different treatments, 100 μL of fresh reaction mixture was added to each well and incubated for 30 min, and the OD values at 490 nm were measured using a microplate reader.

Animal experiments

Animal procedures were performed in compliance with the Institutional Animal Care and Use Committee of Wuhan Servicebio Technology Co., Ltd., China (No. 2022231). Four-week-old male mice (BALB/c nude mice) were used to establish a hypoxia-induced PAH mouse model. The mice were obtained from Wuhan Servicebio Technology Co., Ltd. (Wuhan, China) and cared for in strict accordance with the Guidelines for the Care and Use of Laboratory Animals of the National Institutes of Health. All animals were housed in the same specific pathogen-free room under a constant temperature and humidity on a 12-h light and 12-h dark cycle, and the animals were fed sterile food and water *ad libitum*. Each animal was considered one experimental unit. Researchers who analysed the data were blinded to the group allocation until all the statistical results were finally obtained.

The mice (totally 42) were numbered and divided into the following seven groups based on a table of random numbers: Control group: The mice received phosphate buffered saline (PBS) (n = 6); hypoxia group: The mice were exposed to hypoxia under 10% O_2 for 4 wk (n = 6); HUCMSCs group: After 2 wk of exposure to hypoxia, the mice were injected with 1.5 × 10^5 HUCMSCs-LUC per mouse *via* the tail vein and then housed under hypoxia for 2 wk (n = 6); HUCMSCs + erastin group: After 2 wk of exposure to hypoxia, the mice were infected with 1.5 × 10^5 HUCMSCs-LUC that were treated with erastin (4 μM, 6 h) per mouse *via* the tail vein and then housed under hypoxia for 2 wk (n = 6); HUCMSCs/CSE + erastin group: After 2 wk of exposure to hypoxia, the mice were injected with 1.5 × 10^5 HUCMSCs-LUC/CSE that were treated with erastin (4 μM, 6 h) per mouse *via* the tail vein and then housed under hypoxia for 2 wk (n = 6); HUCMSCs + Fer-1 group: After 2 wk of exposure to hypoxia, the mice were injected with 1.5 × 10^5 HUCMSCs-LUC that were treated with Fer-1 (4 μM, 6 h) per mouse *via* the tail vein and then housed under hypoxia for 2 wk (n = 6); and HUCMSCs/sh-CSE + Fer-1 group: After 2 wk of exposure to hypoxia, the mice were injected with 1.5 × 10^5 HUCMSCs-LUC/sh-CSE that were treated with Fer-1 (4 μM, 6 h) per mouse *via* the tail vein and then housed under hypoxia for 2 wk (n = 6).

One day and seven days after intravenous injection *via* the tail, mice were anaesthetized using isoflurane and placed in an IVIS Lumina imaging station. Images of regions of interest were collected 10 min after the intraperitoneal injection of D-luciferin (L6152, Sigma-Aldrich, United States), the luciferase substrate, at 3.75 mg per 25 g mouse weight.

Measurement of pulmonary artery pressure and right ventricular hypertrophy

After 4 wk, the mice were anaesthetized using isoflurane for haemodynamic assessment. Briefly, a Miler catheter was used to obtain the right ventricular systolic pressure (RVSP) *via* insertion into the right external jugular vein. After exsanguination and collection of the blood, the cardiopulmonary tissues were removed. The right ventricle (RV) free wall and the left ventricle plus septum (LV + S) were weighed separately. The degree of right ventricular hypertrophy was determined by the ratio RV/(LV + S).

Assessment of pulmonary vascular morphometry

After the lung tissue was embedded in paraffin and cut into slices with a thickness of 5 μm, the slices were dewaxed, rehydrated, and stained with haematoxylin and eosin staining. Then, the ratio of the vascular medial cross-sectional area to the total arterial cross-sectional area was calculated as a measurement of distant small pulmonary artery (50-100 μm) remodelling.

For immunofluorescence staining of the lung tissue, after deparaffinization and washing with PBST, lung tissue slides were heated for 20 min at 95 °C in a Tris-EdTA solution for antigen retrieval and then blocked with 3% H_2O_2 for 15 min to block endogenous peroxidase activity and 5% goat serum for 1 h to eliminate nonspecific staining. These slides were incubated with VEcadherin rabbit polyclonal antibody (1:100, ab205336, Abcam) and alpha-smooth muscle actin rabbit monoclonal antibody (1:100, 19245S, CST) at 4 °C overnight and then incubated with the secondary antibody: Antirabbit immunoglobulin G (IgG) (1:500, 4413s, CST) or antirabbit IgG (1:500, 4412S, CST). Nuclei were counterstained with DAPI (D9542, Sigma-Aldrich, United States) at room temperature for another 2 min. Immunofluorescence was visualized under a microscope.

Analysis of cell apoptosis

After treatment, the cells were washed, trypsinized, resuspended, and stained with 5 μL of Annexin V/FITC (331200, Invitrogen, United States) and 5 μL of propidium iodide (PI, P1304MP, Invitrogen, United States) at room temperature for 15 min. Then, cell apoptosis was evaluated by flow cytometry.

Iron assays

Two different methods were used to measure the levels of intracellular ferrous iron. For a colorimetric method using the Iron Assay Kit (ab83366, Abcam, United Kingdom), cells were collected, homogenized (in cold iron assay buffer), and centrifuged. After adding 5 μL of iron reducer to each sample, the supernatant was incubated for 30 min at 37 °C. Next, 100 μL of iron probe was added to each sample and incubated for 60 min at 37 °C in the dark. The absorbance at 593 nm was measured using a microplate reader. For FeRhoNox-1 staining, cells were incubated away from light in a 37 °C, 5% CO_2 incubator for 40 min after the addition of 5 μM FeRhoNox-1 (MX4558, MKbio, CHN). Then, the cells were washed with PBS three times and imaged by fluorescence microscopy.

Reactive oxygen species assay

Intracellular reactive oxygen species (ROS) levels were measured by applying DCFH-DA (S0033, Beyotime, CHN). Briefly, after treatment, the cells were washed with PBS three times and treated with 10 μM DCFH-DA for 30 min away from light. Then, the cells were washed with PBS and observed under a fluorescence microscope.

Lipid peroxide measurement

Cells were labelled with BODIPY™ 581/591 C11 (D3861, Thermo Fisher Scientific, United States) at a final concentration of 2 μM for 20 min at 37 °C. After trypsinization and resuspension in PBS, lipid peroxidation was analysed using a flow cytometer. A lipid peroxidation [malonaldehyde (MDA)] assay (ab118970, Abcam, United Kingdom) was used according to the manufacturer's protocol to quantify the MDA concentration. The results were quantified colorimetrically (OD = 532 nm). The reduced glutathione/oxidized glutathione disulfide (GSH/GSSG) ratio in cells was determined using the GSH/GSSG Ratio Detection Assay Kit (ab205811, Abcam, United Kingdom) following the manufacturer's instructions.

Cystine uptake

Cystine uptake was measured with BioTracker Cystine-FITC Live Cell Dye (SCT047, Sigma-Aldrich, United States). The pretreated cells were incubated with complete medium containing 5 μM cystine-FITC in the dark for 30 min. Then, the cells were washed with PBS and harvested by trypsinization. The cells were resuspended in PBS and assessed by flow cytometry.

Transmission electron microscopy

Cells were fixed, postfixed, dehydrated, cut, and stained as previously described[15]. The cells were viewed under a transmission electron microscope (JEM1200, Tokyo, Japan), and images were taken.

Measurement of the H_2S concentration

The dye 7-azido-4-methylcoumarin (AzMC) was used to measure the H_2S concentration *in vitro*. Cells were plated at a density of 10000 cells per well in 96-well plates. After treatment, cells were loaded with the fluorogenic dye AzMC (802409, Sigma-Aldrich, United States) at 10 μM for 30 min. Then, the cells were washed three times with PBS and measured on a SpectraMax M5 plate reader.

Nrf2 activity assay

Nuclear lysates were isolated following extraction using NE-PER Nuclear and Cytoplasmic Extraction Reagents (78835, Thermo Fisher Scientific, United States) according to the manufacturer's instructions. Nrf2 transcriptional activity was then measured by ELISA using an Nrf2 Transcription Factor Assay Kit (ab207223, Abcam, United Kingdom) in accordance with the manufacturer's guidelines.

S-sulfhydration assay

Kelch-like ECH-associating protein 1 (Keap1) S-sulfhydration was detected with standard procedures using the "tag-switch" method[16]. The Keap1 protein was pulled down by immunoprecipitation. The proteins were dissolved in solution buffer, purified with streptavidin-agarose beads, and subjected to western blotting with anti-Keap1 (sc-365626, Santa Cruz Biotechnology, United States). Cells were treated with 1 mmol/L 1,4-dithio-DL-threitol (DTT, 43815, Sigma-Aldrich, United States) for 3 h as a negative control group.

Quantitative real-time polymerase chain reaction

qPCR was performed as previously described[15,17]. Human GAPDH expression was used for normalization. Fold changes were calculated using the comparative Ct method (ΔΔCt). The sequences of the primers used are as follows: CSE: Forward: GGCCTGGTGTCTGTTAATTGT and reverse: GCCATTCCGTTTTTGAAATGCT; GAPDH: forward: GACATCAAGAAGGTGGTGAAGCAGG and reverse: GTGTCGCTGTTGAAGTCAGAGGAGA.

Western blot analysis

Whole-cell, cytosolic, and nuclear proteins were extracted using RIPA Lysis and Extraction Buffer (89900, Thermo Fisher Scientific, United States) or NE-PER Nuclear and Cytoplasmic Extraction Reagents (78835, Thermo Fisher Scientific, United States). The extractions were performed as previously described[17]. Primary antibodies against the following were used: Glutathione peroxidase 4 (GPX4, 1:1000, 59735S, CST), intracellular ferritin heavy chain 1 (FTH1, 1:1000, 4393S, CST), nuclear receptor coactivator 4 (NOCA4, 1:1000, 66849S, CST), Fe^{3+}-bound transferrin receptor 1 (TFRC1, 1:1000, ab214039, Abcam), 4-hydroxynonenal (4-HNE, 1:1000, ab46545, Abcam), SLC7A11 (1:1000, ab175186, Abcam), Nrf2 (1:1000, ab62352, Abcam), Keap1 (sc-365626, Santa Cruz Biotechnology), CSE (1:1000, 19689S, CST), GAPDH (1:1000, 5174S, CST), and Histone H3 (1:1000, ab1791, Abcam). The intensity of the resulting bands was analysed with ImageJ software.

Statistical analysis

All experimental data are presented as the mean ± SEM. Statistical significance was analysed with GraphPad Prism version 5.01 (San Diego, CA, United States) using one-way analysis of variance (ANOVA). Differences at $P < 0.05$ were considered statistically significant. All experiments were performed with at least three independent replicates.

RESULTS

In vitro assessment of HUCMSCs

HUCMSCs-LUC were analysed *in vitro* by bioluminescence imaging (BLI), cell morphology assessment, flow cytometry, and differentiation potential determination to confirm the properties typical of HUCMSCs. A linear relationship between the number of cells and the bioluminescent signal was observed (Figure 1A). Cells displayed a spindle-like shape and were arranged in radial concentric circles (Figure 1B). Adipogenic and osteogenic differentiation confirmed the multipotentiality and differentiation capacity of the HUCMSCs-LUC (Figure 1B). Flow cytometry confirmed the presence of the following stem cell-specific molecules on the cell surface: CD90 in 94.25% of the cells, CD73 in 83.35%, CD105 in 90.18%, CD44 in 82.16%, CD34 in 0.21%, CD45 in 0.45%, and HLA-DR in 1.36% (Figure 1C).

Ferroptosis could be induced in HUCMSCs

To verify whether ferroptosis could be induced in HUCMSCs and to ascertain the optimal concentration and time, HUCMSCs were exposed to increasing doses (1 μM, 2 μM, 3 μM, 4 μM, and 5 μM) of erastin, a ferroptosis inducer, for three different durations (12 h, 24 h, and 48 h). As shown in Figures 2A-C, the CCK-8 assay illustrated that compared to that in untreated cells, cellular viability was notably reduced to 50% by erastin treatment at concentrations greater than 3 μM for less than 24 h of exposure. In addition, because cell membrane structures can be destroyed by ferroptosis, which leads to the release of LDH from the cytoplasm into the culture medium[18], the levels of LDH in the supernatant were monitored after treatment with increasing erastin concentrations for 12 h, 24 h, and 48 h (Figures 2E-G). The results showed that LDH release increased in a time- and dose-dependent manner. Similarly, treatment with erastin at a concentration greater than 3 μM for 24 h significantly increased LDH release to about 50% compared with that of the untreated HUCMSCs. Thus, HUCMSCs were treated with erastin at a concentration of 3 μM for 24 h in subsequent experiments.

Fer-1 was used to determine whether ferroptosis inhibition could protect HUCMSCs from erastin-induced cell death. Erastin-treated HUCMSCs were cotreated with Fer-1 at concentrations of 0, 2, 4, 6, and 8 μM for 24 h. As shown in Figures 2D and H, Fer-1 above 4 μM had a significant protective effect over treatment without Fer-1.

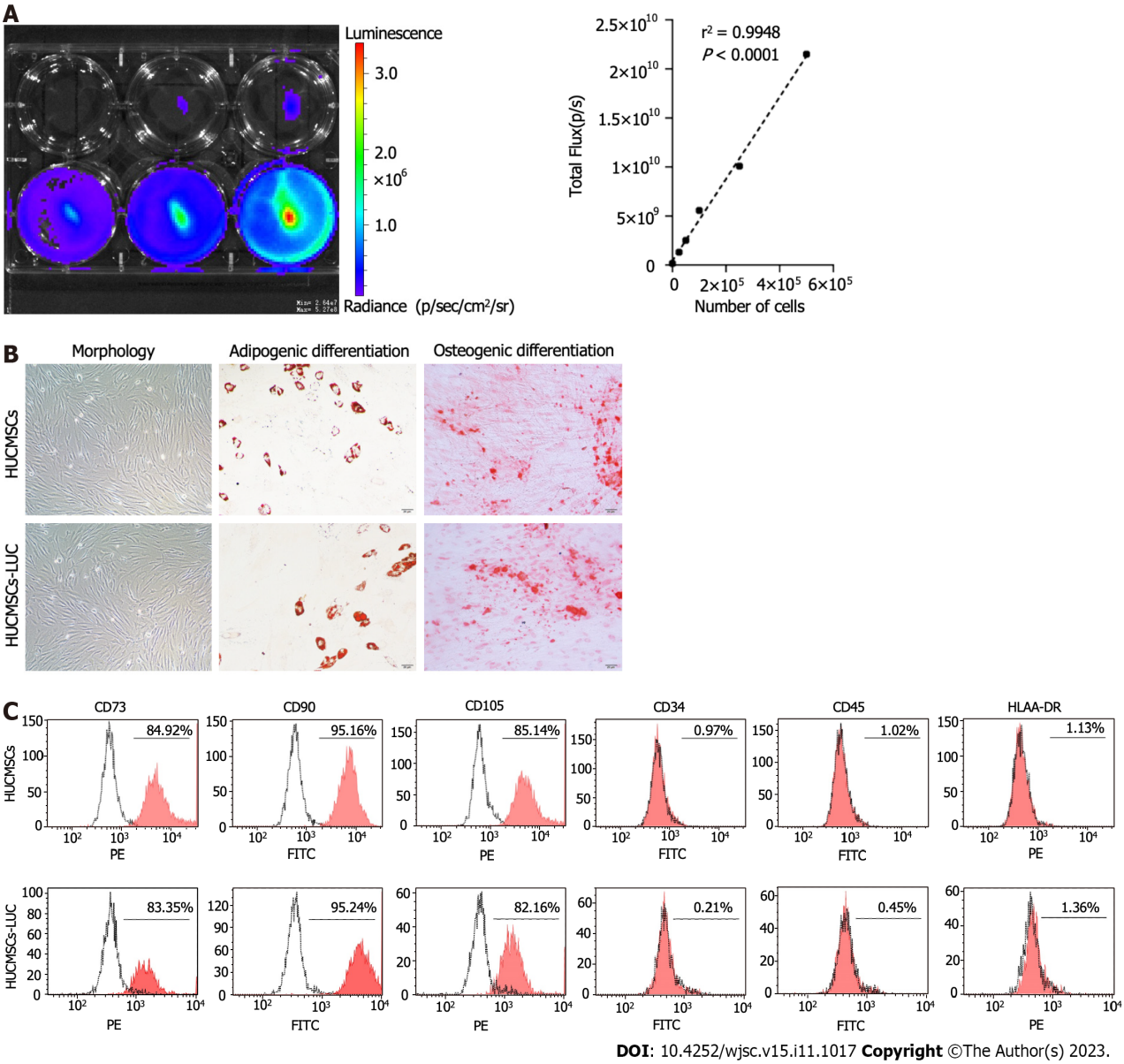

DOI: 10.4252/wjsc.v15.i11.1017 **Copyright** ©The Author(s) 2023.

Figure 1 Characteristics of human umbilical cord mesenchymal stem cells expressing firefly luciferase gene. A: Luciferase activity of human umbilical cord mesenchymal stem cells expressing firefly luciferase gene (HUCMSCs-LUC). Representative luciferase imaging is shown using *in vivo* imaging system; B: Morphologies of HUCMSCs-LUC. HUCMSCs-LUC differentiated into adipocytes (stained with oil red O for lipid droplets) and osteocytes (stained with alizaline red for mineral deposition); C: Surface marker expression of HUCMSCs-LUC in flow cytometry analysis. HUCMSCS: Human umbilical cord mesenchymal stem cells; HUCMSCs-LUC: Human umbilical cord mesenchymal stem cells expressing firefly luciferase gene; PE: Phycoerythrin; FITC: Fluorescein isothiocyanate.

Longitudinal in vivo BLI of HUCMSC grafts

After 1.5 × 10^5 HUCMSCs-LUC were grafted in each mouse, longitudinal *in vivo* BLI was performed on day 1 post-implantation. For quantitative analysis of the observed BLI signals, cell graft-specific BLI signals from fixed regions on the mouse chest and the mean background BLI signals from fixed control regions on the mouse head were plotted *vs* time post-implantation (Figure 3A). The BLI signal was decreased in the HUCMSCs + erastin group and increased in the HUCMSCs + Fer-1 group compared to the HUCMSCs group (Figure 3B). In addition, the signal was further increased in the HUCMSCs/CSE + erastin group but decreased in the HUCMSCs/sh-CSE + Fer-1 group (Figure 3B).

Pulmonary artery remodelling in each group

In PAH, pulmonary artery remodelling results in progressively elevated pulmonary arterial pressure, which ultimately leads to right heart failure[19]. As shown in Figures 3C, F, G, and I, the administration of HUCMSCs or HUCMSCs + Fer-1 decreased the RVSP and RV/(LV + S) ratio in mice with hypoxia-induced PAH ($P < 0.01$). Interestingly, compared to those in the HUCMSCs group, the RVSP and RV/(LV + S) decreased to a greater extent in the HUCMSCs + Fer-1 group (17.000 ± 2.215 *vs* 22.280 ± 3.115, 23.376 ± 0.537 *vs* 28.781 ± 2.311, both $P < 0.01$) and increased in the HUCMSCs + erastin group (34.363 ± 4.065 *vs* 22.280 ± 3.115, 39.158 ± 0.809 *vs* 28.781 ± 2.311, both $P < 0.01$). Moreover, compared to those in the HUCMSCs + erastin group, the RVSP and RV/(LV + S) were decreased in the HUCMSCs/CSE + erastin group (25.817 ± 2.843 *vs* 34.363 ± 4.065, 33.082 ± 2.405 *vs* 39.158 ± 0.809, both $P < 0.01$). Furthermore, the RVSP and RV/(LV + S) were

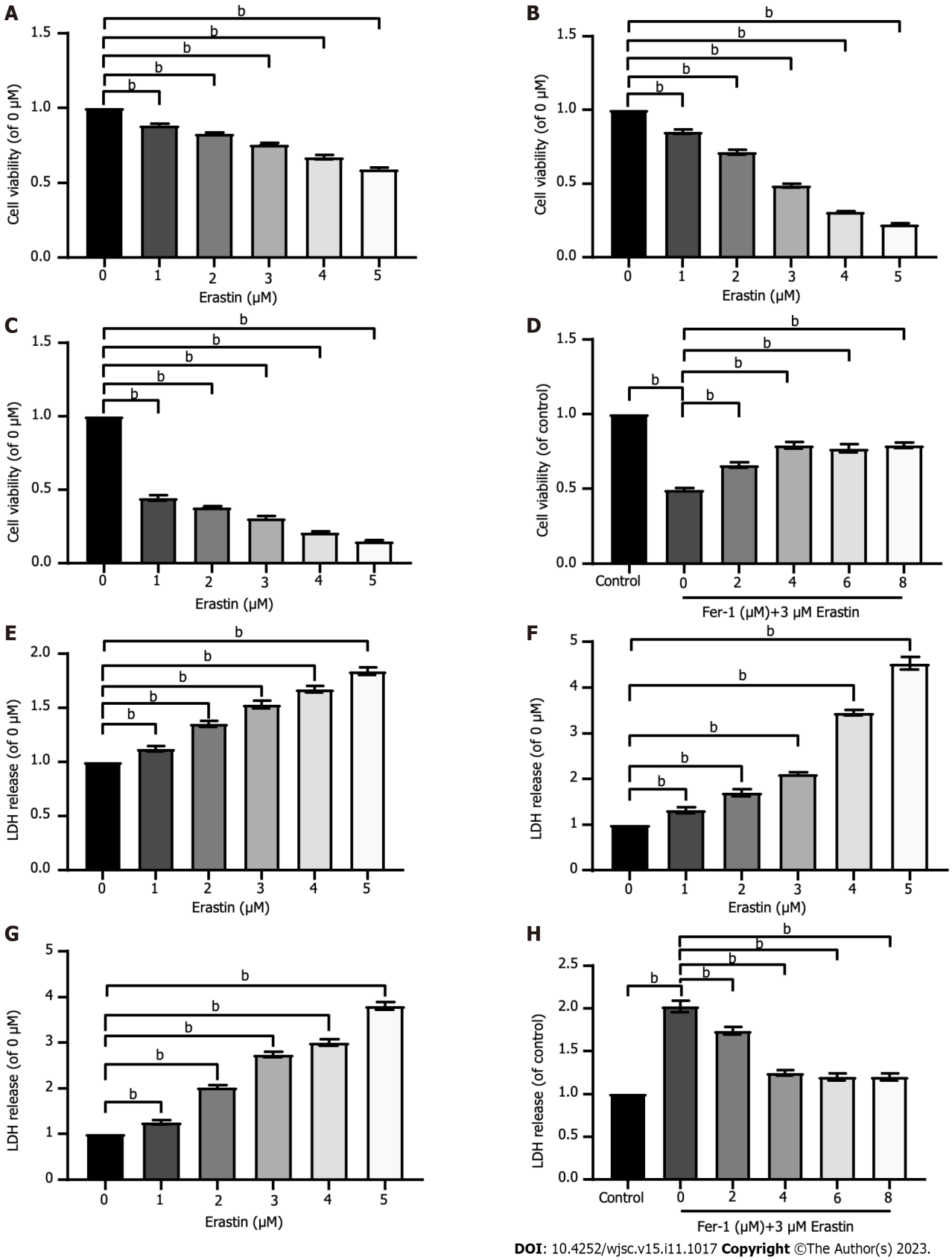

DOI: 10.4252/wjsc.v15.i11.1017

Figure 2 Ferroptosis exists in human umbilical cord mesenchymal stem cells. A-C: Cell viability was assessed after exposure to different concentrations of erastin for different times (12 h, 24 h, and 48 h); D: Cell viability was assessed after exposure to 3 μM erastin and different concentrations of ferrostatin-1 (Fer-1). Cell viability was measured with Cell Counting Kit-8 kit; E-G: Lactic dehydrogenase (LDH) release was assessed after exposure to different concentrations of erastin for different times (12 h, 24 h, and 48 h); H: LDH release was assessed after exposure to 3 μM erastin and different concentrations of Fer-1. LDH release was measured with LDH cytotoxicity detection kit. The data were from at least three independent experiments. Data were quantified for cells subjected to erastin (0 μM), and values are represented as the mean ± SD. Fer-1: Ferrostatin-1; LDH: Lactic dehydrogenase. $^{b}P < 0.01$.

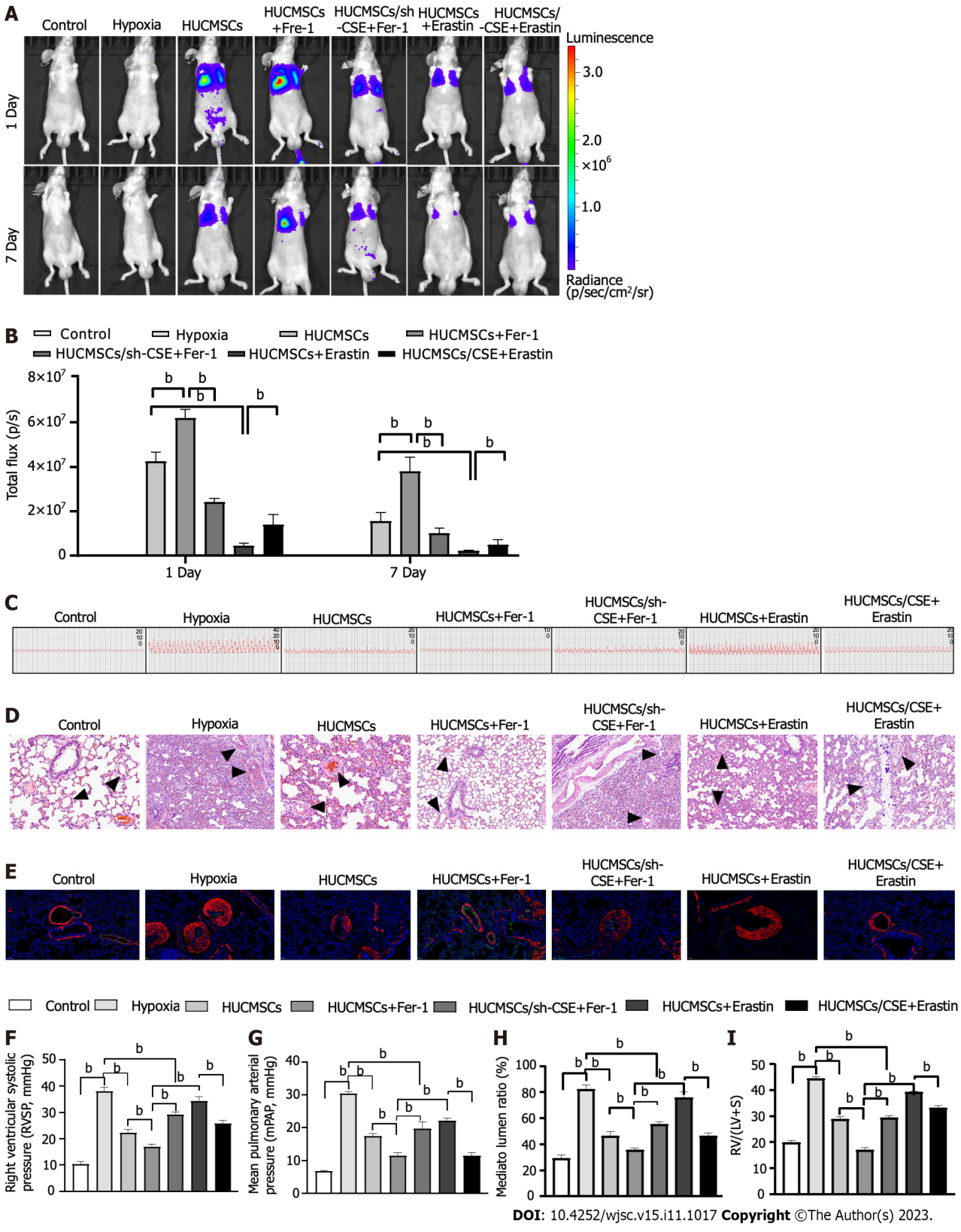

DOI: 10.4252/wjsc.v15.i11.1017

Figure 3 Change of pulmonary arterial remodeling. A: *In vivo* bioluminescence imaging (BLI). Representative time course image showing *in vivo* BLI of mice grafted with living human umbilical cord mesenchymal stem cells expressing firefly luciferase gene in the lungs. Images were acquired at 24 h and 7 d post-implantation. Regions of interest are drawn on the mouse lung and on the mouse shoulder, considered as background signal; B: *In vivo* BLI. Quantitative analysis of *in vivo* BLI at days 1 and 7 post-implantation; C-H: Representing pulmonary arterial pressure (C, F, and G). Representative haematoxylin and eosin-stained lung sections and quantification of the ratio of the medial wall area to the total vessel cross sectional area of the distal pulmonary artery sections (D and H). Immunofluorescent staining (E). Green fluorescence represents VEcadherin, red fluorescence represents alpha-smooth muscle actin, and blue fluorescence indicates 4',6-diamidino-2-phenylindole nuclear staining; I: Right ventricle/left ventricle plus septum. Data are expressed as the mean ± SEM (n = 6/group). HUCMSCS: Human umbilical cord mesenchymal stem cells; Fer-1: Ferrostatin-1; CSE: Cystathionine γ-lyase; RV/(LV + S): Right ventricle/(left ventricle plus septum). $^{b}P < 0.01$.

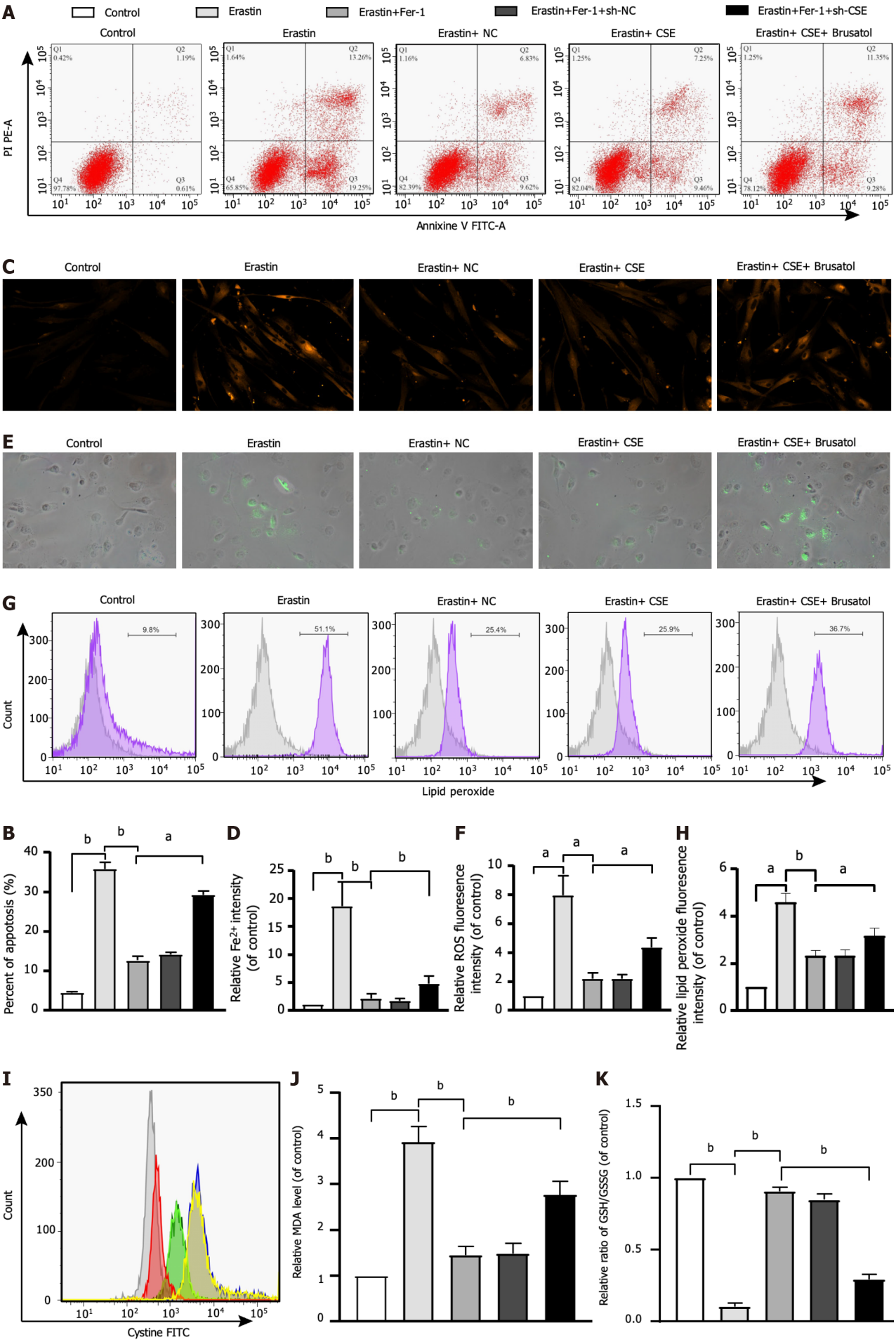
A
Control
Erastin
Erastin+Fer-1
Erastin+Fer-1+sh-NC
Erastin+Fer-1+sh-CSE
Control
Erastin
Erastin+ NC
Erastin+ CSE
Erastin+ CSE+ Brusatol
PI PE-A
Annixine V FITC-A
C
Control
Erastin
Erastin+ NC
Erastin+ CSE
Erastin+ CSE+ Brusatol
E
Control
Erastin
Erastin+ NC
Erastin+ CSE
Erastin+ CSE+ Brusatol
G
Control
Erastin
Erastin+ NC
Erastin+ CSE
Erastin+ CSE+ Brusatol
9.8%
51.1%
25.4%
25.9%
36.7%
Count
Lipid peroxide
B
Percent of appotosis (%)
D
Relative Fe2+ intensity (of control)
F
Relative ROS fluoresence intensity (of control)
H
Relative lipid peroxide fluoresence intensity (of control)
I
Count
Cystine FITC
J
Relative MDA level (of control)
K
Relative ratio of GSH/GSSG (of control)

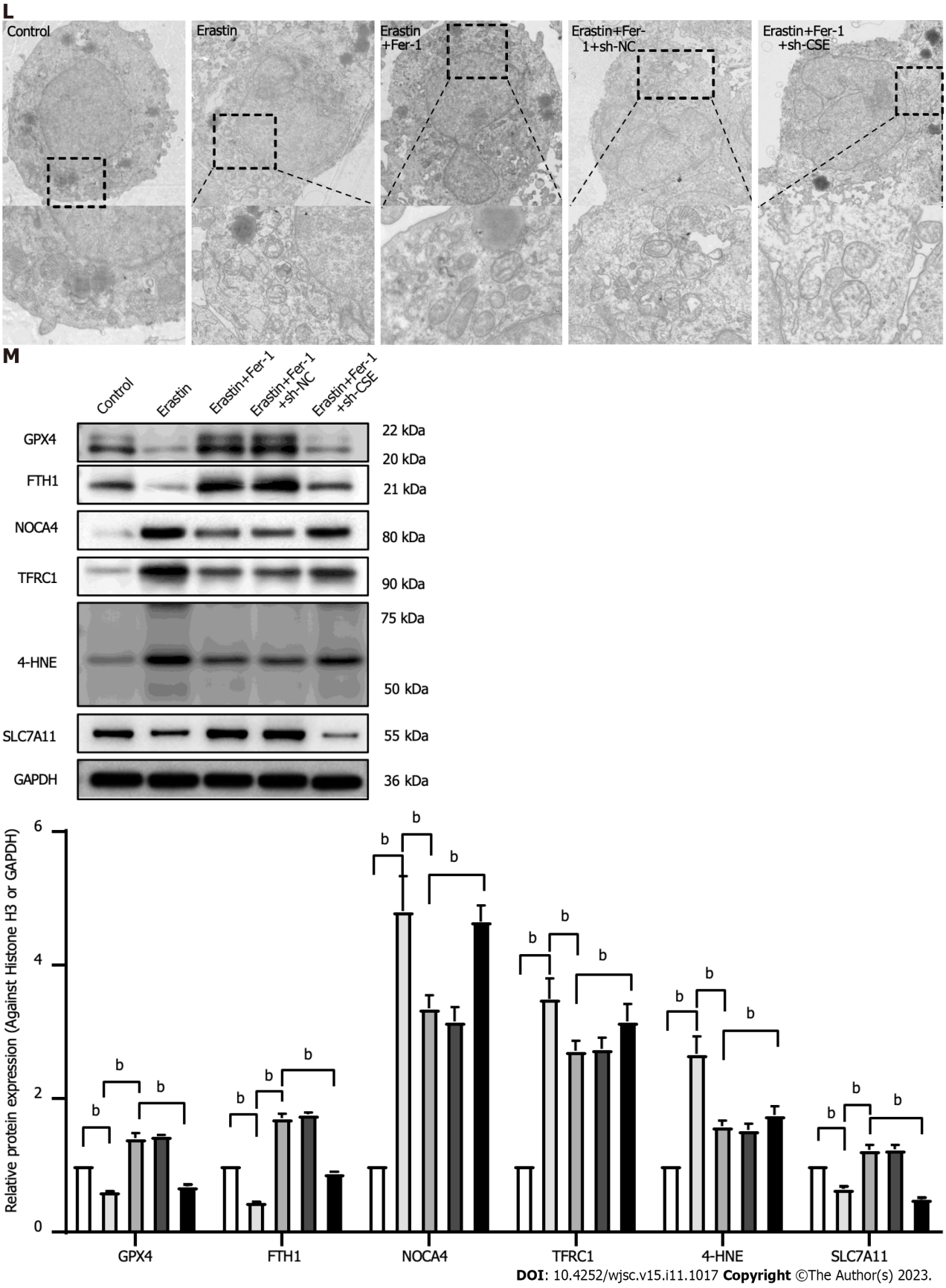

DOI: 10.4252/wjsc.v15.i11.1017

Figure 4 Effect of cystathionine γ-lyase overexpression on ferroptosis in human umbilical cord mesenchymal stem cells. A and B: Cell apoptosis was analyzed by Annexin V-fluorescein isothiocyanate (FITC)/propidine iodide staining using flow cytometry analysis (n = 3), and quantified on the basis of apoptosis rate (n = 3); C and D: Iron level was detected by FeRhoNox-1 staining (C) and iron assay kit (D); E and F: Immunofluorescent staining of total reactive oxygen species; G and H: Level of lipid peroxidation detected by flow cytometry analysis after staining with C11-BODIPY; I: Intracellular cystine-FITC levels measured by flow cytometry. Results represent three independent experiments; J: Malonaldehyde level; K: Ratio of reduced glutathione/oxidized glutathione disulfide;

L: Mitochondrial morphological changes detected by transmission electron microscopy; M: Western blot analysis of expression of the glutathione-dependent antioxidant enzyme glutathione peroxidase, ferritin heavy chain 1, nuclear receptor coactivator 4, Fe^{3+}-bound transferrin receptor 1, 4-hydroxynonenal, and SLC7A11 protein. Glyceraldehyde-3-phosphate dehydrogenase was used for normalization for protein (n = 3). Fer-1: Ferrostatin-1; Annexin V-FITC/PI: Annexin V-fluorescein isothiocyanate/propidine iodide; ROS: Reactive oxygen species; sh-CSE: Short hairpin RNA targeting cystathionine γ-lyase; MDA: Malonaldehyde; GSH/GSSG: Reduced glutathione/oxidized glutathione disulfide; GPX4: Glutathione-dependent antioxidant enzyme glutathione peroxidase; FTH1: Ferritin heavy chain 1; NCOA4: Nuclear receptor coactivator 4; TFRC1: Fe^{3+}-bound transferrin receptor 1; 4-HNE: 4-hydroxynonenal; GAPDH: Glyceraldehyde-3-phosphate dehydrogenase. $^{a}P < 0.05$, $^{b}P < 0.01$.

increased in the HUCMSCs/sh-CSE + Fer-1 group compared with those in the HUCMSCs + Fer-1 group (29.232 ± 2.333 *vs* 17.000 ± 2.215, 29.820 ± 1.526 *vs* 23.376 ± 0.537, both $P < 0.01$).

Endothelial to mesenchymal transition (EnMT) has been causally linked to pulmonary arterial remodelling in PAH[20, 21]. EnMT is a form of cellular plasticity described as a phenotypic conversion whereby endothelial cells lose endothelial characteristics (CD31 expression) and acquire mesenchymal characteristics (VE-cadherin expression)[22]. Here, as shown in Figures 3D, E and H, histological and immunofluorescence staining showed slight pulmonary artery stenosis and EnMT in the groups exposed to hypoxia, and these effects were largely attenuated by treatment with HUCMSCs and HUCMSCs + Fer-1 ($P < 0.01$). Interestingly, the inhibitory effect of HUCMSCs + Fer-1 on small pulmonary artery stenosis and EnMT was stronger than that of HUCMSCs. In addition, compared to those in the HUCMSCs + erastin group, small pulmonary artery stenosis and EnMT were alleviated in the HUCMSCs/CSE + erastin group ($P < 0.01$). Meanwhile, small pulmonary artery stenosis and EnMT were aggravated in the HUCMSCs/sh-CSE group compared with the HUCMSCs/Fer-1 group ($P < 0.05$).

CSE inhibition exacerbates Fer-1-mediated suppression of ferroptosis in HUCMSCs

We observed ferroptosis-related changes in erastin-treated HUCMSCs. As shown in Figure 4, cell apoptosis; the levels of Fe^{2+}, ROS, lipid peroxidation, and MDA; and the expression of 4-HNE, TFRC1, and NOCA4 were significantly increased, while the GSH/GSSG ratio; cystine uptake; and GPX4, FTH1, and SLC7A11 expression were decreased in the erastin group compared with the control group (all $P < 0.05$). Consistent with these results, transmission electron microscopy (TEM) also showed an increased mitochondrial membrane density and shorter mitochondrial cristae in the erastin group (Figure 4L). Moreover, the above changes in erastin-treated HUCMSCs were reversed by Fer-1 administration (all $P < 0.05$). Interestingly, the inhibitory effect of Fer-1 on ferroptosis was aggravated by CSE inhibition (all $P < 0.05$).

CSE overexpression negatively regulates erastin-induced ferroptosis in HUCMSCs

As shown in Figure 5, there was a significant decrease in cell apoptosis; the levels of Fe^{2+}, ROS, lipid peroxidation, and MDA; and the expression of 4-HNE, TFRC1, and NOCA4, whereas there was an increase in the GSH/GSSG ratio; cystine uptake; and the expression of GPX4, FTH1, and SLC7A11 in the erastin + CSE group compared to the erastin group (all $P < 0.05$). Consistent with these results, TEM also showed that the mitochondrial membrane was intact and that the mitochondria were narrower with an increased number of cristae in the erastin + CSE group (Figure 5L). In addition, the inhibitory effect of CSE overexpression on ferroptosis was abolished by brusatol, an Nrf2 inhibitor (all $P < 0.05$).

The CSE/H_2S pathway induces Keap1 S-sulfhydration and nuclear translocation of Nrf2

We examined whether Nrf2 is involved in the protective effect of the CSE/H_2S pathway against the ferroptosis of HUCMSCs. First, we found that CSE inhibition decreased H_2S production (Figure 6A), while CSE overexpression increased H_2S levels in HUCMSCs (Figure 6B). In addition, CSE inhibition further downregulated Fer-1-induced Nrf2 activation (Figure 6C), while CSE overexpression further upregulated erastin-induced Nrf2 inactivation (Figure 6D).

Then, the expression of Nrf2 was examined. Western blot analysis revealed that erastin treatment significantly inhibited Nrf2 nuclear translocation, and this effect was markedly enhanced when erastin treatment was combined with Fer-1 treatment (Figure 6E). Moreover, CSE inhibition upregulated Nrf2 expression in the cytoplasm and downregulated Nrf2 expression in the nucleus (Figure 6E). In contrast, CSE overexpression increased nuclear Nrf2 expression and decreased cytoplasmic Nrf2 expression (Figure 6F).

Next, we found that CSE overexpression-induced ferroptosis inhibition was successfully abolished by treatment with 10 nM brusatol, an Nrf2 inhibitor, for 6 h in HUCSMCs (Figure 6F). We also found no difference in the expression of Keap1 among the groups (Figures 6E and F).

Finally, with the "tag-switch" assay, the S-sulfhydration of Keap1 was tested. S-sulfhydration is a novel posttranslational modification involving H_2S. However, S-sulfhydration, a covalent modification, can be reversed by DDT. Increased S-sulfhydration of Keap1 was found in the HUCMSCs/CSE + erastin group than in the HUCMSCs + erastin group, and decreased S-sulfhydration of Keap1 was detected in the HUCMSCs/sh-CSE + Fer-1 group than in the HUCMSCs + Fer-1 group (Figure 6G). Moreover, the S-sulfhydration of Keap1 was further decreased after treatment with DTT, which indicated that Keap1 is S-sulfhydrated (Figure 6G). As shown in Figure 6H, S- of Keap1 led to decreased nuclear Nrf2 expression, which indicated that the activation of Nrf2 by the CSE/H_2S pathway is dependent on Keap1 S-sulfhydration in HUCMSCs.

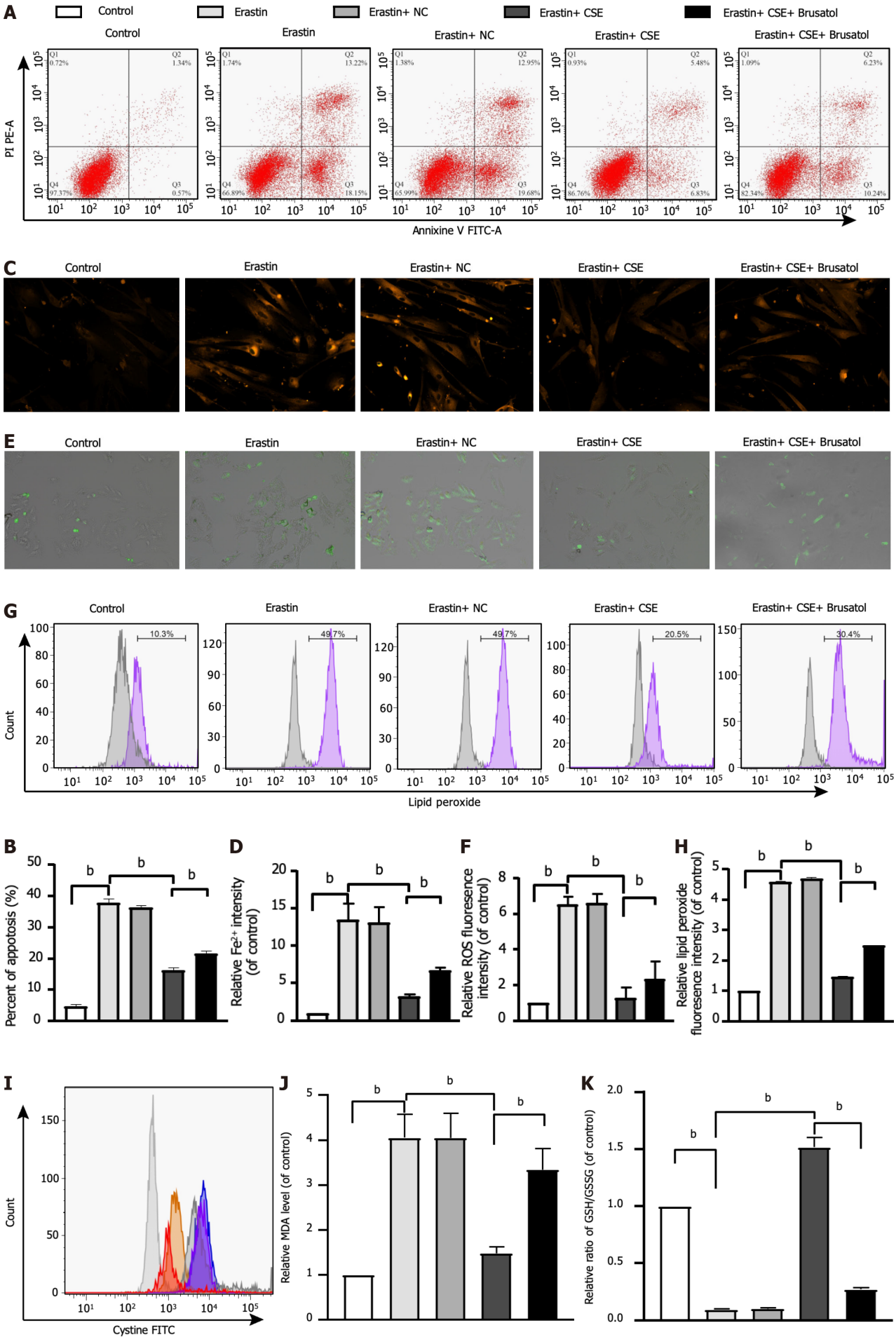
A
Control
Erastin
Erastin+ NC
Erastin+ CSE
Erastin+ CSE+ Brusatol
PI PE-A
Annixine V FITC-A
C
E
G
Count
Lipid peroxide
B
Percent of appotosis (%)
D
Relative Fe2+ intensity (of control)
F
Relative ROS fluoresence intensity (of control)
H
Relative lipid peroxide fluoresence intensity (of control)
I
Cystine FITC
J
Relative MDA level (of control)
K
Relative ratio of GSH/GSSG (of control)

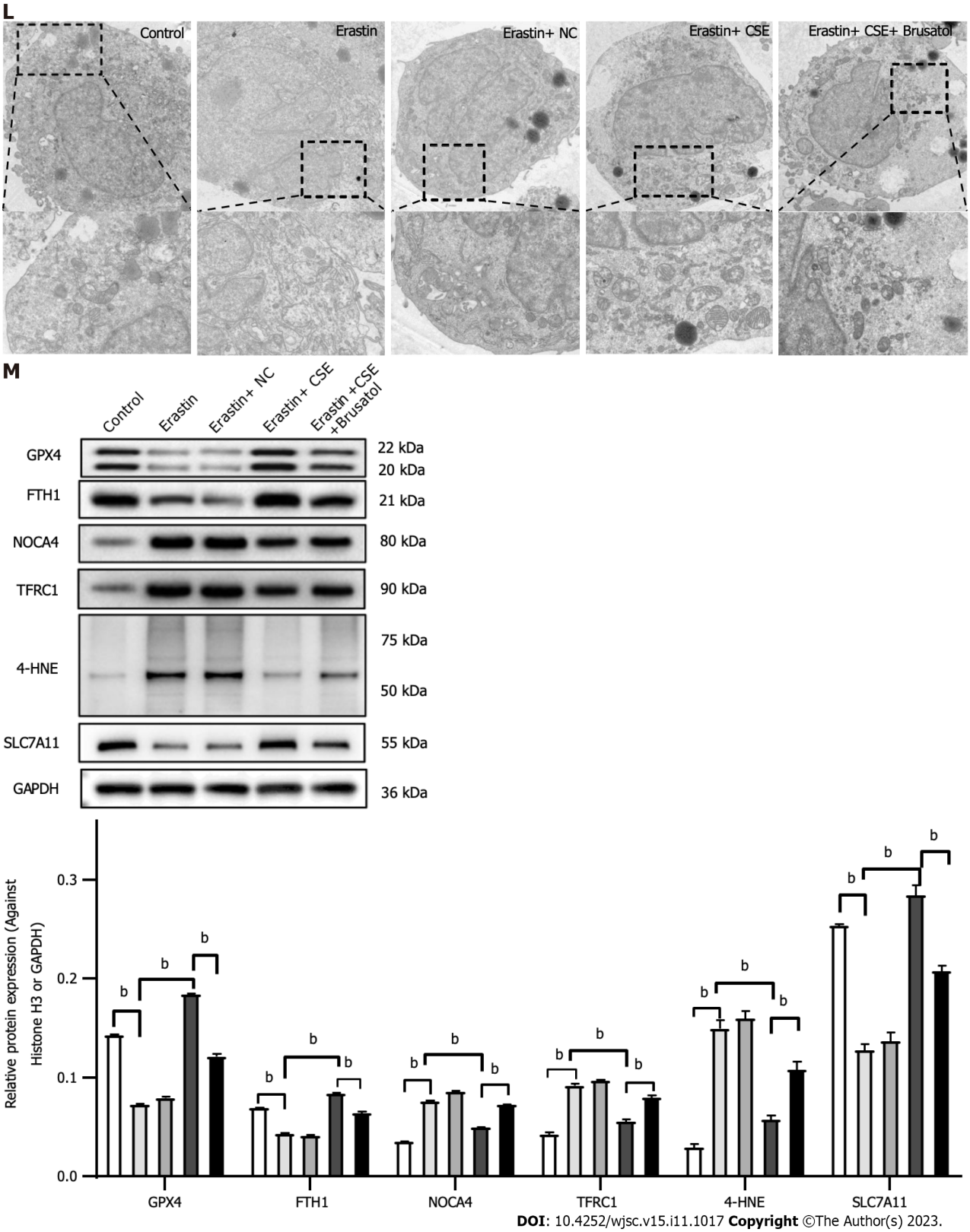

DOI: 10.4252/wjsc.v15.i11.1017

Figure 5 Effect of cystathionine γ-lyase inhibition on ferroptosis in human umbilical cord mesenchymal stem cells. A and B: Cell apoptosis was analyzed by Annexin V-fluorescein isothiocyanate (FITC)/propidine iodide staining using FACS (n = 3), and quantified on the basis of apoptosis rate (n = 3); C and D: Iron level detected by FeRhoNox-1 staining (C) and iron assay kit (D); E and F: Immunofluorescent staining of total reactive oxygen species; G and H: Level of lipid peroxidation detected by flow cytometry after staining with C11-BODIPY; I: Intracellular cystine-FITC levels measured by flow cytometry. Results represent three independent experiments; J: Malonaldehyde level; K: Ratio of reduced glutathione/oxidized glutathione disulfide; L: Mitochondrial morphological changes detected by transmission electron microscopy; M: Western blot analysis of expression of glutathione-dependent antioxidant enzyme glutathione peroxidase, ferritin heavy chain 1, nuclear receptor coactivator 4, Fe^{3+}-bound transferrin receptor 1, 4-hydroxynonenal, and SLC7A11 protein. Glyceraldehyde-3-phosphate dehydrogenase was used for normalization for protein (n = 3). Fer-1: Ferrostatin-1; Annexin V-FITC/PI: Annexin V-fluorescein isothiocyanate/propidine iodide; ROS: Reactive oxygen species;

MDA: Malonaldehyde; CSE: Cystathionine γ-lyase; GSH/GSSG: Reduced glutathione/oxidized glutathione disulfide; GPX4: Glutathione-dependent antioxidant enzyme glutathione peroxidase; FTH1: Ferritin heavy chain 1; NCOA4: Nuclear receptor coactivator 4; TFRC1: Fe^{3+}-bound transferrin receptor 1; 4-HNE: 4-hydroxynonenal; GAPDH: Glyceraldehyde-3-phosphate dehydrogenase. [b]$P < 0.01$.

DISCUSSION

Ferroptosis has been reported as a form of cell death; however, to date, understanding the potential effects of ferroptosis on MSC delivery requires further investigation. In the present study, we showed that ferroptosis occurred during HUCMSC delivery in mice with hypoxia-induced PAH. Moreover, mediation of the CSE/H_2S pathway suppressed ferroptosis in HUCMSCs.

A desirable advantage of MSCs is their ability to home to damaged tissue sites. Evidence has demonstrated that transplanted MSCs can accumulate in lung tissue, inhibit vascular remodelling, and effectively attenuate pulmonary hypertension. In the present study, HUCMSCs were chosen because of their many characteristics, which include their ability to be extracted *via* a noninvasive procedure and high differentiation potential, the ease of their *in vitro* expansion, and their prominent repair properties. To detect transplanted HUCMSCs *in vivo*, HUCMSCs were labelled with firefly luciferase by transduction with a lentiviral vector. Furthermore, we determined that the surface markers and differentiation potential of the HUCMSCs were not disrupted after transduction. In this study, we monitored the survival of HUCMSCs in lung tissue 1 d and 7 d after intravenous injection and found that the HUCMSCs homed to injured lung tissue. Moreover, our data indicated the protective roles of HUCMSCs against pulmonary artery remodelling in mice under hypoxia.

Although MSCs can reach impaired sites due to their homing capacity, cell survival in these places is rare. At present, many potential methods to reduce MSC fate *in vivo* have been identified, including drug pretreatment, genetic modification, and preconditioning. However, our study indicated that pretreatment with Fer-1, an inhibitor of ferroptosis, increased HUCMSC survival in the lung, and combined treatment of HUCMSCs with Fer-1 further decreased vascular remodelling in mice with PAH. Conversely, worse cell survival and decreased therapeutic effects were detected in PAH mice after the delivery of HUCMSCs pretreated with erastin, which induces ferroptosis. Thus, the results showed that ferroptosis may have been linked to HUCMSCs survival in mice with hypoxia-induced PAH.

Researchers have indicated that ferroptosis can be activated by iron overload or the inactivation of GPX4[23-25]. During ferroptosis, following its import through TFRC1, Fe^{3+} is catalysed and converted to Fe^{2+} in the cytoplasm, which then participates in the Fenton reaction, causing ferroptosis. Moreover, Fe^{2+} also binds intracellular FTH1, which can be transported to lysosomes by NCOA4, leading to intracellular iron overload. However, GPX4 is the major endogenous factor that reduces lipid peroxidation[26]. Cystine is converted to cysteine by the cystine/glutamate antiporter system (Xc-), which generates GSH, a cofactor for GPX4[27,28]. In addition, the inhibition of SLC7A11, a key component of system Xc^-, initiates ferroptosis[29], and MDA and 4-HNE, which are byproducts of lipid peroxidation, represent stable markers of oxidative stress that are also associated with ferroptosis[30]. In the present *in vitro* experiments, after Fer-1 administration, we detected decreased cell death, the rebalancing of intracellular iron homeostasis, and reduced levels of lipid peroxidation products, indicating that ferroptosis was suppressed by Fer-1 in erastin-treated HUCMSCs. This is consistent with the ability of Fer-1 and erastin to induce and inhibit ferroptosis, respectively[31].

On the basis of our *in vitro* and *in vivo* experimental results, we suggest that the CSE/H_2S pathway mediates ferroptosis in HUCMSCs. Synthesized by CSE in mammalian cells, H_2S has been shown to directly scavenge ROS[32], facilitate GSH production[33], inhibit GPX4 inactivation[34], and enhance the activity of system Xc[35], mitigating ferroptosis. Indeed, in our study, CSE inhibition decreased endogenous H_2S levels and exacerbated ferroptosis in HUCMSCs, while CSE overexpression increased intracellular H_2S production and inhibited ferroptosis in HUCMSCs. Although emerging evidence has shown that Nrf2 is among the major cellular defences against ferroptosis as it promotes the translation of antioxidant genes, such as FTH1[36], GPX4[37], and Xc[38], the effects of the CSE/H_2S pathway on Nrf2 activation in HUCMSCs have not been described. In our investigation, it was apparent that upregulation of the CSE/H_2S pathway promoted the translocation of Nrf2 into the nucleus, which indicated that Nrf2 was activated. In addition, using an Nrf2 inhibitor, we demonstrated that the inhibitory effects of the CSE/H_2S pathway against ferroptosis were mediated through the activation of Nrf2. Interestingly, we also found that the inactivation of Nrf2, in turn, led to the downregulation of CSE, which may have been caused by excessive oxidative stress-induced oxidation of CSE.

Keap1 is known to bind Nrf2 in the cytoplasm and inhibit it, preventing Nrf2 translocation to the nucleus. Under oxidative stress, the dissociation of Keap1 and Nrf2 results in the entrance of Nrf2 into the nucleus, where it initiates gene transcription[39]. In this study, we found that the CSE/H_2S pathway had little effect on total Keap1 protein expression in HUCMSCs. Thus, to further explore the mechanism underlying the effects of the CSE/H_2S pathway on Nrf2 activation, Keap1 S-sulfhydration was investigated in HUCMSCs. S-sulfhydration is a posttranslational modification induced by H_2S that leads to the attachment of sulfhydryl groups to selective proteins, yielding a hydropersulfide moiety (-SSH)[40]. However, the covalent modification that occurs in sulfhydration is reversable by DTT[40]. Recent publications have revealed that H_2S induces the S-sulfhydration of transcription factors, such as Keap1[41]. In this study, we found that Keap1 S-sulfhydration was inhibited upon ferroptosis. By comparing the difference in Keap1 S-sulfhydration between the HUCMSCs/CSE and HUCMSCs/sh-CSE groups, we demonstrated the significant role of Keap1 S-sulfhydration in the protective effects of the CSE/H_2S pathway against ferroptosis in HUCMSCs.

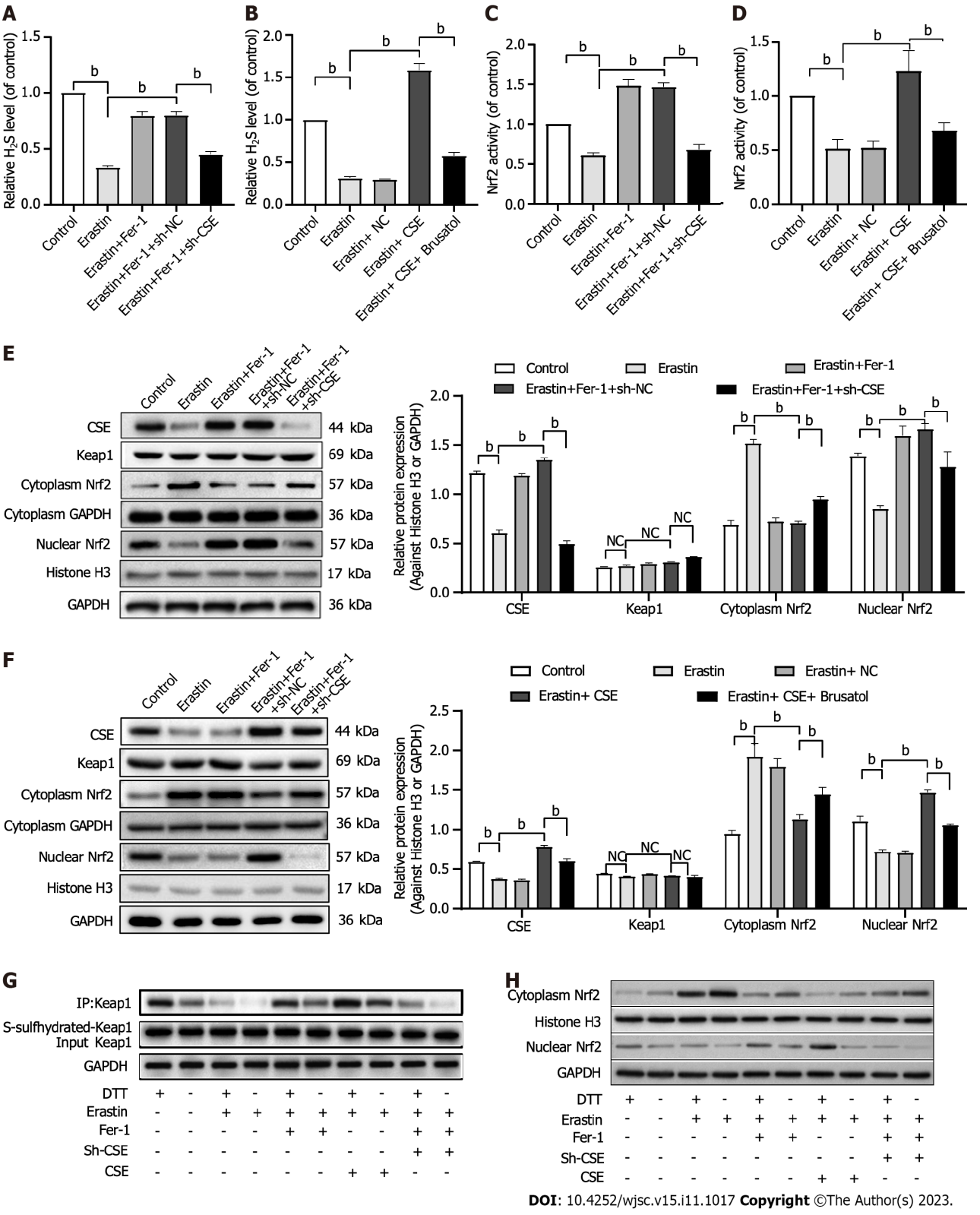

DOI: 10.4252/wjsc.v15.i11.1017

Figure 6 Effect of cystathionine γ-lyase/hydrogen sulfide pathway on nuclear factor erythroid 2-related factor 2 activation and ferroptosis in human umbilical cord mesenchymal stem cells. A and B: Exogenous hydrogen sulfide (H_2S) production; C and D: Nuclear factor erythroid 2-related factor 2 (Nrf2) activity; E and F: Western blot analysis and quantification of cystathionine γ-lyase (CSE) protein, Kelch-like ECH-associating protein 1 (Keap1), and cytoplasmic and nuclear Nrf2 protein; G: Change of Keap1 S-sulfhydration. 1,4-Dithio-DL-threitol (DTT, 1 mmol/L, 3 h) served as a negative control; H: Effect of DTT on cytoplasmic and nuclear Nrf2 expression. Histone H3 was used for normalization for nuclear proteins, and glyceraldehyde-3-phosphate dehydrogenase was used for normalization for whole and cytoplasmic protein (n = 3). CSE: Cystathionine γ-lyase; H_2S: Hydrogen sulfide; Nrf2: Nuclear factor erythroid 2-related factor 2; HUCMSCs: Human umbilical cord mesenchymal stem cells; Fer-1: Ferrostatin-1; sh-CSE: Short hairpin RNA targeting cystathionine γ-lyase; Keap1: Kelch-like ECH-associating protein 1; DTT: 1,4-Dithio-DL-threitol; GAPDH: Glyceraldehyde-3-phosphate dehydrogenase. $^bP < 0.01$.

CONCLUSION

In conclusion, the present data provide evidence for the first time that inhibiting ferroptosis improves the survival of HUCMSC transplanted in mice with hypoxia-induced PAH. Moreover, ferroptosis can be suppressed by regulating the CSE/H_2S pathway *via* S-sulfhydrated Keap1/Nrf2 signalling in HUCMSCs. Collectively, the ability of CSE to inhibit ferroptosis suggests that genetic approaches to manipulate CSE expression and H_2S production may provide a novel therapeutic avenue for improving the protective capacity of transplanted MSCs in PAH.

ARTICLE HIGHLIGHTS

Research background

Ferroptosis can decrease retention and engraftment after mesenchymal stem cell (MSC) delivery, which is considered a major challenge to the effectiveness of MSC-based therapy for pulmonary arterial hypertension (PAH). Interestingly, the cystathionine γ-lyase (CSE)/hydrogen sulfide (H_2S) pathway may contribute to mediating ferroptosis.

Research motivation

We aimed to investigate the influence of the CSE/H_2S pathway on ferroptosis in human umbilical cord MSCs (HUCMSCs).

Research objectives

We aimed to clarify whether the effect of HUCMSCs on vascular remodelling in mice with PAH is by CSE/H_2S pathway-mediated ferroptosis. Furthermore, the effect of the CSE/H_2S pathway on ferroptosis in HUCMSCs and the underlying mechanisms were investigated.

Research methods

Erastin and ferrostatin-1 (Fer-1) were used to induce and inhibit ferroptosis, respectively. HUCMSCs were transfected with a vector that overexpressed or inhibited CSE. A PAH mouse model was established using 4-wk-old male BALB/c nude mice under hypoxic conditions, and pulmonary pressure and vascular remodelling were measured. The survival of HUCMSCs after delivery was observed by *in vivo* bioluminescence imaging. Cell viability, iron accumulation, reactive oxygen species (ROS) production, cystine uptake, and lipid peroxidation in HUCMSCs were tested. Ferroptosis-related proteins and S-sulfhydrated Kelch-like ECH-associating protein 1 (Keap1) were detected by western blot analysis.

Research results

In vivo, CSE overexpression improved cell survival after erastin-treated HUCMSCs were delivered to mice with hypoxia-induced PAH. *In vitro*, CSE overexpression improved H_2S production and ferroptosis-related indexes in erastin-treated HUCMSCs, such as cell viability, the iron level, ROS production, cystine uptake, lipid peroxidation, mitochondrial membrane density, and ferroptosis-related protein expression. In contrast, *in vivo*, CSE inhibition decreased cell survival after Fer-1-treated HUCMSC delivery and aggravated vascular remodelling in the PAH mice. *In vitro*, CSE inhibition decreased H_2S levels and restored ferroptosis in Fer-1-treated HUCMSCs. Interestingly, we found that upregulation of the CSE/H_2S pathway induced the S-sulfhydration of Keap1, which contributed to the inhibition of ferroptosis.

Research conclusions

Regulation of the CSE/H_2S pathway in HUCMSCs contributes to the inhibition of ferroptosis and improves the effect of vascular remodelling suppression in hypoxia-induced PAH mice. Moreover, the protective effect of the CSE/H_2S pathway on ferroptosis in HUCMSCs is mediated *via* S-sulfhydrated Keap1/nuclear factor erythroid 2-related factor 2 (Nrf2) signalling. The present study may provide a novel therapeutic avenue for improving the protective capacity of transplanted MSCs in PAH.

Research perspectives

Regulation of the CSE/H_2S pathway in HUCMSCs contributes to the inhibition of ferroptosis and improves the ability of HUCMSCs to suppress vascular remodelling in mice with hypoxia-induced PAH. Moreover, the protective effect of the CSE/H_2S pathway on ferroptosis in HUCMSCs is mediated *via* S-sulfhydrated Keap1/Nrf2 signalling. The present study may provide a novel therapeutic avenue for improving the protective capacity of transplanted MSCs in PAH.

FOOTNOTES

Co-first authors: Bin Hu and Xiang-Xi Zhang.

Author contributions: Hu B and Zhang XX contributed equally to this work; Yu WC conceived the research; Hu B and Yu WC participated in the design of the study, performed the statistical analysis, and helped to draft the manuscript; Hu B, Zhang XX, Zhang T, and Yu WC performed the experiments; and all authors participated in discussing and revising the manuscript, and approving the final manuscript.

Supported by the Natural Science Foundation of Shandong Province of China, No. ZR2021QH179 and ZR2020MH014.

Institutional animal care and use committee statement: Animal procedures were performed in compliance with the Institutional Animal Care and Use Committee of Shandong Provincial Hospital Affiliated to Shandong First Medical University (No. 2022-333).

Conflict-of-interest statement: All the authors report no relevant conflicts of interest for this article.

Data sharing statement: No additional unpublished data are available.

ARRIVE guidelines statement: The authors have read the ARRIVE guidelines, and the manuscript was prepared and revised according to the ARRIVE guidelines.

Country/Territory of origin: China

ORCID number: Wan-Cheng Yu 0000-0003-3850-3298.

S-Editor: Wang JJ
L-Editor: Wang TQ
P-Editor: Zhang XD

REFERENCES

1 **Pullamsetti SS**, Schermuly R, Ghofrani A, Weissmann N, Grimminger F, Seeger W. Novel and emerging therapies for pulmonary hypertension. *Am J Respir Crit Care Med* 2014; **189**: 394-400 [PMID: 24401129 DOI: 10.1164/rccm.201308-1543PP]
2 **Malliaras K**, Marbán E. Cardiac cell therapy: where we've been, where we are, and where we should be headed. *Br Med Bull* 2011; **98**: 161-185 [PMID: 21652595 DOI: 10.1093/bmb/ldr018]
3 **Zhang Q**, Wan XX, Hu XM, Zhao WJ, Ban XX, Huang YX, Yan WT, Xiong K. Targeting Programmed Cell Death to Improve Stem Cell Therapy: Implications for Treating Diabetes and Diabetes-Related Diseases. *Front Cell Dev Biol* 2021; **9**: 809656 [PMID: 34977045 DOI: 10.3389/fcell.2021.809656]
4 **Lei G**, Zhuang L, Gan B. Targeting ferroptosis as a vulnerability in cancer. *Nat Rev Cancer* 2022; **22**: 381-396 [PMID: 35338310 DOI: 10.1038/s41568-022-00459-0]
5 **Li X**, Zeng J, Liu Y, Liang M, Liu Q, Li Z, Zhao X, Chen D. Inhibitory Effect and Mechanism of Action of Quercetin and Quercetin Diels-Alder anti-Dimer on Erastin-Induced Ferroptosis in Bone Marrow-Derived Mesenchymal Stem Cells. *Antioxidants (Basel)* 2020; **9** [PMID: 32131401 DOI: 10.3390/antiox9030205]
6 **Liu J**, Ren Z, Yang L, Zhu L, Li Y, Bie C, Liu H, Ji Y, Chen D, Zhu M, Kuang W. The NSUN5-FTH1/FTL pathway mediates ferroptosis in bone marrow-derived mesenchymal stem cells. *Cell Death Discov* 2022; **8**: 99 [PMID: 35249107 DOI: 10.1038/s41420-022-00902-z]
7 **Lan D**, Qi S, Yao C, Li X, Liu H, Wang D, Wang Y. Quercetin protects rat BMSCs from oxidative stress *via* ferroptosis. *J Mol Endocrinol* 2022; **69**: 401-413 [PMID: 35900382 DOI: 10.1530/JME-22-0086]
8 **Lan D**, Yao C, Li X, Liu H, Wang D, Wang Y, Qi S. Tocopherol attenuates the oxidative stress of BMSCs by inhibiting ferroptosis through the PI3k/AKT/mTOR pathway. *Front Bioeng Biotechnol* 2022; **10**: 938520 [PMID: 36061427 DOI: 10.3389/fbioe.2022.938520]
9 **Han L**, Ma C, Wu Z, Xu H, Li H, Pan G. AhR-STAT3-HO-1/COX-2 signalling pathway may restrict ferroptosis and improve hMSC accumulation and efficacy in mouse liver. *Br J Pharmacol* 2023 [PMID: 37538043 DOI: 10.1111/bph.16208]
10 **Kajarabille N**, Latunde-Dada GO. Programmed Cell-Death by Ferroptosis: Antioxidants as Mitigators. *Int J Mol Sci* 2019; **20** [PMID: 31597407 DOI: 10.3390/ijms20194968]
11 **Dodson M**, Castro-Portuguez R, Zhang DD. NRF2 plays a critical role in mitigating lipid peroxidation and ferroptosis. *Redox Biol* 2019; **23**: 101107 [PMID: 30692038 DOI: 10.1016/j.redox.2019.101107]
12 **Stein A**, Bailey SM. Redox Biology of Hydrogen Sulfide: Implications for Physiology, Pathophysiology, and Pharmacology. *Redox Biol* 2013; **1**: 32-39 [PMID: 23795345 DOI: 10.1016/j.redox.2012.11.006]
13 **Stipanuk MH**. Sulfur amino acid metabolism: pathways for production and removal of homocysteine and cysteine. *Annu Rev Nutr* 2004; **24**: 539-577 [PMID: 15189131 DOI: 10.1146/annurev.nutr.24.012003.132418]
14 **Huang F**, Gao T, Wang W, Wang L, Xie Y, Tai C, Liu S, Cui Y, Wang B. Engineered basic fibroblast growth factor-overexpressing human umbilical cord-derived mesenchymal stem cells improve the proliferation and neuronal differentiation of endogenous neural stem cells and functional recovery of spinal cord injury by activating the PI3K-Akt-GSK-3β signaling pathway. *Stem Cell Res Ther* 2021; **12**: 468 [PMID: 34419172 DOI: 10.1186/s13287-021-02537-w]
15 **Zhang Q**, Cheng X, Zhang H, Zhang T, Wang Z, Zhang W, Yu W. Dissecting molecular mechanisms underlying H(2)O(2)-induced apoptosis of mouse bone marrow mesenchymal stem cell: role of Mst1 inhibition. *Stem Cell Res Ther* 2020; **11**: 526 [PMID: 33298178 DOI: 10.1186/s13287-020-02041-7]
16 **Park CM**, Macinkovic I, Filipovic MR, Xian M. Use of the "tag-switch" method for the detection of protein S-sulfhydration. *Methods Enzymol* 2015; **555**: 39-56 [PMID: 25747474 DOI: 10.1016/bs.mie.2014.11.033]
17 **Yu WC**, Chen HY, Yang HL, Xia P, Zou CW, Sun TW, Wang LX. rBMSC/Cav-1(F92A) Mediates Oxidative Stress in PAH Rat by

Regulating SelW/14-3-3η and CA1/Kininogen Signal Transduction. *Stem Cells Int* 2019; **2019**: 6768571 [PMID: 31781243 DOI: 10.1155/2019/6768571]

18 **Li B**, Wang C, Lu P, Ji Y, Wang X, Liu C, Lu X, Xu X. IDH1 Promotes Foam Cell Formation by Aggravating Macrophage Ferroptosis. *Biology (Basel)* 2022; **11** [PMID: 36290297 DOI: 10.3390/biology11101392]

19 **Pulido T**, Adzerikho I, Channick RN, Delcroix M, Galiè N, Ghofrani HA, Jansa P, Jing ZC, Le Brun FO, Mehta S, Mittelholzer CM, Perchenet L, Sastry BK, Sitbon O, Souza R, Torbicki A, Zeng X, Rubin LJ, Simonneau G; SERAPHIN Investigators. Macitentan and morbidity and mortality in pulmonary arterial hypertension. *N Engl J Med* 2013; **369**: 809-818 [PMID: 23984728 DOI: 10.1056/NEJMoa1213917]

20 **Arciniegas E**, Frid MG, Douglas IS, Stenmark KR. Perspectives on endothelial-to-mesenchymal transition: potential contribution to vascular remodeling in chronic pulmonary hypertension. *Am J Physiol Lung Cell Mol Physiol* 2007; **293**: L1-L8 [PMID: 17384082 DOI: 10.1152/ajplung.00378.2006]

21 **Zhu P**, Huang L, Ge X, Yan F, Wu R, Ao Q. Transdifferentiation of pulmonary arteriolar endothelial cells into smooth muscle-like cells regulated by myocardin involved in hypoxia-induced pulmonary vascular remodelling. *Int J Exp Pathol* 2006; **87**: 463-474 [PMID: 17222214 DOI: 10.1111/j.1365-2613.2006.00503.x]

22 **Piera-Velazquez S**, Jimenez SA. Molecular mechanisms of endothelial to mesenchymal cell transition (EndoMT) in experimentally induced fibrotic diseases. *Fibrogenesis Tissue Repair* 2012; **5**: S7 [PMID: 23259736 DOI: 10.1186/1755-1536-5-S1-S7]

23 **Yang WS**, Kim KJ, Gaschler MM, Patel M, Shchepinov MS, Stockwell BR. Peroxidation of polyunsaturated fatty acids by lipoxygenases drives ferroptosis. *Proc Natl Acad Sci U S A* 2016; **113**: E4966-E4975 [PMID: 27506793 DOI: 10.1073/pnas.1603244113]

24 **Battaglia AM**, Chirillo R, Aversa I, Sacco A, Costanzo F, Biamonte F. Ferroptosis and Cancer: Mitochondria Meet the "Iron Maiden" Cell Death. *Cells* 2020; **9** [PMID: 32575749 DOI: 10.3390/cells9061505]

25 **Park E**, Chung SW. ROS-mediated autophagy increases intracellular iron levels and ferroptosis by ferritin and transferrin receptor regulation. *Cell Death Dis* 2019; **10**: 822 [PMID: 31659150 DOI: 10.1038/s41419-019-2064-5]

26 **Doll S**, Freitas FP, Shah R, Aldrovandi M, da Silva MC, Ingold I, Goya Grocin A, Xavier da Silva TN, Panzilius E, Scheel CH, Mourão A, Buday K, Sato M, Wanninger J, Vignane T, Mohana V, Rehberg M, Flatley A, Schepers A, Kurz A, White D, Sauer M, Sattler M, Tate EW, Schmitz W, Schulze A, O'Donnell V, Proneth B, Popowicz GM, Pratt DA, Angeli JPF, Conrad M. FSP1 is a glutathione-independent ferroptosis suppressor. *Nature* 2019; **575**: 693-698 [PMID: 31634899 DOI: 10.1038/s41586-019-1707-0]

27 **Fujii J**, Homma T, Kobayashi S. Ferroptosis caused by cysteine insufficiency and oxidative insult. *Free Radic Res* 2020; **54**: 969-980 [PMID: 31505959 DOI: 10.1080/10715762.2019.1666983]

28 **Lu SC**. Glutathione synthesis. *Biochim Biophys Acta* 2013; **1830**: 3143-3153 [PMID: 22995213 DOI: 10.1016/j.bbagen.2012.09.008]

29 **Dixon SJ**, Lemberg KM, Lamprecht MR, Skouta R, Zaitsev EM, Gleason CE, Patel DN, Bauer AJ, Cantley AM, Yang WS, Morrison B 3rd, Stockwell BR. Ferroptosis: an iron-dependent form of nonapoptotic cell death. *Cell* 2012; **149**: 1060-1072 [PMID: 22632970 DOI: 10.1016/j.cell.2012.03.042]

30 **Yan B**, Xie D, Wu Y, Wang S, Zhang X, Zhao T, Liu L, Ma P, Li G, Yang Y, Zhao Y, Zheng T, Geng R, Li B, Zheng Q. Ferroptosis is involved in PGPS-induced otitis media in C57BL/6 mice. *Cell Death Discov* 2022; **8**: 217 [PMID: 35449198 DOI: 10.1038/s41420-022-01025-1]

31 **Shou Y**, Yang L, Yang Y, Xu J. Inhibition of keratinocyte ferroptosis suppresses psoriatic inflammation. *Cell Death Dis* 2021; **12**: 1009 [PMID: 34707088 DOI: 10.1038/s41419-021-04284-5]

32 **Kimura H**. Hydrogen sulfide: its production, release and functions. *Amino Acids* 2011; **41**: 113-121 [PMID: 20191298 DOI: 10.1007/s00726-010-0510-x]

33 **Kimura Y**, Goto Y, Kimura H. Hydrogen sulfide increases glutathione production and suppresses oxidative stress in mitochondria. *Antioxid Redox Signal* 2010; **12**: 1-13 [PMID: 19852698 DOI: 10.1089/ars.2008.2282]

34 **Wang Q**, Wang XL, Liu HR, Rose P, Zhu YZ. Protective effects of cysteine analogues on acute myocardial ischemia: novel modulators of endogenous H(2)S production. *Antioxid Redox Signal* 2010; **12**: 1155-1165 [PMID: 19842912 DOI: 10.1089/ars.2009.2947]

35 **Kimura Y**, Kimura H. Hydrogen sulfide protects neurons from oxidative stress. *FASEB J* 2004; **18**: 1165-1167 [PMID: 15155563 DOI: 10.1096/fj.04-1815fje]

36 **Sun X**, Ou Z, Chen R, Niu X, Chen D, Kang R, Tang D. Activation of the p62-Keap1-NRF2 pathway protects against ferroptosis in hepatocellular carcinoma cells. *Hepatology* 2016; **63**: 173-184 [PMID: 26403645 DOI: 10.1002/hep.28251]

37 **Shin D**, Kim EH, Lee J, Roh JL. Nrf2 inhibition reverses resistance to GPX4 inhibitor-induced ferroptosis in head and neck cancer. *Free Radic Biol Med* 2018; **129**: 454-462 [PMID: 30339884 DOI: 10.1016/j.freeradbiomed.2018.10.426]

38 **Fan Z**, Wirth AK, Chen D, Wruck CJ, Rauh M, Buchfelder M, Savaskan N. Nrf2-Keap1 pathway promotes cell proliferation and diminishes ferroptosis. *Oncogenesis* 2017; **6**: e371 [PMID: 28805788 DOI: 10.1038/oncsis.2017.65]

39 **Abed DA**, Goldstein M, Albanyan H, Jin H, Hu L. Discovery of direct inhibitors of Keap1-Nrf2 protein-protein interaction as potential therapeutic and preventive agents. *Acta Pharm Sin B* 2015; **5**: 285-299 [PMID: 26579458 DOI: 10.1016/j.apsb.2015.05.008]

40 **Mustafa AK**, Gadalla MM, Sen N, Kim S, Mu W, Gazi SK, Barrow RK, Yang G, Wang R, Snyder SH. H2S signals through protein S-sulfhydration. *Sci Signal* 2009; **2**: ra72 [PMID: 19903941 DOI: 10.1126/scisignal.2000464]

41 **Xie L**, Gu Y, Wen M, Zhao S, Wang W, Ma Y, Meng G, Han Y, Wang Y, Liu G, Moore PK, Wang X, Wang H, Zhang Z, Yu Y, Ferro A, Huang Z, Ji Y. Hydrogen Sulfide Induces Keap1 S-sulfhydration and Suppresses Diabetes-Accelerated Atherosclerosis *via* Nrf2 Activation. *Diabetes* 2016; **65**: 3171-3184 [PMID: 27335232 DOI: 10.2337/db16-0020]

Published by **Baishideng Publishing Group Inc**
7041 Koll Center Parkway, Suite 160, Pleasanton, CA 94566, USA
Telephone: +1-925-3991568
E-mail: bpgoffice@wjgnet.com
Help Desk: https://www.f6publishing.com/helpdesk
https://www.wjgnet.com